NUREG/CR–5889
LA–UR–88–1937

Posttest Analysis of MIST Test 330302 Using TRAC–PF1/MOD1

Prepared by
B. E. Boyack

Los Alamos National Laboratory

Prepared for
U.S. Nuclear Regulatory Commission

AVAILABILITY NOTICE

Availability of Reference Materials Cited in NRC Publications

Most documents cited in NRC publications will be available from one of the following sources:

1. The NRC Public Document Room, 2120 L Street, NW., Lower Level, Washington, DC 20555

2. The Superintendent of Documents, U.S. Government Printing Office, P.O. Box 37082, Washington, DC 20013-7082

3. The National Technical Information Service, Springfield, VA 22161

Although the listing that follows represents the majority of documents cited in NRC publications, it is not intended to be exhaustive.

Referenced documents available for inspection and copying for a fee from the NRC Public Document Room include NRC correspondence and internal NRC memoranda; NRC bulletins, circulars, information notices, inspection and investigation notices; licensee event reports; vendor reports and correspondence; Commission papers; and applicant and licensee documents and correspondence.

The following documents in the NUREG series are available for purchase from the GPO Sales Program: formal NRC staff and contractor reports, NRC-sponsored conference proceedings, international agreement reports, grant publications, and NRC booklets and brochures. Also available are regulatory guides, NRC regulations in the *Code of Federal Regulations*, and *Nuclear Regulatory Commission Issuances*.

Documents available from the National Technical Information Service include NUREG-series reports and technical reports prepared by other Federal agencies and reports prepared by the Atomic Energy Commission, forerunner agency to the Nuclear Regulatory Commission.

Documents available from public and special technical libraries include all open literature items, such as books, journal articles, and transactions. *Federal Register* notices, Federal and State legislation, and congressional reports can usually be obtained from these libraries.

Documents such as theses, dissertations, foreign reports and translations, and non-NRC conference proceedings are available for purchase from the organization sponsoring the publication cited.

Single copies of NRC draft reports are available free, to the extent of supply, upon written request to the Office of Administration, Distribution and Mail Services Section, U.S. Nuclear Regulatory Commission, Washington, DC 20555.

Copies of industry codes and standards used in a substantive manner in the NRC regulatory process are maintained at the NRC Library, 7920 Norfolk Avenue, Bethesda, Maryland, for use by the public. Codes and standards are usually copyrighted and may be purchased from the originating organization or, if they are American National Standards, from the American National Standards Institute, 1430 Broadway, New York, NY 10018.

DISCLAIMER NOTICE

NUREG/CR--5889

TI93 003213

Posttest Analysis of MIST Test 330302 Using TRAC–PF1/MOD1

Manuscript Completed: April 1992
Date Published: September 1992

Prepared by
B. E. Boyack

Los Alamos National Laboratory
Los Alamos, NM 87545

Prepared for
Division of Systems Research
Office of Nuclear Regulatory Research
U.S. Nuclear Regulatory Commission
Washington, DC 20555
NRC FIN A7311

ISBN 0-16-038194-0

For sale by the U.S. Government Printing Office
Superintendent of Documents, Mail Stop: SSOP, Washington, DC 20402-9328
ISBN 0-16-038194-0

CONTENTS

TABLES

FIGURES

POSTTEST ANALYSIS OF MIST 330302 USING TRAC-PF1/MOD1*

by

Brent E. Boyack

ABSTRACT

A posttest analysis of Multi-Loop Integral System Test (MIST) 330302 has been performed using TRAC-PF1/MOD1. This test was one of group performed in the MIST facility to investigate high-pressure injection (HPI)–power-operated relief valve (PORV) cooling, also known as feed-and-bleed cooling. In Test 330302, HPI cooling was delayed 20 min after opening and locking the PORV open to induce extensive system voiding. MIST 330302 displayed many phenomena of interest. These included a steam-generator-secondary boiloff, slow primary-system pressurization at constant primary-system inventory, single- and two-phase fluid flows through the PORV, hot-leg spillover events, cold-leg and downcomer flow interruption and recovery, effects of late HPI injection into a voided primary system, and primary-system refill. We have concluded that the TRAC-calculated results are in reasonable overall agreement with the data for Test 330302. All major trends and phenomena were correctly predicted. Differences observed between the measured and calculated results have been traced and related, in part, to deficiencies in our knowledge of the facility configuration and operation. We have identified two models for which additional review is appropriate. However, in general, the TRAC closure models and correlations appear to be adequate for the prediction of the phenomena expected to occur during feed-and-bleed transients in the MIST facility. We believe that the correct conclusions about trends and phenomena will be reached if the code is used in similar applications. Conclusions reached regarding use of the code to calculate similar phenomena in full-size plants (scaling implications) and regulatory implications of this work are also presented.

EXECUTIVE SUMMARY

A posttest analysis of Multi-Loop Integral System Test (MIST) 330302 has been performed using TRAC-PF1/MOD1. This test was one of a group performed in the MIST facility to investigate high-pressure injection (HPI)–power-operated relief valve (PORV) cooling, also known as feed-and-bleed cooling. In Test 330302, HPI cooling was delayed 20 min after opening and locking the PORV open to induce extensive system voiding. MIST 330302 displayed many

* This work was funded by the US Nuclear Regulatory Commission, Office of Nuclear Regulatory Research, Division of Reactor and Plant Systems.

phenomena of interest. These included a steam-generator-secondary boiloff, slow primary-system pressurization at constant primary-system inventory, single- and two-phase fluid flows through the PORV, hot-leg spillover events, cold-leg and downcomer flow interruptions and flow recovery, effects of late HPI injection into a voided primary system, and primary-system refill. Our lessons learned and key conclusions have been subdivided into areas related to (1) knowledge of facility configuration and operation, (2) the facility input model used with TRAC, and (3) code models and correlations; we have also considered scaling implications and regulatory implications.

Knowledge of Facility Configuration and Operation

We identified two cases in which our knowledge of MIST facility operation was deficient. First, we did not have an adequate understanding of the initial pressurizer liquid temperature distribution. Sufficient transient data were available for us to infer a more correct initial or steady-state temperature distribution. However, our procedures have not generally included the plotting and review of all transient data in advance of our transient calculation as this is a costly procedure. Second, we believe that measurement of steam-generator-secondary liquid level is incorrect for Test 330302. We recommend that Babcock & Wilcox (B&W) review the apparent inconsistency between test measurements. If one or more of the details of instrumentation are in error, we recommend that other tests in which the error could be important be reviewed, corrected, and flagged, as necessary.

We believe that our calculation of MIST 330302 should be rerun with an improved pressurizer initial liquid temperature distribution and with the correct steam-generator-secondary liquid level, once defined by B&W.

Input Model

We found the input model, with one exception, to be adequate for feed-and-bleed transients in the MIST facility. For Test 330302, the steam-generator-secondary initial liquid levels were quite low and resided within the first level of the standard MIST steam-generator (SG) model. We found that TRAC had to use a small time step to deal with this situation. A noding study was conducted and we found that by dividing the bottom cell into smaller nodes the calculation time was improved. We also noted that finer noding of the pressurizer may be required for an improved prediction of the primary-system pressurization following transient initiation. No noding study was conducted to investigate this area.

Code Models and Correlations

We found two areas of concern regarding TRAC constitutive models and correlations. First, the critical flow model during liquid flow shows a sensitivity to subcooling not observed in the data for Test 330302. Second, we found that TRAC has the potential for overpredicting the steam-generator primary-side heat transfer during natural-circulation flow.

Scaling Implications

Two categories of scaling information can be derived from this test. The first category is a collection and analysis of assessment results at the component level that can be considered to be full scale. For example, the facility core heater rods are full scale in diameter and height. Thus, subchannel phenomena occurring in the core can be assessed as if they were full scale. For Test 330302, the measured and predicted core thermal-hydraulic parameters were

in reasonable agreement. The SG tubes are also full scale such that phenomena occurring at the inner and outer surfaces of the tubes can be assessed. We determined that the liquid heat-transfer coefficients calculated on the inside of the tubes by TRAC were 15 to 30% high. Finally, the facility is full height so that phenomena related to density differences such as flow interruptions and recovery may be assessed. The agreement between the calculated and measured loop phenomena such as flow interruption and recovery was reasonable.

The second category considers this assessment as one element or piece of evidence that is accumulated to determine whether TRAC-PF1/MOD1 is able to predict the phenomena occurring in a feed-and-bleed transient. We note that this result is specific to one facility, MIST, which is characterized by a scaled-volume reduction of 817 relative to a full-size lowered-loop B&W plant. For the TRAC-PF1/MOD1 posttest assessment of MIST 330302, a feed-and-bleed test with HPI injection delayed 20 min following PORV actuation, we concluded that the overall agreement between test and calculated results was reasonable. This result can be accumulated and weighed with other assessments for a variety of transients and facilities by qualified technical people charged with the responsibility for determining whether TRAC-PF1/MOD1 can be used as a predictive tool for full-plant transients.

Candidate approaches for assessing the scaling capability of a code such as TRAC-PF1/MOD1 have been reviewed. We concluded that each posttest assessment contributes to the determination of code-scaling capability. We also concluded that the posttest assessment of a single experiment will usually provide only a small fraction of the information needed for a complete statement about code-scaling capability. Given the importance of this issue, initiation of an effort to define and plan an approach to determine the code-scaling capability of TRAC-PF1/MOD1 is recommended. This approach, once defined, would be applicable to other codes. The effort would include collecting, reviewing and applying existing posttest assessment data. In addition, this effort would identify the need for additional work, if any, related to assessments of full-plant transients, assessments of counterpart tests and the assessment of code-scaling capability by focusing on the correlations and models used in the code for given scaled integral or full-plant transients.

Regulatory Implications

It is possible to draw important conclusions regarding HPI-PORV or feed-and-bleed cooling in the MIST facility. First, the feed-and-bleed procedure was successful in cooling and depressurizing the primary system in each of the tests conducted. Second, the parametric cases for reduced HPI (Test 330201) and delayed HPI (Test 330302) demonstrate that the feed-and-bleed procedure, as scaled and applied in the MIST facility, can still successfully cool and depressurize the plant. These two cases provide an indication of the margin against reductions in the amount of HPI delivered or in the time of delivery. The two cases do not define the limits of the margin. Third, the MIST feed-and-bleed tests do not address the issues of equipment survivability or willingness of the operator to initiate a feed-and-bleed procedure. Fourth, the test results cannot be directly extrapolated to full-size B&W plants. The extension to full-size plants must be made through the use of assessed computer codes. Fifth, TRAC-PF1/MOD1 predicts the time to PORV actuation to occur earlier than measured in the MIST facility for Test 330302. The result is conservative in that more time would be available to PORV opening on high primary-system pressure than predicted by TRAC. Sixth, the TRAC-calculated results

for Test 330302 are in reasonable overall agreement with the data. All major trends and phenomena were correctly predicted. Differences observed between the measured and calculated results have been traced and related, in part, to deficiencies in our knowledge of the facility configuration and operation. We have also identified two models for which additional review is appropriate. However, in general, the TRAC closure models and correlations appear to be adequate for the prediction of the phenomena expected to occur during feed-and-bleed transients in the MIST facility.

Finally, we have analyzed the use of feed-and-bleed procedures using models of two full-size B&W plants, Oconee-1 and Davis-Besse. A feed-and-bleed procedure was found to successfully cool and depressurize the Oconee-1 plant following a postulated loss of feedwater provided the procedure was initiated no later than the time the primary system would have saturated had the primary system been maintained at a pressure near the PORV setpoint by cycling the PORV open and shut. In addition, phenomena predicted to occur in the full-size Oconee-1 plant were similar to those observed in MIST 330302. These included primary-system heatup and expansion following loss of the SG-secondary heat sink, primary-system inventory depletion following PORV actuation, and primary-system refill following HPI initiation. Studies show that a feed-and-bleed procedure would have successfully cooled and depressurized the Davis-Besse plant if such a procedure had been used following the actual loss-of-feedwater event of June 9, 1985. Again, the global characteristics of the calculated Davis-Besse feed-and-bleed transient were similar to those observed in MIST 330302 and in our calculation of a postulated feed-and-bleed transient in the Oconee-1 plant. Based on the successful calculation of MIST 330302 and the prediction of similar phenomena in full-size plants (Oconee-1 and Davis-Besse), we conclude that TRAC-PF1/MOD1 will correctly predict the major trends for feed-and-bleed transients in full-size plants.

I. INTRODUCTION

The Multi-Loop Integral System Test (MIST) facility is a scale model of a Babcock & Wilcox (B&W) nuclear power plant. The facility is located in Alliance, Ohio, and is designed to experimentally investigate transients occurring after reactor trip and primary-pump coastdown. The MIST facility is scaled to a 2×4 lowered-loop prototype plant with 177 fuel assemblies. The scale factor is 1/817 for volume and power; component elevations are scaled one to one. Data from the MIST facility are used to help resolve current plant licensing issues and also to assess and refine computer codes used to analyze plant thermal-hydraulic behavior.

Thermal-hydraulic systems codes such as the Transient Reactor Analysis Code (TRAC) have been developed as tools for the prediction of transients in full-size plants. To be used in this manner, the codes must be verified as predictive. Thus, a primary goal of a code-assessment activity is to evaluate the adequacy of the correlations and models in the TRAC. A related goal is to assist in developing an understanding of the phenomena occurring during the experiment. A secondary goal of the assessment process is to evaluate input-modeling practices and develop user guidelines. To achieve these goals, the analyst must come to an understanding of the measured test data and phenomena, the calculated data and phenomena, and the reasons for differences between test data and calculated values and phenomena. We have found it helpful to divide the differences we identify into three categories. First, a difference may be due to an incomplete or inaccurate knowledge of the facility or its operation, including the instrumentation and the resulting data. Although this might seem to be a minor problem,

it has not been minor for many facilities. Differences of this type may be difficult to isolate and can mask problems with the input model or the code. The documentation of the MIST facility, its operation, and its data qualification are excellent, although there have been occasional problems as occur in any complex facility or test sequence. Second, the input model may be inadequate because of modeling compromises, noding, use of one-dimensional instead of three-dimensional models, etc. Third, inadequacies in the code closure models and correlations can cause differences. A major task of an analyst in code-assessment calculations is to understand the differences between calculation and test within this framework, and in the case of code deficiencies, to identify the particular code model or correlation causing the difference.

The objective of this report is to document assessment studies performed using TRAC-PF1/MOD1, version 14.3 (Ref. 1), by comparing their results with the experimental data for MIST 330302 (Refs. 2 and 3). Test 330302 was conducted to examine an extended period of pressure-operated relief valve (PORV) actuation without makeup and with the steam generators unavailable. In addition, high-pressure injection (HPI) was delayed to permit extensive voiding in the primary system to occur. It was anticipated that the HPI, when finally actuated, would perturb system conditions because of condensation and depressurization. A pretest analysis of MIST 330302 was completed and reported in Ref. 4.

II. TEST DESCRIPTION

Test 330302 is the delayed HPI feed-and-bleed test. In this test there was no primary system leak; the initiating event was a complete loss of auxiliary feedwater (AFW) to the steam generators (SGs). In the Phase III MIST facility, AFW is the only source of feedwater supply to the SGs. The PORV was actuated at 16.2 MPa (2350 psi) and maintained manually open for the remainder of the test. Nominal HPI flow was initiated 1200 s after PORV actuation, thereby establishing feed-and-bleed cooling.

A. Test Conduct

Following AFW termination, the SG secondaries were allowed to boil off in Test 330302. The reactor-vessel vent valve (RVVV) control in Test 330302 was transferred from manually closed to automatic/independent when the AFW flow was terminated at the beginning of the test; the RVVVs immediately opened. The actuation set points for the RVVV automatic mode are 862 Pa (0.125 psi) to open and 275 Pa (0.04 psi) to close. Core power decay was started in the test when the PORV actuated. Before PORV actuation, the core power was maintained at its initial value. The transient controls for Test 330302 are provided in Table I.

During the secondary boiloff process, the set point for the steam discharge valves was maintained at its initial value of 6.96 MPa (1010 psia). Near the end of the boiloff, the secondary pressures fell below this set point, and the discharge valves closed. Afterward, the secondary pressure slowly decayed as a result of heat losses from the secondaries. When the secondary pressure fell to 6.55 MPa (950 psia), the SGs were pressurized with nitrogen at 6.55 MPa (950 psia) for the remainder of the test. This was done to maintain the primary-to-secondary pressure difference within the structural limits of the SGs.

B. Test Phenomena Overview

Feed-and-bleed transient 330302 was initiated at time zero from the steady state reported in Table II by terminating all AFW to both SG secondaries. An overview of the resultant test transient is shown in Fig. 1. Only test data are presented in Fig. 1.

With the termination of AFW to the SG secondaries, the SG-secondary inventory begins to boil off. However, this process removes only part of the core energy, and the primary system begins to heat up and pressurize as shown in Fig. 1.a. In the test the primary pressurizes to the PORV set point of 16.41 MPa (2350 psia) at 942 s. During this period the pressurizer liquid level is increasing as a result of primary-system swelling as shown in Fig. 1.b. The rate of steam generation in the SG secondary during the boiloff is shown in Fig. 1.e. The RVVVs open immediately following test initiation; the resultant total RVVV flow is shown in Fig. 1.f. The Loop-A1 and downcomer mass flows following test initiation are shown in Figs. 1.g and 1.h, respectively. The period from test initiation to PORV actuation is designated as Phase 1, SG dryout.

Phase 2 of the transient covers the period between PORV actuation and HPI initiation 1200 s later. This period is a time of primary-system inventory depletion as shown in Fig. 1.i and covers the time between 942 and 2142 s in the test. Boiling begins in the hottest regions of the primary system at 1000 s as shown in Fig. 1.j. Immediately following PORV actuation the pressurizer filling rate increases; the pressurizer fills with water at about 1070 s as shown in Fig. 1.b. Two-phase fluid is released through the PORV while the pressurizer fills. At about 1185 s liquid flow through the PORV begins and the flow continues at a nearly constant rate until the start of HPI. The PORV mass flow is shown in Fig. 1.c. Because HPI flow is delayed for 1200 s after PORV actuation and there is no other primary coolant makeup, primary-system liquid levels begin to decline. The reactor-vessel collapsed liquid level is shown in Fig. 1.j. Measured hot-leg and cold-leg collapsed liquid levels are shown in Figs. 1.k and 1.l, respectively. Voiding occurs in the hot legs first and is followed by several U-bend spillover events. The interactions between the hot-leg liquid levels and the Loop-A1 cold-leg and downcomer mass flows are shown in Fig. 1.g and 1.f, respectively. The Loop-A1 cold-leg mass flow stagnates following the hot-leg liquid-level spillover event that occurs beginning at approximately 1475 s. There is a subsequent short-lived hot-leg spillover event at 1870 s (Fig. 1.k) that briefly re-establishes flow in the Loop-A1 cold leg as shown in Fig. 1.g. Steam generation decreases markedly once voiding and flow interruptions begin in the hot leg at about 1000 s, as shown in Fig. 1.e. Steam is still being generated in the Loop-A SG at approximately 1600 s when the SG is isolated and filled with nitrogen.

Phase 3 of the transient covers the period between HPI initiation and about 4650 s, the end of the posttest assessment calculation. HPI was activated at 2142 s in the test. There were several direct consequences of the HPI activation. First, the primary-system pressure, which had slowly oscillated while generally trending upward during Phase 2, began to slowly decrease as shown in Fig. 1.a. Second, the PORV flow rate abruptly decreased as shown in Fig. 1.c, indicating that two-phase flow was established through the PORV. The pressurizer liquid levels provided in Fig. 1.b show that a small vapor space is established at the top of the pressurizer. First the reactor vessel and then the cold legs begin to refill, as shown in Figs. 1.j and 1.l, respectively. Finally, an intraloop cold-leg circulation began at about 2770 s as shown in Fig. 1.g.

MIST 330302 displayed many phenomena of interest. These included an SG-secondary boiloff, slow primary-system pressurization at constant primary-system inventory, single- and two-phase fluid flows through the PORV, hot-leg spillover events, cold-leg and downcomer flow interruptions and the flow recovery, the effects of late HPI injection into a voided primary system, and primary-system refill.

III. TRAC MODEL OF MIST FACILITY

The TRAC-PF1/MOD1 input model of the MIST facility is constructed entirely of one-dimensional components. The model consists of 77 components that have been subdivided into 276 fluid cells. A detailed description of the input model is provided in Appendix A. Archival information related to the input model used in the calculation of MIST 330302 is found in Appendix B. Model development was based on information found in Refs. 5 and 6.

IV. CODE DESCRIPTION

The calculations reported herein were performed with TRAC-PF1/MOD1, version 14.3, with a MIST-specific update (see Appendix B). The TRAC-PF1/MOD1 code (Ref. 1) was developed at Los Alamos National Laboratory to provide best-estimate predictions of postulated accidents in light-water reactors. The code features a two-phase, two-fluid nonequilibrium hydrodynamics model with a noncondensable gas field; flow-regime-dependent constitutive equation treatment; either one- or three-dimensional treatment of the reactor vessel; complete control-systems modeling capability; a turbine component model; and a generalized steam-generator component model.

Code modifications were necessary for this application. We made changes in the TRAC-PF1/MOD1 code to improve the calculation of falling-film heat transfer on the secondary side of the SG tubes when the AFW is active. A code update was prepared and used for all steady-state and transient calculations. The falling-film heat transfer from the AFW was calculated in the updated code version by redistributing the liquid in the single-channel secondary to the heat slabs connected to the three-tube primary channel (see Appendix A for a description of the SG model). In addition to the liquid redistribution, a multiplier was applied to the Chen correlation heat-transfer coefficient for the wetted-channel heat slabs. These code changes resulted in a more accurate calculation of the heat-transfer distribution and the thermal-center elevation in the SGs; a result confirmed by an improved calculation of the steady-state natural-circulation flow rate. We note that the code update produced (see Appendix B) is specific to the MIST facility and not for general application.

Archival information about the TRAC-PF1/MOD1 version used for this study is presented in Appendix B. A draft document describing the TRAC-PF1/MOD1, version 14.3 models and correlations has been prepared.[7] In addition, a TRAC-PF1/MOD1 user's manual[8] is available.

V. CODE PERFORMANCE

There are several measures of code performance that are of interest to the user of a particular code. These measures are used to assign value to the code-calculated result. As used here, value is a combination of the quality of the technical result produced and the cost required to produce that result. First, the user is interested in the degree to which the code predicts phenomena occurring in nature (test facility or full-size plant). In this report, we have attempted to characterize the degree to which the TRAC-calculated results agree with the test results. To better communicate this information, we use the standard set of code assessment

descriptor definitions found in Appendix C. The defined assessment descriptors are "excellent," "reasonable," "minimal," and "insufficient" agreement. The reader's understanding of the analyst's assessment judgments will be enhanced if the definitions in Appendix C are reviewed before proceeding further.

Second, the user is interested in performance parameters or run statistics that provide an indication of how much it cost to produce the result. Several parameters are generally used to convey this information. These include the central processing unit (CPU) time versus real time, the number of calculation steps required versus real time, the time-step size versus real time, and a single-value "grind" parameter indicative of the entire calculation. Identification of the machine used to perform the calculation is also required. For the calculation of MIST 330302, a Cray-1S computer was used. The reader is referred to Appendix D for information about the performance parameters specific to the calculation of MIST 330302.

Third, the user is interested in any performance failures encountered during the calculation. No such failures occurred during the calculation of MIST 330302.

VI. COMPARISON OF TEST AND CALCULATED RESULTS

In this section we present and compare the TRAC-PF1/MOD1 calculated results with the measured and observed results for MIST 330302. We have attempted to develop an understanding of both the test and calculated results and will discuss these. The assessment descriptors appearing in Appendix C are used to characterize the degree of agreement between measured and calculated results.

A. Steady-State

The TRAC-calculated steady-state conditions are presented in Table II and compared to key measured steady-state parameters. We conclude that the calculated steady-state parameters are in reasonable agreement with the measured values. As previously discussed, definitions for code assessment descriptors such as "reasonable agreement" are found in Appendix C. The calculated steady state provides the initial conditions for the transient calculation. Our posttest assessment studies conducted to date for the MIST facility have shown accurate calculation of MIST transient performance requires that the calculated steady state be in reasonable to excellent agreement with the test data. Similar sensitivities to small differences in the facility "initial conditions and boundary system controls" have been observed and reported.[9]

B. Transient

We have chosen to describe and discuss the measured and calculated transient results in two ways. We first provide an overview discussion describing the code–experiment comparisons. This discussion will focus on the major phenomena occurring in the test, both measured and calculated. This discussion (1) identifies major phases that occurred during the test, (2) provides an overview of measured and calculated phenomena occurring in the test, and (3) identifies major areas of agreement and disagreement between the measured and calculated results. We next provide a detailed discussion of the transient results, with a more extensive examination of the calculated phenomena that diverge from those observed and measured in the test. Additional studies needed to clarify the reasons for the divergence are identified and the results of these studies summarized. Detailed discussions of the additional studies are presented in Sec. VI.C.

1. Code-Experiment Comparison Overview. Feed-and-bleed transient 330302 was initiated at time zero from the steady state reported in Table II by terminating all AFW to both SG secondaries. An overview of the resultant test and calculated transients is shown in Fig. 2.

With the termination of AFW to the SG secondaries, the SG-secondary inventory begins to boil off. However, this process removes only part of the core energy and the primary system begins to heat up and pressurize as shown in Fig. 2.a. In the test the primary pressurizes to the PORV set point of 16.41 MPa (2350 psia) at 942 s. The same primary-system pressurization and heatup phenomena are calculated, but the pressurization is more rapid than measured and the PORV set point is reached at 730 s. We believe that this discrepancy is related to our modeling of the pressurizer and surge line, specifically to the initial fluid temperature distributions in the surge line and pressurizer and the pressurizer noding. During this period the pressurizer liquid level is increasing as a result of primary-system swelling as shown in Fig. 2.b. The calculated rate of steam generation in the SG secondary during the boiloff is greater than measured as shown in Fig. 2.e. Thus, TRAC seems to predict excessive heat transfer to the SG secondary during the SG-boiloff period. Primary-system mass flows are provided for the RVVVs, Loop-A1 cold leg, and downcomer in Figs. 2.f through 2.h. The early RVVV flow is underpredicted. The predicted loop and downcomer flows display the same trends as seen in the test but the magnitude of flow swings is underpredicted. As previously noted, the period from test initiation to PORV actuation is designated as Phase 1, SG dryout, and will be discussed in greater detail in subsequent sections.

Phase 2 of the transient covers the period between PORV actuation and HPI initiation 1200 s later. This period is a time of primary-system inventory depletion and covers the time between 942 and 2142 s in the test. The corresponding calculated times are 730 and 1930 s. Boiling begins in the hottest regions of the primary following PORV actuation as shown in Fig. 2.d. Boiling is predicted to occur earlier than measured because the PORV is opened earlier as previously discussed. Immediately following PORV actuation, the pressurizer-filling rate increases in both the calculation and test. Two-phase fluid is released through the PORV while the pressurizer fills and then liquid is released through the PORV. The PORV mass flow is shown in Fig. 2.c. Because HPI flow is delayed for 1200 s after PORV actuation and there is no other primary-coolant makeup, primary-system liquid levels begin to decline. The reactor-vessel collapsed liquid level is shown in Fig. 2.j. The calculated and measured level trends display a similar character but the observed liquid levels were lower. This is a direct result of the underprediction of PORV mass flow during Phase 2 as shown in Fig. 2.c. Calculated and measured hot-leg and cold-leg collapsed liquid levels are shown in Figs. 2.k and 2.j, respectively. In both the calculation and the test, voiding occurs in the hot legs first and is followed by several U-bend spillover events. The effect of the U-bend voiding and spillover events is observed in the Loop-A1 cold-leg and downcomer mass flows (see Figs. 2.g and 2.h). The Loop-A1 cold-leg mass flow stagnates following the hot-leg liquid spillover event that occurs in the test at approximately 1475 s and a similar stagnation is predicted, although it occurs slightly earlier. There is a subsequent short-lived hot-leg spillover event that occurs in the test at 1870 s and re-establishes flow in the Loop-A1 cold leg; this phenomenon was predicted. There is a marked difference between measured and calculated SG performance as shown in Fig. 2.e. Dryout was predicted to occur at about 680 s while the SG was still steaming in the test when it was

isolated at about 1600 s. We have determined that our initial specification of SG-secondary liquid level based on measured liquid levels was low. In addition, we have determined that the predicted primary-to-secondary heat transfer was too high.

Phase 3 of the transient covers the period between HPI initiation and about 4650 s, the end of the posttest assessment calculation. HPI was activated at 2142 s in the test. There were several direct consequences of the HPI activation. First, the primary-system pressure, which had slowly oscillated while generally trending upward during Phase 2, began to slowly decrease in both the test and the prediction as shown in Fig. 1.a. Second, the PORV flow rate abruptly decreased as shown in Fig. 1.c, indicating that two-phase flow was established through the PORV. The pressurizer liquid levels provided in Fig. 1.b show that a small vapor space is established at the top of the pressurizer. First the reactor vessel and then the cold legs begin to refill, as shown in Figs. 1.j and 1.l, respectively. In each case, the major test trends were predicted. Finally, an intraloop cold-leg circulation began at about 2770 s as shown in Fig. 1.g. The predicted start of intraloop circulation was about 1900 s later.

MIST 330302 displayed many phenomena of interest. These included an SG-secondary boiloff, slow primary-system pressurization at constant primary-system inventory, single- and two-phase fluid flows through the PORV, hot-leg spillover events, cold-leg and downcomer flow interruptions and the flow recovery, the effects of late HPI injection into a voided primary system, and primary-system refill. In general, the TRAC-calculated results are in reasonable agreement with the observed phenomena. Thus, TRAC-PF1/MOD1 provides an acceptable prediction of the test. All major trends and phenomena are correctly predicted. Two areas of concern observable in Fig. 1 were identified. First, the calculated PORV flow rate is less than measured. Because the MIST system behaviors are very sensitive to primary-system inventory, a more accurate prediction of the PORV flow rate is desirable. Second, TRAC predicts the too-rapid transfer of heat from the primary to the SG secondaries during Phase 1, SG dryout. This resulted in the too-rapid pressurization of the primary to the PORV setpoint.

2. Detailed Discussion of Transient Results. In this section, the test and calculated nominal or base-case results are examined and discussed in detail. Where calculated phenomena diverge from the measured phenomena, the postulated reasons are identified. Additional studies conducted to clarify the reasons for the divergence are identified and the results of these studies summarized. Detailed descriptions of the additional studies are provided later in Sec. VI.C.

Phase 1—Steam Generator Dryout. The period from test initiation to PORV actuation has been designated as Phase 1; during the test this phase covered the period between 0 and 942 s. This phase began at test initiation with a total cessation of AFW to both SG secondaries.

The indicated core power was maintained at the steady-state value of 128.3 kW (note that a portion of this power is dissipated in the rod stubs that project below the vessel and the estimated delivered core power is 126.7 kW, the value used in the TRAC input). A portion of the provided core power is rejected to the SG secondaries and causes evaporation of the SG secondary liquid inventory. A small fraction of the total core power is transferred to the atmosphere from vessel flanges, supports and RVVVs; hot-leg viewports, gamma densitometer, and supports; SG supports; cold-leg reactor-coolant pumps, cooled thermocouple, and gamma densitometer. These heat losses are simulated in the TRAC input model. The remainder of the core energy is deposited in the primary coolant and heats the primary coolant and structures in contact with the primary coolant. Because the primary is liquid-full with the exception

of the steam space in the pressurizer, the primary-system liquid inventory expands and the primary-system pressure increases.

The measured primary-system pressurization during Phase 1 is shown in Fig. 3. The pressurization begins immediately after AFW termination and continues until the PORV opening pressure of 16.2 MPa (2350 psia) is reached at 942 s. The swelling of the primary system during the Phase 1 heatup is shown by the pressurizer liquid level as seen in Fig. 4. The calculated primary-system pressure also begins to increase immediately after AFW termination. However, the rate of pressure increase is more rapid than measured; the calculated primary-system pressure reaches the PORV opening pressure of 16.2 MPa (2350 psia) at 730 s.

We have identified potential causes of this problem and analyzed them; we discuss them here in the order they were identified and examined. First, the total core power input to the TRAC model could be in error. The measured indicated core power and input indicated core power are shown in Fig. 5. The core power remains constant in both the test and the calculation until PORV opening when the power follows a programmed decay heat curve. The reason for the differences between the measured indicated and the provided input core powers has been previously explained. After 1500 s, the core power used in the calculation is slightly high. This is caused by an error in the TRAC code that results in an incorrect shifting of the core power curve; this error has been identified and a code error correction prepared. For the period before 1500 s, the input core power correctly matches the measured value. Thus, we do not believe that an error in the core power is the source of the too-rapid primary-system pressurization during Phase 1. The second possible cause identified is the failure of one or more primary-system guard-heater zones. If such failures occurred, they would result in uncompensated heat losses. We have found no indication of such failures through inspection of the guard-heater power data. The third possible cause identified is that the primary-system metal mass is underspecified. However, we have performed hand calculations that show the increase in metal-mass energy storage required to account for the excess primary-system heatup is not physically realistic. The fourth possible cause identified is that too little energy is rejected from the primary to the secondary through the SGs. Figures 6 and 7 display the measured and calculated SG-secondary steam flows in loops A and B, respectively. An inspection of these figures appears to show that too much energy is calculated to be transferred from the primary to secondary as measured by steam production. This conclusion is most easily verified by comparing the integrated measured and calculated SG-secondary steam flows in loops A and B and shown in Figs. 8 and 9, respectively. These figures clearly show that the calculated steam production, and hence energy transfer from the primary to secondary, exceeds the measured values. At 500 s, the Loop-A and Loop-B steam productions are 27 and 16 percent high, respectively. A fifth possible cause identified was an error in the TRAC thermodynamic and transport fluid properties. For example, we examined the possibility that the energy required to either heat water (primary side) or evaporate water (secondary side) could be low. However, the TRAC quality assurance effort has recently verified that the property routines in TRAC are reasonably accurate (Ref. 7, Appendix A, Sec. III).

The sixth and last possible cause identified focused on the modeling of the hot-leg surge line and pressurizer, particularly focusing on the initial conditions and the pressurizer noding. The locations of MIST pressurizer instrumentation are shown in Fig. 10 (Ref. 10, Fig. 2.2). The surge-line fluid temperature is measured at two locations. Temperature measurement

PZTC01 is taken in the surge line near the hot leg. Temperature measurement PZTC02 is taken in the horizontal section of the surge line. These two surge-line temperatures as well as the calculated values are shown in Fig. 11. The fluid temperatures measured near the hot leg and in the horizontal section were about 582 K and 519 K, respectively. For the input model, we assumed that the surge line was completely filled with liquid at about 520 K at transient initiation. A comparison of the measured and calculated temperatures in the horizontal surge-line section indicates that the fluid moving past thermocouple PZTC02 from the direction of the hot leg as the primary inventory swells was slightly warmer than input. We believe that the slight difference between the actual fluid state (inferred) and the input fluid state is not significant.

We have found what we believe to be a significant difference between the actual fluid state and that input at the bottom of the pressurizer at transient initiation. Figure 12 shows the measured fluid temperature at the 5.8 m (19.01 ft) level in the pressurizer; the identification for the temperature measurement is PZTC03 (see Fig. 11). As the primary-system liquid begins to heat up and swell, liquid at the bottom of the pressurizer begins to move upward in the pressurizer past the thermocouple. As seen in Fig. 13, the liquid moving past the thermocouple is cool; a minimum fluid temperature of 571.5 K (569.3°F) was measured at about 160 s. By referring to Fig. 4, we see that the pressurizer liquid level had increased only 0.4 m (1.31 ft). Since the bottom of the pressurizer is at 5.47 m (17.95 ft), it is clear that this cold fluid was in the pressurizer at test initiation, *i.e.*, 5.8 m−0.4 m = 5.4 m, which is just slightly lower than the bottom of the pressurizer. This volume of cold liquid was not present in the input model, which was assumed to contain saturated liquid at 597 K (615.2°F). We believe that the liquid in the pressurizer was stratified. The pressurizer guard heaters fulfilled their design function of creating a near-adiabatic condition for the pressurizer. With minimal heat losses through the surface, there was no recirculation of liquid in the heater zones to the lower reaches of the pressurizer while the liquid from the bottom of the pressurizer heaters to the liquid interface just above the top of the pressurizer heaters was heated. The thermal stratification of the pressurizer fluid can be observed in Fig. 13 which shows the measured temperatures across a vertical thermocouple rake between the levels of 6.46–6.56 m (21.19–21.52 ft, thermocouple identification PZTC04-8). The passage of the cool liquid from the bottom of the pressurizer and the surge line can be easily observed. When we embarked upon the posttest analysis effort at Los Alamos, we decided that we could not plot every measured variable. Figures 11 and 13 were included in our standard plot package; Fig. 12 was not. Lacking the fluid temperature information provided in Fig. 12, and using only digital steady-state measurements which showed the pressurizer liquid to be saturated, we incorrectly specified the pressurizer fluid temperature distribution. We believe the colder liquid present at the bottom of the pressurizer played a significant role in slowing the rate of primary-system pressurization during the test.

In addition to the specified pressurizer fluid-temperature distribution, pressurizer noding may also play a significant role. In Fig. 12 we observe that the measured and calculated timing and rate of temperature decrease near the bottom of the pressurizer are the same. However, the passage of the cooler liquid at higher elevations occurs much earlier than measured, as shown in Fig. 13. The current pressurizer model contains four levels. Figure 12 displays the fluid temperature for the lowest level while Fig. 13 displays the fluid temperature for the next

highest level. It appears that finer noding is required to capture the delay because the cold-liquid stratification is effectively lost with the current noding. At the present time, it is not clear to us whether this noding effect is significant. A noding study would be required to quantify this effect.

The modeling of the thermal-hydraulic and heat-transfer processes in the MIST once-through SGs (OTSGs) is a challenging task. We have found that using one-dimensional components to model these processes is problematic. For the steady-state operation of the SGs with the high AFW injection in use, we have identified code modifications that produce the correct result; these modifications, however, are more in the nature of "fitting" modifications than physically based. Our efforts to produce an acceptable steady-state SG heat-transfer model are documented in Ref. 11. The resultant update to TRAC-PF1/MOD1 is provided in Appendix B.

We have also encountered difficulties in modeling the transient behavior of the MIST OTSGs during Test 330302. We consider the SG secondary transient in Phase 1 to be divided into two subphases dominated by different thermal-hydraulic phenomena. The first subphase begins with termination of AFW injection at test initiation and covers the transition to heat transfer by pooling boiling only. During the first subphase, the thermal center of the SG moves from a position high in the steam generator (AFW-injection dominated) to one that is low in the SG (pool boiling only) as residual AFW-supplied liquid drains downward to the pool at the bottom of the SG secondary. The secondary-side steam flow during this period is under predicted by TRAC as shown in Figs. 6–9, although the impact of this under prediction on key transient phenomena is thought to be small. This subphase covers the period between 0 and about 90 s. During the second subphase, secondary-side heat transfer is to a pool of decreasing height as liquid is evaporated. This subphase ends when either the SG secondary is isolated and heat transfer is terminated (at 1680 s in the test, Ref. 2) or the SG secondary boils dry (at about 680 s in calculation). During the second subphase from 90 to 680 s, TRAC overpredicted the rate of secondary steam flow as shown in Figs. 8 and 9. Additional detailed studies were conducted to identify the cause of the excess heat transfer. We found that increased secondary-side noding increased the time to SG-secondary dryout. Thus, there is a degree of noding sensitivity. We also reviewed the primary-side SG heat-transfer processes and determined that the potential for overpredicting the heat transfer exists. Thus, a combination of several factors appears to result in the TRAC-predicted excess generation of steam during subphase 2. The additional studies we conducted will be reviewed in more detail in Sec. VI.C. The estimated time of SG dryout and subsequent PORV opening is potentially an important parameter for a feed-and-bleed transient because in some plant types the operators must take early action if they are to utilize a feed-and-bleed procedure.[12,13]

Although our studies reported thus far have focused on possible input model sensitivities and TRAC deficiencies, an important area of inquiry is an assessment of our knowledge of the facility and its operation, including instrumentation and data. As seen in Figs. 6 and 7, secondary-side steam flow continued to be measured long after the predicted dryout of the SG secondaries. Further, it is demonstrable that liquid still remained in the SG secondaries at the time the they were isolated (1680 s), although the rate of SG had decreased prior to that time. The integral SG-secondary steam flows shown in Figs. 8 and 9 further substantiate this conclusion. These liquid levels appear to understate the actual total liquid inventory of the SG

secondaries by about 30%. One consequence of the lower input SG-secondary liquid levels is that the calculated SG-secondary thermal center during subphase 2 is lower than measured. A more detailed discussion of this problem is provided in Sec. VI.C.1.

We now turn to a comparison of the measured and predicted primary-flow rates. The downcomer mass flow is provided in Fig. 14. Subphase 1 is characterized by a rapid decrease in mass flow as the thermal center of the SG secondaries migrates from a high level associated with AFW injection to a lower level associated with pool boiling. At the end of subphase 1, the mass flow has overshot the natural-circulation flow that can be maintained given the thermal center in the SG-secondary pool; the measured mass flow recovers as subphase 2 begins. The TRAC-calculated overshoot during subphase 1 is not as great as predicted. More importantly, however, the mass flow does not recover to as high a value as measured as subphase 2 begins. We believe that this is a direct consequence of the input SG-secondary liquid levels which are about 30% lower than in the test as inferred from measurements other than the SG-secondary liquid level and discussed above. The mass flows in cold-legs A1, A2, B1, and B2 are presented in Figs. 15–18, respectively. These flows summed together are equal to the downcomer flow when the RVVVs are closed and so will not be discussed further. The RVVV flow is presented in Fig. 19.

For completeness, a set of primary-system fluid-temperature comparisons are presented. The core inlet and exit fluid temperatures are provided in Figs. 20 and 21, respectively. The measured and calculated inlet values are in reasonable agreement during Phase 1. The calculated core outlet fluid temperature closely tracks the measured value until about 190 s, after which the calculated temperature is higher. This is caused by the lower core mass flow as inferred from the downcomer mass flow shown in Fig. 14. Upper-plenum fluid temperatures are compared in Fig. 22. The Loop-A and Loop-B SG inlet and outlet plenum fluid temperatures are provided in Figs. 23 and 24, respectively. The Phase-1 trends closely track those of the core inlet and outlet. The Loop-A1, Loop-A2, Loop-B1, and Loop-B2 pump-suction fluid temperatures are provided in Figs. 25–28, respectively.

Overall, we conclude that the calculated results are in reasonable agreement with the test data during Phase 1.

Phase 2—Primary System Inventory Depletion. This phase covers the period between PORV actuation and HPI initiation 1200 s later. This period is a time of primary-system inventory depletion and covers the time between 942 and 2142 s in the test; the corresponding calculated times are 730 and 1930 s. During the test, there was little heat rejection to the SG secondaries between 942 and 1680 s when the SG secondaries were isolated. The small steam flows and the SG-secondary isolation are shown by the secondary steam flows presented in Figs. 6 and 7. There was no calculated heat rejection to the SG secondaries during Phase 2 because the SG secondaries dried out during Phase 1. The discussion provided in Phase 1 identified two reasons that the SG secondary dryout was predicted to occur early; these are further discussed in Sec. VI.C.

The hydraulic phenomena occurring during Phase 2 are closely related to the "bleed" or flow through the PORV and the "feed" or HPI. Comparisons of measured and calculated PORV and HPI mass flows are provided in Fig. 29. The major trends and magnitudes are similar during Phase 2. There are, however, several differences to be noted. First, flow through the PORV is predicted to occur at 730 s after the primary pressure increases to the PORV set

point, about 210 s earlier than measured. This may be related to the initial liquid temperature distribution in the surge line and PORV and the PORV noding as described in the discussion of Phase 1. Additional calculations are required to confirm and quantify the importance of these factors.

Second, the calculated transition from two-phase fluid to single-phase liquid flow through the PORV seems to occur over a longer period than measured. This conclusion is an inference arising from comparing the increases in PORV mass flows during the period immediately following PORV actuation while two-phase fluid is passing through the PORV. The calculated vapor fraction upstream of the PORV is shown in Fig. 30 and the time at which two-phase flow through the PORV terminates is provided by annotation on Fig. 29. It appears that for void fractions between 0.8 and 0.0, the predicted mass flow through the PORV is less than measured. This difference may be either noding sensitive (no noding study was done) or may be related to the critical-flow model in TRAC.

Third, the magnitude of the calculated PORV single-phase liquid flow through the PORV peaks at a smaller value than measured. In addition, the measured mass flow is essentially steady, while the calculated mass flow oscillates. The integrated PORV mass flow is provided in Fig. 31. During the period of single-phase liquid flow through the PORV, the slope of the calculated integrated mass flow is less than measured. Accounting for the time shift caused by the earlier calculated PORV actuation, more mass passes through the PORV in Phase 2 during the test. This effect is also seen in the comparison of primary-system water mass as shown in Fig. 32. Again, accounting for the time shift associated with PORV actuation, more mass is calculated to remain in the primary than measured in the test. For completeness, we note that a critical-flow multiplier of 1.0 was used for the calculation of Test 330201.

The calculated oscillations in PORV mass flow show a sensitivity of the TRAC critical-flow model to liquid subcooling not evident in the data. For example, the measured and calculated primary-system pressures are presented in Fig. 3. Following PORV actuation, pressure oscillations are seen in both the test and calculated results. The calculated liquid subcooling upstream of the PORV is shown in Fig. 33 and there is a one-to-one correspondence between the the subcooling peaks and the pressure peaks in Fig. 3. There is also a one-to-one correspondence between the subcooling peaks and the PORV mass flow peaks during liquid flow. The predicted PORV flow is at a maximum when the subcooling is at a maximum. This result suggests that the formulation of the TRAC critical-flow model during periods of subcooled liquid flow should be reviewed. We do note, however, the importance of correctly specifying the initial liquid temperature distribution in the surge line and pressurizer. For example, if these initial temperatures had been correctly specified, the subcooling at the PORV inlet would have been greater. Given that the TRAC critical-flow model is sensitive to liquid subcooling, we anticipate a greater PORV mass flow would have been calculated.

Liquid levels throughout the primary system are shown in Figs. 34–42. The reactor-vessel and downcomer collapsed liquid levels are shown in Figs. 34 and 35. The major measured and calculated trends throughout the transient are similar. Immediately after opening the PORV, the reactor-vessel collapsed liquid levels begin to decrease. The liquid-level decline pauses at the level of the RVVVs and then continues. The measured liquid level then resumes its sharp rate of decline until the level of the hot-leg nozzles is approached. The decline of the liquid level again pauses and then starts sharply downward and continues to a liquid-level minimum

of about 5 m (16.4 ft). Although the same trends are calculated, there are differences after the level of the RVVVs is passed. The calculated level decrease pauses before the level of the hot-leg nozzles is reached. This is caused by the backward drainage of liquid from the hot-leg into the upper plenum. Evidently, the predicted backward drainage is greater than in the test. Figure 36 shows the measured and calculated hot-leg collapsed liquid levels. During the period in which the calculated reactor-vessel liquid level pauses (1235–1580 s), the liquid level in the hot legs is falling below the calculated liquid level, reaching a maximum difference of about 1 m (3.3 ft) at 1500 s. One possible cause for this may be that the TRAC-calculated horizontal interfacial shear is too low for this case. At 1800 s, the reactor-vessel, downcomer, and hot-leg liquid levels reach a local minimum. The primary-side SG collapsed liquid levels (Figs. 37 and 38) and cold-leg collapsed liquid levels (Figs. 39–42) are also at a local minimum at this time. These all appear to be related to the underprediction of PORV mass flow when passing single-phase liquid. All the major liquid-level trends throughout the primary system were calculated by TRAC. We note, for example, that several hot-leg spillover events were seen shortly after PORV actuation in the test and these were also calculated by TRAC although with a time shift caused by the earlier PORV actuation. The effect of these spillover events can be clearly seen in the comparison of measured and calculated downcomer mass flow rates as shown in Fig. 14.

Overall, we conclude that the calculated results during Phase 2 are in reasonable agreement with the test data.

Phase 3—Primary-System Refill Following HPI Initiation. This phase covers the period between HPI initiation and about 4650 s, the end of the calculated transient. HPI was activated at 2142 s in the test and at 1930 s in the calculation. The measured and calculated HPI flows are shown in Fig. 29. HPI flow in both the test and the calculation (via the input model) is a function of the primary-system pressure. The calculated HPI flow is about 10% low because the calculated primary-system pressure is always high, as shown in Fig. 3.

As part of our examination of the primary-system pressure comparison for Phase 3, we first consider the pressure difference at the beginning of Phase 3 and then the trends during Phase 3. During Phase 2, less mass flow is calculated through the PORV than measured. Thus, TRAC predicted less mass (and energy) to leave the primary system through the PORV during Phase 2. This accounted, in part, for the higher predicted primary pressure during Phase 2. In addition, the SGs were active during the test for a part of Phase 2 while the calculation predicted the SGs boiled dry during Phase 1. Thus, there was some primary-to-secondary energy rejection in the test whereas none occurred in the calculation. This accounted for the remainder of the higher predicted primary pressure during Phase 2. Improved input of the surge line and pressurizer initial (steady state) liquid temperature distribution, and possibly finer pressurizer noding, may result in an improved primary-system pressure prediction. A more correct specification of the SG-secondary initial liquid level may also result in some improvement in the pressure prediction.

Again referring to Fig. 3, we note that both the calculated and measured primary pressures begin to decrease shortly after HPI initiation. The initial depressurization rate in the test is greater than calculated. This may be due, in part, to the greater cold-leg condensation potential in the test. By referring to Figs. 39–42, we see that there is greater cold-leg pump-suction voiding in the test than calculated. The depth of the measured pump-suction liquid-level

depression would seem to indicate some voiding in the cold legs near the HPI injection port. In contrast, the smaller voiding calculated by TRAC may be insufficient to produce significant voiding in the cold leg at the HPI injection sites.

Shortly before 3500 s, the calculated rate of primary-system pressure decrease increases. This is caused by subcooled HPI liquid flowing into the Loop B1 and B2 pump suction (Figs. 27 and 28). The measured Loop-B1 and -B2 fluid temperatures show the same decline but about 650 s earlier at 2700 s. In addition, the decrease is at a slower rate. We believe that the calculated temperature trace would compare to the measured more closely if finer cold-leg noding were used. However, we believe that the TRAC-calculated result is sufficiently good and that the computational penalty would be too large. Therefore, we do not recommend a noding change. The same trends are predicted in the Loop-A1 and -A2 pump suctions as shown in Figs. 25 and 26. The calculated delivery of subcooled HPI to the pump suction in Loop A is delayed even more relative to the calculation; the delay is about 1400 s. Given the differences in cold-leg voiding at HPI initiation, it is difficult to draw any conclusions about the TRAC condensation model.

Shortly after HPI initiation, the PORV mass flow decreased sharply (Fig. 29). The decline was related to the primary-system pressure decrease and contraction of the primary-system steam volume by condensation. The fluid upstream of the PORV changed from single-phase liquid to two-phase fluid as shown in Fig. 30. The measured PORV flow in Fig. 29 is oscillatory but oscillations are not predicted by TRAC. However, the two-phase flow predicted by TRAC during Phase 3 appears to be in reasonable agreement with the measured flow, although differences in the slope indicate the TRAC-calculated mass flow was, on average, slightly less. The reactor-vessel and downcomer refilling process begins with HPI initiation as shown in Figs. 34 and 35. However, the hot legs continue to decrease past the time of HPI initiation as shown in Fig. 36. Refilling of cold-leg pump-suction risers begins immediately in the calculation as shown in Figs. 39–42 because little voiding was predicted to exist at HPI initiation. In contrast, the refilling of the cold-leg pump-suction risers was delayed because of the greater cold-leg voiding occurring in the test.

Finally, we review the primary-system mass flows during Phase 3. The downcomer mass flow is presented in Fig. 14. We can consider this as an overall mass flow consisting of the four cold-leg loop flows and the RVVV flow. The calculated mass flow is slightly high between 2000 and 3000 s, but agrees closely with the data thereafter. During the period 2000–2500 s, the measured cold-leg A1 and A2 loop flows are stagnant. Beginning at about 2600 s, the loop flows restart with an intraloop natural circulation. Loop A1 flows in a direction reverse to normal flow and Loop A2 flows in the normal flow direction. TRAC predicts the same flow startup and direction to occur but near the end of the calculated transient at about 4550 s. During the period 2000–2700 s, the measured cold-leg B1 and B2 loop flows are stagnant. Beginning at about 2700 s, the loops flows restart with an intra-loop natural circulation. Loop B1 flows in a direction reverse to normal flow and Loop B2 flows in the normal flow direction. TRAC predicts intraloop natural circulation to begin at about 3600 s. However, the flow directions are opposite to those measured in the test. We acknowledge the differences in loop flow but believe that the MIST facility is sufficiently sensitive to variations in initial and boundary conditions such that improved calculations may not be possible. We note the loop-to-loop differences do

not appear to be significant and that the integrated conditions, *e.g.*, the downcomer flow, are found to be in reasonable agreement with the data.

Overall, we believe that the calculated results for Phase 3 are in reasonable agreement with the test data.

C. Additional Studies

During the course of our analysis of MIST 330302, we either identified or performed additional studies with the objective of resolving issues and answering questions. We have collected and grouped the resultant information in three categories. The first category provides information developed regarding our understanding of facility configuration and operation. Ideally, the analyst would have a perfect knowledge of facility configuration and operation. However, it has been our experience that problems often occur in this area for tests performed in integral systems. We document our efforts for MIST 330302 in the hope that this information will assist other analysts of MIST tests and other TRAC users. The second category provides information developed regarding the adequacy of the TRAC input model of the MIST facility. We believe that the results of our studies in this area will assist other TRAC users. The third category provides information regarding the adequacy of the closure models and correlations in the TRAC code. We hope that this information will assist those involved in the development and improvement of TRAC.

1. Studies Related to Knowledge of the Facility. During the process of reviewing the calculated results from the nominal or base-case calculation of MIST 330302, several deficiencies in our knowledge of the facility operation were identified. These deficiencies were reflected in the values entered into the TRAC model of the MIST facility for Test 330302.

The first deficiency relates to the initial or steady-state liquid-temperature distribution in the surge line and pressurizer. After a thorough examination of the available test results for the pressurizer, we have concluded that a stagnant layer of cold liquid was formed in the lower portion of the pressurizer below the elevation of the lowest pressurizer heater. As shown in Fig. 12, thermocouple PZTC03 at the 5.8 m (19.01 ft) level, shows a minimum temperature of 571.5 K (569°F). Pressurizer and surge-line instrumentation locations are shown in Fig. 10. Thermocouple PZTC03 is measuring the temperature of liquid moving upward into the pressurizer from below during the swelling of the primary-system inventory caused by primary-system heatup during Phase 1 of the transient. The initial or steady-state temperature of all water in the pressurizer selected for input in the TRAC model was about 598 K (617°F), the saturation temperature at the pressurizer steady-state pressure. Clearly, a nonuniform initial liquid temperature distribution should be input for the pressurizer. We now infer that the appropriate distribution would be for the temperature of the liquid between the bottom of the pressurizer and the elevation of the lowest pressurizer heater to be specified as about 570 K (567°F). Note that the actual temperature is unknown. Lacking better information, we believe that the temperature of the liquid in the surge line between thermocouple PZTC02 and the bottom of the pressurizer should be input at the steady-state value measured by PZTC02 or 519 K (475°F) as shown in Fig. 11. We believe that correction of this input deficiency will reduce the Phase 1 overprediction of primary-system pressure shown in Fig. 3.

We wish to provide a brief description of the procedures leading to this input discrepancy. The MIST facility is highly instrumented; it tracks about 1200 measured variables per test. Because of the volume of data, Los Alamos has prepared a digital listing of the initial or

steady-state values for each measurement. We review this list and use the steady-state data in preparing our input. We have also selected a standard set of variables for comparison of measured and calculated results but we usually do not produce these plots until calculated results are also available. For Test 330302, all thermocouples in the pressurizer (PZTC03 and the thermocouple rake PZTC04-8) showed saturation temperatures of 598 K (617°F). There is no thermocouple reading below the pressurizer heaters and so we did not detect the cold liquid pool existing there. In addition, the surge-line thermocouples did not indicate the presence of the pool; in fact, the surge-line temperatures are warmer than those found to exist at the bottom of the pressurizer. Finally, we neither anticipated nor identified the presence of the cold liquid pool at the bottom of the pressurizer. This was due, in part, to this being the first MIST posttest analysis for a transient other than a small-break loss-of-coolant accident (SBLOCA). We conclude from this experience that availability of a complete set of data plots at the time the input model is prepared would be useful.

The second deficiency relates to the specified initial or steady-state values of the SG-secondary liquid levels. The measured and calculated intact- and broken-loop SG-secondary liquid levels are presented in Figs. 37 and 38. At transient initiation, the measured and calculated values are in close agreement. They should agree closely because we used the steady-state values for instrumentation S1LV20 and S2LV20 to specify the initial SG-secondary liquid levels in the TRAC input model. As seen in Figs. 6 and 7, secondary-side steam flow continued to be measured long after the predicted dryout of the SG secondaries. This result implies that there was more liquid in the SGs during the test than available per the input specification. Further, it is demonstrable that liquid still remained in the SG secondaries at the time that they were isolated (1680 s). The integral SG-secondary steam flows shown in Figs. 8 and 9 further substantiate this conclusion. An addition of SG-secondary mass using data only shows that the integrated Loop-A SG steam flow to SG isolation at 1680 s was 6.7 kg (14.8 lbm, integral of Tag ID SSOR20), the integrated Loop-B SG steam flow was 6.4 kg (14.1 lbm, integral of Tag ID SSOR21), and the total 13.1 kg (28.9 lbm). The initial total SG-secondary mass using levels, Tag ID SLML20, was 18.45 kg (40.6 lbm) and the total SG-secondary mass at SG-secondary isolation was 6.2 kg (13.7 lbm). Taking the sum of the residual SG-secondary mass of 6.2 kg (13.7 lbm) from Tag ID SLML20, the Loop-A integrated steam flow of 6.7 kg (14.8 lbm) and the Loop-B integrated steam flow of 6.4 kg (14.1 lbm), a total SG-secondary mass of 19.3 kg (42.5 lbm) is obtained. This is in reasonable agreement with the measured initial total SG-secondary mass using liquid levels of 18.45 kg (40.6 lbm) from Tag ID SLML20. We again note, however, that we initialized our transient using SG-secondary liquid levels also obtained from test data (Tag IDs S1LV20 and S2LV20 for the SG1 and SG2 secondary-side levels, respectively). These liquid levels appear to understate the actual total liquid inventory of the SG secondaries by about 30%. Finally, we have checked our modeling of the SG secondary to ensure that an accurate representation of volume versus elevation is input. At this time, we conclude that the SG-secondary liquid-level measurements are not consistent with other available test data.

2. Studies Related to the Input Model. During the course of this study we identified two areas of potential noding studies that could be conducted with the objective of quantifying the adequacy of the TRAC input model.

First, we believe that a study of the pressurizer noding should be conducted. Such a study has not been conducted to date. The primary objective of such a study would be to develop noding guidelines for improved modeling of such events in the future. For the present transient, only the timing of events would potentially change; we do not believe the conclusions presented in this report would be altered. For transients in which the pressurizer either fills or empties over a short period, finer noding is probably not warranted. This would seem to include all SBLOCA transients, with the possible exception of very small break sizes. For the slow pressurizer filling that occurred during Phase 1 of the MIST 330302 transient, a more finely noded pressurizer may improve the comparison of measured and calculated results. The current pressurizer model contains four cells of unequal heights. The lowest pressurizer cell height is 0.539 m (1.77 ft) and the next-highest cell height is 1.0 m (3.28 ft). The cell-center elevations of lowest and adjoining cell above are 5.731 m (18.8 ft) and 6.500 m (21.3 ft), respectively. The positions of these cell centers relative to instrumentation can be seen from Fig. 10.

One outcome of the current pressurizer noding can be seen by comparing the calculated liquid temperatures of Fig. 12 (bottom pressurizer cell) and Fig. 13 (next-highest pressurizer cell). During the test, thermal stratification persisted. As seen in Fig. 12, the temperature began to drop immediately after test initiation in both the test and calculation. As previously discussed, the measured temperature decreased further because the correct liquid temperature below the pressurizer heaters was not used in the input model. At the next-higher level, however, the measured and calculated results diverge (Fig. 13). The calculated temperature begins to decrease immediately while the effect of thermal stratification is clearly shown at the thermocouple rake. Within each TRAC cell a mixed mean temperature is calculated for the cell fluid volume. With fluid swelling, some of this cooler liquid is moved into the next higher cell and mixed with the existing liquid there. The direct outcome of this is a too-rapid propagation of the cooler liquid temperature upward. Thus, the calculated liquid temperature in the pressurizer cell immediately above the bottom cell, decreases too early. Without conducting the noding study, it is not possible to determine whether increased noding would contribute to an improved calculation of the primary-system pressure response.

Second, we believed that a study of SG noding should be performed. In fact, such a study has been completed as part of the MIST 330302 posttest analysis effort and the results will now be reported. The noding study was necessitated by the specific test conditions used for MIST 330302. The initial SG secondary liquid levels (as recorded for Tag IDs S1LV20 and S2LV20) were 1.048 m (3.44 ft) and 0.9038 m (2.97 ft) for the Loop-A and Loop-B SG-secondary initial liquid levels, respectively. The majority of the noding studies were conducted with a standalone model of the SG. This was done to speed running time and to permit the isolation of calculated results to the SG only.

The standard MIST SG noding used for SBLOCA calculations has cell heights of 1.5 m (4.92 ft). Thus, with the standard noding, the entire SG-secondary dryout process of Test 330302 was to take place within a single secondary level at the bottom of the SG. An initial calculation was performed with the standard noding. We noted that TRAC required a small time step to handle the boiling processes in the single cell. In addition, dryout was predicted to occur too early. During the initial stages of our calculations and analyses, we thought that the early dryout might be a key contributor to the too-rapid pressurization of the the primary.

The noding study was performed by dividing the bottom SG cell of height 1.5 m (4.92 ft) into first five (0.3 m, 0.984 ft) levels and then ten (0.15 m, 0.492 ft) levels. We found that the calculated time to SG-secondary dryout was noding sensitive when evaluated using the SG standalone model. However, we also determined that when finer noding was used in the full-plant model, the time to PORV actuation was affected only moderately. Thus, we were led to conclude that the prediction of too-rapid primary-system pressurization, was not related in a major way to the prediction of SG secondary dryout. The results of our SG noding studies are presented in Table IV. However, faster computation times were obtained by subdividing the bottom cell into smaller cells and so a SG model with the bottom cell of the standard model further divided into five smaller cells was used for the nominal or base-case calculation.

3. Studies Related to Code Models and Correlations. We have identified several TRAC closure models and correlations that show deficiencies when compared to the test data. First, the subcooling critical flow model seems to show a sensitivity to upstream liquid subcooling not seen in the data. This sensitivity in mass flow through the PORV is shown in Fig. 28. The peaks in mass flow correlate to the peaks in liquid subcooling upstream of the PORV as shown in Fig. 32. The origin of subcooling oscillations are the primary-system pressure oscillations as shown in Fig. 2. However, although the primary-system pressure oscillations exist in both the data and the calculation, flow oscillations in the PORV flow are observed only in the calculation.

We have considered the possibility that the measured PORV mass flow (measurement VVMM01) might be in error. The estimated uncertainty for this measurement is given in Ref. 14 (Fig. 5.34). At a measured mass flow of 0.09 kg/s (713 lbm/h) the stated uncertainty is about 0.00063 kg/s (5 lbm/h) or less than 1 percent. The span for this instrument is listed at 0–0.315 kg/s (0–2500 lbm/h) (Ref. 14, Table 5.8). Given the span of this instrument, it is clear that the flow was not sufficiently large to saturate the flowmeter. In addition, the instrument was rapidly responding to changes in upstream conditions as illustrated by the flow reduction when the fluid conditions upstream of the PORV changed from liquid to two-phase fluid (Fig. 28).

This information suggests several possible deficiencies in the calculation of phenomena related to the calculation of the PORV mass flow rather than deficiencies in the data. The first of these is that the actual subcooling upstream of the PORV in the test may not be as large as calculated. Given that similar pressure oscillations are measured and calculated, this would imply physical processes reducing the local pressure near the PORV in the test that are not captured in the calculation. A second possible deficiency lies in the formulation of the subcooled critical-flow model. We have examined the TRAC-PF1/MOD1 correlations and models document (Ref. 7, Sec. 7.2) as part of our review of the critical-flow model. The model as formulated does show a sensitivity to liquid subcooling, but this sensitivity is believed to reflect real physics. We believe that the MIST data could be used to support a separate study of the TRAC critical-flow model if it were used with a standalone model of the PORV and the pressurizer. A boundary condition could be modeled at the level of the pressurizer thermocouple rake and measured liquid temperature, pressure, and flow provided as functions of time. We recommend that such a study be conducted if further information about the adequacy of the TRAC-PF1/MOD1 critical-flow model is desired.

We have also examined the formulation of the fluid-to-wall heat-transfer model for single-phase liquid in forced and natural-circulation flow. The incentive for doing so was the apparent overprediction of primary-to-secondary heat transfer during the SG-secondary boiloff of Phase 1. As shown in Figs. 7 and 8, the calculated rate of steam generation in both SGs exceeds that measured. There is the possibility, of course, that in an integral calculation the excess steam-generation rate is related to differences in the measured and calculated primary-side flow conditions. To clarify this matter, we again used the SG standalone model. The model was driven with inlet and outlet boundary conditions directly derived from the test measurements. We found that the time to SG-secondary dryout was essentially the same as when using boundary conditions derived from the integral calculation. Thus, we concluded that TRAC predicts excessive primary-to-secondary heat transfer during Phase 1.

We again reviewed the TRAC-PF1/MOD1 models and correlations document (Ref. 7, Sec. 4.2) as part of our review of wall-to-fluid heat transfer. During Phase 1, TRAC appears to identify the SG primary-side wall-to-fluid heat-transfer regime as either forced convection to a single-phase liquid or liquid natural convection. In effect, however, TRAC calculates heat-transfer coefficients for both regimes and selects the maximum heat-transfer coefficient. Thus, when either forced convection to single-phase liquid or liquid natural circulation is possible, laminar and turbulent heat-transfer coefficients are calculated for both forced convection to single-phase liquid and liquid natural circulation, and the maximum value is selected. It is evident that this approach, which was selected to eliminate discontinuities associated with switching between these two regimes, would always maximize the predicted heat transfer. Referring to Figs. 7 and 8, the calculated integrated steam mass flow is high by 27% in the Loop-A SG and by 16% in the Loop-B SG. These figures provide an estimate of the amount by which the average calculated heat-transfer coefficient exceeds the actual value. To examine the impact of reducing the calculated SG primary-side heat-transfer coefficient, we arbitrarily reduced the calculated value by 10% and recalculated the time to SG-secondary dryout using the standalone SG model. The time to dryout increased from 680 s for the nominal standalone calculation (Table IV) to 780 s.

As we were using the comparison of measured and calculated SG-secondary steam mass flow to infer an excessive primary-to-secondary heat transfer, we felt it prudent to examine the possibility that condensation might be occurring at the outer wall of the SG. If this were the case, the TRAC-calculated heat transfer could be correct but the secondary steam flow high because outer wall condensation processes were not modeled. We examined the guard-heater control ΔT's and found that condensation on the walls was unlikely as the guard heaters kept the walls near saturation. We also examined the SG downcomer for the same effect. We found that condensation was possible in the downcomer. However, we estimate that the condensation was only about 1/50th that required to account for the difference between the calculated and measured SG-secondary steam mass flows.

It appears that data exist that could be used to resolve this issue. B&W has conducted loss-of-feedwater (LOFW) tests using the 19-tube laboratory OTSG located at the Alliance Research Center.* This OTSG appears to be one of the MIST SGs. The tests were conducted

* H. R. Carter and D. D. Schleappi, "Nuclear Once-Through Steam Generator (OTSG and IEOTSG) Loss-Of-Feedwater Flow (LOFW) Test," Babcock & Wilcox proprietary data.

with forced, scaled full-power primary-side conditions. The initial SG-secondary liquid levels were high and the SG secondary was allowed to boil off. Secondary-side steam flows were measured throughout each test. Los Alamos believes that the data taken by B&W during this program would be useful for further examining the heat transfer processes in OTSGs during LOFW events. Because the standalone-OTSG TRAC input model already exists, we believe that the assessment process using the B&W data would not be costly. We have requested that B&W examine whether the data can be made available to Los Alamos and the review is currently underway.

VII. LESSONS LEARNED, CONCLUSIONS, AND RECOMMENDATIONS

MIST 330302 displayed many phenomena of interest. These included a SG secondary boiloff, slow primary-system pressurization at constant primary-system inventory, single- and two-phase fluid flows through the PORV, hot-leg spillover events, cold-leg and downcomer flow interruptions and the flow recovery, the effects of late HPI injection into a voided primary system, and primary-system refill. We feel that MIST 330302, feed and bleed with delayed HPI, was an excellent vehicle for assessment of the TRAC-PF1/MOD1 code. Our lessons learned and key conclusions are further subdivided into the areas of (1) adequacy of facility knowledge, (2) adequacy of facility input model, (3) adequacy of code models and correlations, (4) scaling considerations, and (5) regulatory implications.

A. Knowledge of the Facility

We identified two cases in which our knowledge of MIST facility operation was deficient. First, we did not have an adequate understanding of the initial pressurizer liquid-temperature distribution. Sufficient transient data were available for us to infer an improved initial or steady-state temperature distribution. However, our procedures have not generally included the plotting and review of all transient data in advance of a transient calculation. Such a procedure can be followed in the future if the cost and schedule impacts are acceptable. In addition, B&W does not routinely provide a complete set of transient plots to MIST program participants. Finally, test results are reported in group reports such as Ref. 3. These reports covering a group of tests are, of necessity, brief and focus on major phenomena. Detailed reports of test phenomena would be helpful, but, again, there would be cost and schedule impacts associated with providing detailed reporting for each test.

Second, we believe that measurement of SG-secondary liquid level is incorrect for Test 330302. When using the reported liquid levels as initial conditions for the TRAC model, an early dryout of the SG secondary is calculated. This may be partially caused by the prediction of an excessive rate of heat transfer from the primary to the SG secondary. However, a comparison of measured and calculated integrated SG-secondary steam mass flows shows that more steam mass passed into the steam line during the test than was calculated. In addition, the steam generators contained residual liquid at SG-secondary isolation while the calculation predicted early and complete SG-secondary dryout. We recommend that B&W review the apparent inconsistency between test measurements. If one or more of the instruments are in error, we recommend that other tests in which the error could be important be reviewed and corrected and flagged, as necessary.

We believe that our calculation of MIST 330302 should be rerun with an improved pressurizer initial liquid-temperature distribution and with the correct SG-secondary liquid level, once defined by B&W.

B. Input Model

We found the input model, with one exception, to be adequate for feed-and-bleed transients in the MIST facility. For Test 330302, the SG-secondary initial liquid levels were quite low, being 1.048 m (3.44 ft) and 0.9038 m (2.97 ft) for the Loop-A and Loop-B SG-secondary initial liquid levels, respectively. These liquid levels reside within the first level of the standard MIST SG model. We found that TRAC had to use a small time step to deal with this situation. A noding study was conducted and we found that by dividing the bottom cell of 1.5 m (4.92 ft) into five cells of 0.3 m (0.984 ft), the calculation time was improved even though the SG was more finely noded. We also noted that finer noding of the pressurizer may be required for an improved prediction of the primary-system pressurization following transient initiation. No noding study was conducted to investigate this area.

C. Code Models and Correlations

We found two areas of concern regarding TRAC constitutive models and correlations. First, the critical flow model during liquid flow shows a sensitivity to subcooling not observed in the data for Test 330302. However, the observed sensitivity may also be affected by the incorrect specification of the pressurizer liquid temperature distribution since greater subcooling would be expected in that case. Again, a recalculation of this Test 330302 with the correct pressurizer liquid temperature distribution would remove this uncertainty. Second, we found that TRAC has the potential for overpredicting the SG-primary-side heat transfer during natural-circulation flow and this seems to have occurred during the calculation of Phase 1.

D. Scaling Implications

The issue of scaling is one of the most difficult with which to deal. Nevertheless, it is a key issue in providing closure to the US Nuclear Regulatory Commission (NRC) research program in the area of thermal-hydraulics. The objective of this section is to summarize the issues, results, and conclusions related to scaling that may be derived from MIST 330302.

1. Background. A primary objective of the NRC's thermal-hydraulic research program has been to develop the data base for development and validation of thermal-hydraulics systems codes such as TRAC. From the early years of the research program, it has been acknowledged that thermal-hydraulic data from scaled integral facilities would have limited direct applicability for the prediction of phenomena in plants. Therefore, the assumption that the thermal-hydraulics systems codes would correctly scale and provide the bridge between scaled integral facilities and the plant was inherent in both the experimental and code-development programs conducted by the NRC.

In its long-range research plan,[16] the NRC notes "The principal products of thermal-hydraulic research are analytical tools to understand and predict the plant response to disturbances from normal operating conditions. . . . . An integral facility is a scaled representation of a plant with all the major components present to provide information on overall system response and the interactions of different phenomena. In contrast, a separate-effects facility studies a particular component or phenomenon in greater detail. Each experimental facility has its own particular limitations associated with scaling and other design compromises that preclude direct extrapolation of experimental results to the full-scale plant. Rather, the computer code provides the required link."

There appears to be no single accepted technique or rationale for demonstrating the ability of thermal-hydraulic systems codes to scale up from sub-scale tests to full-scale plants. However, there are several candidate techniques and these will be reviewed. It appears that the demonstration of a scale-up capability will combine elements of the techniques described below.

The first scale-up technique is based on assessments using full-scale plant data. The importance of such assessments is that these efforts effectively bypass the scaling question by comparing code-calculated results to data taken during either plant operational testing or plant transients. If the plant transient data base were sufficiently broad and contained good quality data, use of this technique would be sufficient to determine the accuracy of code predictions at full scale. However, there are several limitations associated with this technique. First, the plant operational transients are relatively benign and, therefore, exercise only limited portions of the TRAC-encoded phenomenology (*e.g.*, single-phase flow) for assessment purposes. Second, neither planned nor unplanned plant transients cover a sufficiently broad spectrum of plant transients and their associated phenomena, particularly when plant-specific geometries are considered. Third, although plant transients such as the accident at Three Mile Island and the Ginna SG tube-rupture event do result in a broader class of phenomena for assessment purposes, there are frequently difficulties in defining and interpreting the transient initial and boundary conditions from the plant instrumentation.[13] Nevertheless, valuable assessment information has been obtained using this technique.

The second scale-up technique is based on assessments of either coupled full-scale plant transients and simulations of those transients in scaled facilities or coupled experiments between different scaled facilities. Examples of the former are tests planned in the MIST Phase IV testing program[17,18] using the Rancho Seco and Crystal River transients, respectively. Once counterpart tests to an actual plant transient are conducted, a limited assessment of code scale-up capability and trends can be provided by completing assessment calculations using the identical code for both the full-size plant transient and the counterpart transient in the scaled facility. If the calculated results for each are found to be in reasonable agreement with the plant and experimental facility transients, the code can be judged to scale for the types of phenomena occurring in the given transient. An example of the latter is a test conducted in the Cylindrical Core Test Facility (CCTF) as a counterpart to the test conducted in the FLECHT-SET (Phase B) facility. The boundary conditions for CCTF Test 75 (Ref. 19) were designed to be similar to those in FLECHT-SET experiment 2714B (Ref. 20). The volume-scale reduction for the CCTF facility is 20 while the volume-scale reduction for the FLECHT-SET facility is 2000, a scaling range factor of 100. Thus, the ability of a code to predict the scale effect between facilities at different scales with boundary conditions designed for similarity could provide significant contributions to assessing the ability of a code to scale correctly.

The third scale-up technique verifies the ability of a code to scale up to the full-size plant following a two-track approach. The first track includes validation of the code's predictive capability against data for full-size components. Examples of such components are the reactor coolant pumps, upper plenum, downcomer, hot legs, and breaks. In this manner, the ability of a code to model the phenomena in a given component at full scale is assessed. The ability of the code to integrate and couple these various component models is not assessed in such activities. The second track includes validation of code predictive capability against

data from integral facilities at various scales. The objective of tests in scaled facilities is to verify the ability of the code to integrate the component models and obtain reasonable to excellent overall comparisons with the data from integral tests. Among the facilities available for such assessment activities and their volume-scale reduction are FLECHT SEASET (2000), Semiscale (1600), LOBI (700), PKL (150), LOFT (50), ROSA-IV (48), CCTF (20), SCTF (20), and UPTF (1). The MIST volume-scale reduction is 817. Frequently, additional scaling assumptions beyond the volume-scale reduction have been made in the design and operation of these facilities. Results from these two tracks are combined and at some point the accumulated evidence is judged sufficient for qualified technical people to agree that the ability of the code to scale-up important thermal-hydraulic phenomena has been demonstrated.

The fourth scale-up technique relies on identifying the most important correlations and models used by the code for a given subscale integral test or plant transient. These correlations and models are then examined in detail to assess their adequacy at full scale. In addition, the analyst checks to ensure that correlations and models exist in the code that simulate all key phenomena and processes occurring during the transient under examination. A description of the correlations and models in the TRAC-PF1/MOD1 code is provided in Ref. 7. A correlations and models document is essential for this technique as it identifies the specific correlations and models in the code as well as the basis and data base for each. In addition, selected assessments are documented that identify and quantify the usage of a given model or correlation outside the range of its original data base. Because this technique focuses on and considers correlations and models one at a time, it does not provide insights into the integration of individual models and correlations into the architecture and numerics of the code. Thus, it appears that this technique is best viewed as supportive of an effort to provide an overall statement of code scalability when combined with information from the first three techniques described above.

There is a large effort currently in progress to quantify the uncertainty of using TRAC-PF1/MOD1 for prediction of large-break loss-of-coolant accidents.[21] A similar effort should follow to quantify the uncertainty of applying TRAC for predicting SBLOCA phenomena in full-size plants. The elements of the Code Scaling Applicability and Uncertainty (CSAU) method described in Ref. 22 include (1) availability of a full set of code-specific documentation, (2) a ranking of key components, processes, and phenomena, (3) review and use of separate-effects test data to determine uncertainty ranges on key parameters identified during the ranking process, (4) use of integral-effects test data directly where results can be considered to be scale independent, and (5) a combination of uncertainty contributions. Los Alamos supports addressing the scaling question through application of the CSAU or similar methodology.

2. Conclusions. In the previous section, four techniques for assessing the ability of a code to scale up to full-size plant calculations were described. We will now describe the scaling conclusions based on each of these four techniques as related to MIST 330302.

- No full-scale plant data exist for a feed-and-bleed transient. Therefore, it has not been possible to assess the code-scaling capability of TRAC-PF1/MOD1 using this technique.
- Given that no full-scale plant data exist for a feed-and-bleed transient, counterpart testing has not been conducted. In addition, MIST 330302 was not designed as a counterpart to a similar test in another scaled facility. Therefore, it has not been possible to assess the code-scaling capability of TRAC-PF1/MOD1 using this technique.

- Two categories of scaling information can be derived from this test. The first category is a collection and analysis of assessment results, at the component level, that can be considered to be full scale. For example, the facility core-heater rods are full scale in diameter and height. Thus, subchannel phenomena occurring in the core can be assessed as if they were full scale. For Test 330302, the measured and predicted core thermal-hydraulic parameters were in reasonable agreement during those periods of time when the measured and calculated vessel boundary conditions were in reasonable agreement. The SG tubes are also full scale such that phenomena occurring at the inner surfaces of the tubes can be assessed. We determined that the liquid heat-transfer coefficients calculated on the inside of the tubes by TRAC were 15 to 30% high. Finally, the facility is full height so that phenomena related to density differences such as flow interruptions and recovery may be assessed. The agreement between the calculated and measured loop phenomena such as flow interruption and recovery was reasonable.

  The second category considers this assessment as one element or piece of evidence that is accumulated to determine whether TRAC-PF1/MOD1 is able to predict the phenomena occurring in a feed-and-bleed transient. We note that this result is specific to the MIST facility, which is characterized by a scaled volume reduction of 817 relative to a full-size lowered-loop B&W plant. For the TRAC-PF1/MOD1 posttest assessment of MIST 330302, a feed-and-bleed test with HPI injection delayed 20 min following PORV actuation, we concluded that the overall agreement between test and calculated results was reasonable. Phenomena both occurring in the test and predicted to occur by TRAC included steam-generator-secondary boiloff, slow primary-system pressurization at constant primary-system inventory, single- and two-phase fluid flows through the PORV, hot-leg spillover events, cold-leg and downcomer flow interruptions and flow recovery, effects of late HPI injection into a voided primary system, and primary-system refill from a voided condition. As noted in the discussion of scale-up technique three, this result can be accumulated and weighed by qualified technical people charged with the responsibility for determining whether TRAC-PF1/MOD1 can be used as a predictive tool for full-plant transients.
- A TRAC-PF1/MOD1 correlations and models draft document[7] that was recently prepared provides detailed descriptions of the various correlations and models utilized by the code. It also provides the basis for each model and correlation through references to original literature and/or a description of the development process, lists the assumptions made in the implementation, and describes the details of implementation. A limited range of assessments of some of the more important, less well founded correlations and models has been provided to indicate their inherent accuracy. Several extensive reviews of the draft models and correlation document are underway with the objective of providing review comments that will be considered before final release of the TRAC-PF1/MOD1 correlations and models document. In addition, a brief review of the document by members and consultants of the Advisory Committee on Reactor Safeguards Thermal-Hydraulic Phenomena Subcommittee has been completed and impressions recorded during a recent subcommittee meeting.[23] There

were diverse opinions expressed by the subcommittee members and consultants; several are of significance relative to the issue of scaling. One consultant stated that the code is "working quite well" for the large-break loss-of-coolant accident (Ref. 23, p. 327) and another that the code did "quite well" in predicting transient phenomena in a spectrum of facilities (Ref. 23, pp. 344 and 351). Another consultant expressed concerns that even though TRAC is predicting the experiments it does not scale to the full plant (Ref. 23, p. 354). All committee members and consultants expressed concern that there was either insufficient basis or justification for too many of the individual models and correlations included in the code (Ref. 23, pp. 317, 326, 311, 344, 352, and 386).

I conclude that this technique can be an important contributor to determining the code-scaling capability of TRAC-PF1/MOD1 (Ref. 7). However, the effort to apply this technique could be large, particularly the first few times it is used. Because the effort required is beyond the current defined scope of a single assessment calculation, I recommend that the NRC consider defining and funding a separate activity to demonstrate and document this approach for a selected transient or set of transients. Within the MIST program the set of SBLOCA transients would be the logical and recommended choice for such a demonstration activity.

In this section an effort has been made to review candidate approaches for assessing the scaling capability of a code such as TRAC-PF1/MOD1. In addition, the code-scaling contributions from the posttest assessment of MIST 330302 using TRAC-PF1/MOD1 have been described. It is clear that each posttest assessment contributes to the determination of code-scaling capability. It is equally clear that the posttest assessment of a single experiment will usually provide only a small fraction of the information needed for a complete statement about code-scaling capability. Given the importance of this issue, I recommend that an effort be initiated to define and plan an approach to determine the code-scaling capability of TRAC-PF1/MOD1. This effort would include collecting, reviewing, and applying existing posttest assessment data. In addition, this effort would identify the need for additional work, if any, related to assessments of full-plant transients (technique 1), assessments of counterpart tests (technique 2), and the assessment of code-scaling capability by focusing on the correlations and models used for given scaled-integral or full-plant transients (technique 4).

E. Regulatory Implications

The objective of this section is to summarize our understanding of issues, results, and conclusions that may be used in support of the regulatory process for B&W plants.

1. Background. The US NRC has identified a number of nuclear-safety issues requiring further investigation. These have been designated as either generic or unresolved safety issues (USIs), and action plans have been prepared to resolve them. USI A-45, Shutdown-Decay-Heat Removal is one such issue. Feed and bleed has been considered as one method of removing decay heat from pressurized water reactors (PWRs) following total loss of feedwater.[12] Feed and bleed is a procedure in which coolant is injected into the primary system by safety- and/or non-safety-grade systems (feed), absorbs the core-decay heat, and is released to the containment (bleed) through the PORV. Successful implementation of a feed-and-bleed procedure requires that needed valves and pumps work, the energy relief rate of the PORV exceeds the

core decay heat over an extended time period, emergency core-cooling (ECC) water can be supplied to the primary system faster than primary-system inventory is released through the PORV over an extended time period, and the plant operators start the process sufficiently early. This later requirement highlights the importance of timing to successful implementation of a feed-and-bleed procedure.

Questions about the use of feed-and-bleed procedure are being considered by the NRC. Shortly after the Davis-Besse event, some NRC staff questioned whether feed and bleed would have failed if implemented during the Davis-Besse transient event on June 9, 1985 (Ref. 24, p. 9); *i.e.*, cooldown and depressurization of the plant would have failed. Three specific reservations are identified in Ref. 25. The first reservation is related to whether or not the electrical equipment, pumps and vents needed for the process will work in an environment of high-pressure, radioactive steam to which they could be exposed for an extended period of time following opening of the PORV. The second reservation is that initiation of the feed-and-bleed procedure has a time limit that varies from plant to plant. Thus, there is a concern that the operators will wait too long to implement the feed-and-bleed procedure while trying to restore feedwater to the system. A third and related reservation is whether the operators will use feed and bleed in a timely fashion, even when written procedures identify it. There is some supporting evidence for this concern in that during the Davis-Besse loss-of-feedwater event, the operators did not use the feed-and-bleed procedure even though such actions were directed by emergency guidelines.[23]

2. MIST Feed-and-Bleed Tests. The MIST facility was designed to address perceived deficiencies in the thermal-hydraulic data base for B&W plants. As stated in Ref. 5 (Appendix A.1, p. I.A-1), "Due to the unique configuration of the B&W NSS, previous large integral test facilities did not model the unique B&W hot leg configuration or the OTSG and, as a result, did not simulate the appropriate natural circulation conditions. In particular, there was uncertainty about the effects of two-phase flow, noncondensable gases, and the validity of the boiler-condenser mode of heat removal. In addition, the hydraulic stability, effects of high point vents, and internal reactor vessel valves . . . . were items of interest."

A Test Advisory Group (TAG) was formed in September 1982 with representatives of the NRC, B&W owners, B&W and the Electric Power Research Institute participating. After an extensive review, a list of seventeen technical issues were identified by the TAG as those that should be addressed through an integral systems test facility. This list is reproduced from Ref. 5 (Table 2.1, p. I.2-7) as Table V and includes the consensus prioritization of the issues developed by the TAG. This list includes feed and bleed as a procedure containing phenomena requiring testing and evaluation. Overall, the evaluation used ratings from A to D to represent a measure of the priority. An "A" rating was defined as top priority. A "D" rating was used to indicate a lower priority, although issues rated as "D" were still considered to be of sufficient importance to warrant investigation. The NRC representative to the TAG noted, for example, that the TAG issues list (Table V) represented a culling from a more extensive list of potential issues. All issues remaining on the TAG list are thought to be important. A compromise on the priority was reached on all issues except the understanding of the high point vents as they affect natural circulation. The B&W owners rated this issue of "D" priority but the NRC rated this issue as "A" priority. A priority ranking of "D" was assigned by consensus to the feed-and-bleed issue.

Key SBLOCA events were also identified. A group of B&W personnel with extensive plant and thermal-hydraulic experience then reviewed the phenomena and ranked them by their relevance to the TAG issues. This B&W produced priority ranking of SBLOCA events by their relevance to the TAG issues is reproduced from Ref. 5 (Table 2.3, p. I.2-10) as Table VI. Feed-and-bleed primary cooldown was assigned a rank of 13 in a group of 25 SBLOCA events, thereby placing the importance of feed-and-bleed primary cooldown near the middle of identified events occurring during SBLOCA transients.

As discussed in Ref. 5 (Sec. 2.1.3, p. I.2-3), the TAG agreed not only to the testing issues but also to a test matrix and to the essentials of a test facility. Thus, the MIST facility design definition and test matrix were direct outcomes of a process of identifying thermal-hydraulic issues for B&W plant designs. As noted in Ref. 5, the facility and tests were recommended by the TAG ". . . . . *to provide a sufficient data base for use in computer code assessment. The assessed computer code is the link between the test data and the operating plant. Test facility results cannot be extrapolated to predict plant performance.*"

MIST group 33 examined HPI-PORV or feed-and-bleed cooling. A primary objective of MIST group 33 was to determine whether feed-and-bleed cooling could effectively cool and depressurize the MIST facility following a complete loss of feedwater to the SG secondaries. Both nominal and off-nominal tests were conducted. For the nominal test of group 33, Test 33001BB, full HPI was initiated at the time of PORV opening. Reduced HPI (evaluation model) was provided for MIST 330201; the reduced HPI was initiated at PORV actuation as in the nominal case.

For MIST 330302, the key parametric variation from nominal conditions was the time to delivery of full HPI, which was delayed 20 min after PORV actuation. An additional objective of MIST 330302 was to examine an extended period of PORV actuation without ECC makeup and with the SGs unavailable. An expected outcome of the delay in providing HPI was extensive primary-system voiding; in this condition, primary-system condensation and depressurization phenomena were of interest. Specifically, the test was designed to determine whether condensation phenomena induced major system perturbations and whether a controlled primary-system depressurization could be sustained.

3. Conclusions. It is possible to draw important conclusions regarding HPI-PORV or feed-and-bleed cooling in the MIST facility.

First, the feed-and-bleed procedure was successful in cooling and depressurizing the primary system in each of the tests conducted. Observations regarding feed-and-bleed Tests 3301BB, 330201, and 330302 are reported in Ref. 3. For the nominal Test 3301BB, the core remained covered and cooled throughout the test. For the reduced-HPI Test 330201, the HPI-injection rate was approximately one-half the nominal injection rate. The relatively large imbalance between the PORV discharge rate and the HPI-injection rate caused the primary system to void extensively. However, the trend of primary-system mass depletion was reversed following pressurizer surge line uncovery. The core remained covered throughout the transient. During the delayed-HPI Test 330302, the liquid level approached the top of the core and the downcomer level briefly descended a few feet below the top of the core. Primary-system inventory depletion was reversed shortly after HPI initiation.

Second, the parametric cases for reduced HPI (Test 330201) and delayed HPI (Test 330302) demonstrate that the feed-and-bleed procedure, as scaled and applied in the MIST

facility, can still successfully cool and depressurize the facility. These two cases provide an indication of the margin against reductions in the amount of HPI delivered or in the time of delivery. The two cases do not define the limits of the margin. For example, the percentage reduction in HPI that would lead to core heatup was not determined, nor was the time of delay in HPI delivery beyond which the primary system could not be cooled and depressurized.

Third, the MIST feed-and-bleed tests do not address the issues of equipment survivability or willingness of the operator to initiate a feed-and-bleed procedure.

Fourth, the test results cannot be directly extrapolated to full-size B&W plants. This conclusion has been reached and documented by the TAG but is repeated here for emphasis. The extension to full-size plants must be made through the use of assessed computer codes. Results of such efforts for the Davis-Besse loss-of-feedwater transient of June 9, 1985 are reported in Refs. 13 and 26.

Fifth, TRAC-PF1/MOD1 predicts the time to PORV actuation to occur earlier than measured in the MIST facility for Test 330302. Thus, the Davis-Besse transient results in Ref. 13 may underestimate the time available for operator action. The result is conservative in that more time would be available to PORV opening on high primary-system pressure than predicted by TRAC.

Sixth, the TRAC-calculated results for Test 330302 are in reasonable overall agreement with the data. All major trends and phenomena were correctly predicted. Differences observed between the measured and calculated results have been traced and related, in part, to deficiencies in our knowledge of the facility configuration and operation. We have also identified two models for which additional review is appropriate. However, in general, the TRAC closure models and correlations appear to be adequate for the prediction of the phenomena expected to occur during feed-and-bleed transients in the MIST facility.

Seventh, we have analyzed feed-and-bleed procedures using models of two full-size B&W plants, Oconee-1[12] and Davis-Besse.[13] A feed-and-bleed procedure was found to successfully cool and depressurize the Oconee-1 plant following a postulated loss-of-feedwater provided the procedure was initiated no later than the time the primary would have saturated had the primary system been maintained at a pressure near the PORV setpoint by cycling the PORV open and shut. In addition, phenomena predicted to occur in the full-size Oconee-1 plant were similar to those observed in MIST 330302. These included primary-system heatup and expansion following loss of the SG-secondary heat sink, primary-system inventory depletion following PORV actuation, and primary-system refill following HPI initiation. Studies show that a feed-and-bleed procedure would have successfully cooled and depressurized the Davis-Besse plant if such a procedure had been used following the actual loss-of-feedwater event of June 9, 1985. The outcomes of postulated feed-and-bleed procedures initiated at approximately 15 min, 20 min, and 35 min following the transient initiator were calculated. In the first two cases, feed-and-bleed was directly calculated to be successful. The characterization of a successful feed-and-bleed operation for the final case was based on extrapolation. Again, the global characteristics of the calculated Davis-Besse feed-and-bleed transient were similar to those observed in MIST 330302 and our calculation of a postulated feed-and-bleed transient in the Oconee-1 plant. Based on the successful calculation of MIST 330302 and the prediction

of similar phenomena in full-size plants (Oconee-1 and Davis-Besse), we conclude that TRAC-PF1/MOD1 will correctly predict the major trends for feed-and-bleed transients in full-size plants.

Eighth, an independent study of the Davis-Besse transient was conducted at the Idaho National Engineering Laboratory.[24] It was concluded that a calculation of the Davis-Besse loss-of-feedwater transient was in good qualitative and quantitative agreement with the measured data. This agreement was attained for a calculation of the transient using RELAP5/MOD2. The maximum deviation between calculated and measured reactor-coolant system pressure was about 0.3 MPa (50 psi). The deviations between calculated and measured reactor-coolant-system temperatures were generally less than 3 K (6°F). It was noted that the differences between an earlier RELAP5/MOD2 calculation, the TRAC-PF1/MOD1 calculation reported in Ref. 13, and the RELAP5/MOD2 calculation reported in Ref. 24 "were primarily due to the assumption of different core powers, feedwater flows, and pressurizer spray flows." The first RELAP5 calculation and the TRAC calculation were performed shortly after the Davis-Besse event; at this time there was significant uncertainty regarding key boundary conditions. The subsequent RELAP5 calculation used more accurate representations of these key boundary conditions resulting from additional study of the plant transient. We conclude that a TRAC-PF1/MOD1 calculation using the improved boundary conditions specification would have produced similar results. This information strengthens our confidence that the major trends to be expected during a feed-and-bleed transient in a full-size B&W plant would be calculated using TRAC-PF1/MOD1.

REFERENCES

1. Safety Code Development Group, "TRAC-PF1/MOD1: An Advanced Best-Estimate Computer Program for Pressurized Water Thermal-Hydraulic Analysis," Los Alamos National Laboratory report LA-10157-MS (NUREG/CR-3858) (July 1986).
2. "Immediate Report, Test 330302: Group 33 (Feed and Bleed) Test 3, Delayed HPI," Babcock & Wilcox document BAW-1938 (October 1986).
3. J. R. Gloudemans (principal author), "Group Report, MIST Test Group 33, HPI-PORV Cooling," Babcock & Wilcox document BAW-1965 (July 1987).
4. B. E. Boyack and J. L. Steiner, "Pretest Analysis of MIST Test 330302," Los Alamos National Laboratory document LA-CP-86-267 and NUREG/CR-5889 (November 1986).
5. "Multi-Loop Integral System Test (MIST) Facility Specification," Babcock & Wilcox document RDD-84:4091-01-01:01 (1984).
6. J. A. Klingenfus, "Multi-Loop Integral System Test Design Verification Report," Babcock & Wilcox document NRC-04-83-168/RP 2399-1 (November 1984).
7. D. R. Liles, J. W. Spore, T. D. Knight, R. A. Nelson, M. W. Cappiello, K. O. Pasamehmetoglu, *et al.*, "TRAC-PF1/MOD1 Correlations and Models," Los Alamos National Laboratory report LA-11208-MS and NUREG/CR-5069 (January 1989).
8. B. E. Boyack, H. Stumpf, and J. F. Lime, "TRAC User's Guide," Los Alamos National Laboratory report LA-10590-M and NUREG/CR-4442 (November 1985).
9. J. R. Gloudemans (principal author), "Group Report, MIST Test Group 31, Boundary Conditions," Babcock & Wilcox document BAW-1958 (March 1987).
10. Multi-Loop Integral System Test (MIST) Instrumentation, Babcock & Wilcox document RP 2399-1, Revision 3 (March 1987).

11. J. L. Steiner and D. A. Siebe, "Posttest Analysis of MIST Test 3109AA Using TRAC-PF1/MOD1," Los Alamos National Laboratory report LA-UR-89-2158 and NUREG/CR 5887 (September 1992).
12. B. E. Boyack, R. J. Henninger, E. Horley, J. F. Lime, B. Nassersharif, and R. Smith, "Los Alamos Decay-Heat-Removal Studies Summary Results and Conclusions," Los Alamos National Laboratory report LA-10637-MS (also NUREG/CR-4471) (March 1986).
13. J. F. Lime, B. Nassersharif, and B. E. Boyack, "Rapid-Response Analysis of the Davis-Besse Loss-of-Feedwater Event on June 9, 1985," Los Alamos National Laboratory document LA-UR-85-3083 (August 1985).
14. Multi-Loop Integral System Test (MIST) Instrumentation and Derived Quantity Uncertainty Analysis, Babcock & Wilcox document RDD:84:4091-01001:02 (July 1987).
15. Cancelled.
16. "Long-Range Research Plan, FY 1987 - FY 1991," Office of Nuclear Regulatory Research report NUREG-1080, Vol. 3 (August 1986).
17. "Test Specification for Ranch Seco Scaling Transient Test," B&W IST Program Communication with PMG No. 4-7 (August 21, 1987).
18. "Crystal River 3 Scaling Transient Test Specification," B&W IST Program Communication with PMG No. 4-30 (December 7, 1987).
19. T. Okubu, *et al.*, "Quick-Look Report on CCTF Core-II Reflood Test C2-15 (Run 75) – Investigation of FLECHT-SET Coupling Test Results," Japan Atomic Energy Research Institute memorandum 60-225 (September 1985).
20. J. P. Waring, *et al.*, "PWR FLECHT-SET Phase B1 Data Report," Westinghouse report WCAP-8431, UC-78a (December 1984).
21. K. R. Katsma, R. A. Dimenna, and G. E. Wilson, "TRAC-PF1/MOD1 Uncertainty Quantification for LBLOCA Blowdown Peak Cladding Temperature," Idaho National Engineering Laboratory, Fifteenth Water Reactor Safety Information Meeting, October 26–30, 1987, Gaithersburg Maryland, NUREG/CP-0090 (October 1987).
22. "Compendium of ECCS Research for Realistic LOCA Analysis," US Nuclear Regulatory Commission, NUREG-1230 (December 1988).
23. Transcript of Proceedings, The Advisory Committee on Reactor Safeguards Thermal Hydraulic Phenomena, Los Alamos, New Mexico, January 21–22, 1988.
24. *Inside N.R.C.*, McGraw-Hill Publishing, July 22, 1985.
25. D. E. White, "Davis-Besse: Will Feed & Bleed Work?," The Kiplinger Program Report, The Ohio State University School of Journalism, Vol III, No. 1, Spring 1987.
26. C. B. Davis, "Davis-Besse Uncertainty Study," EG&G Idaho, Inc. document EGG-RTH-7453 (November 1986).

TABLE I

TEST 330302 TRANSIENT CONTROLS

Parameter	Control
PORV	Actuate at 16.2 MPa (2350 psia): manually open after actuation.
Core power	Trip at PORV actuation.
RVVV	Automatic/Independent.
HPI	Full scaled head-flow 1200 s after PORV actuation.
CFT	Actuate at 4.14 MPa (600 psia): Manual isolation when core exit subcooling > 27.8 K (50°F) for 30 min and primary pressure > 4.93 MPa (715 psia) and primary pressure not increasing.
Primary pumps	Locked rotors.
SG secondary pressure	Initially controlled at 6.96 MPa (1010 psia): pressure maintained with nitrogen after decreasing to 6.55 MPa (950 psia).
AFW	Off.

TABLE II

STEADY-STATE CONDITIONS FOR TEST 330302

Parameter	Unit	Test	TRAC
Core power	kW	128.4	126.7[notes 1,2]
Pressurizer pressure	MPa	11.964	11.98
	psia	1735.2	1715.4
Core-exit subcooling	K	12.9	13.1
	(°F)	23.3	23.6
Hot-leg temperatures	K	584.6	584.2
	(°F)	592.9	592.2
Cold-leg A1 pump suction temperature	K	561.7	560.7
	(°F)	551.7	549.9
Downcomer flow	kg/s	0.870	0.879
	lbm/s	1.916	1.936
Pressurizer water level (elevation)	m	6.05	6.08[note 2]
	ft	19.85	19.95
Steam-generator secondary 1 level	m	1.048[note 4]	1.048[note 3]
	ft	4.5	3.438
Steam-generator secondary 2 level	m	0.904[note 4]	0.904[note 3]
	ft	4.3	2.966
Steam-generator secondary 1 pressure	MPa	6.997	6.964
	psia	1014.8	1010.0[notes 3,5]
Steam-generator secondary 2 pressure	MPa	6.997	6.964
	psia	1014.8	1010.0[notes 3,5]

NOTES:

1. TRAC core power reduced to account for ex-core energy losses in facility.
2. Specified in TRAC input.
3. Control system controls to specified value.
4. Obtained from TAGs S1LV20 and S2LV20. We believe that these measurements are in error and that actual initial liquid levels were about 1.37 m (4.5 ft) and 1.31 m (4.3 ft) for the loop 1 and loop 2 SGs, respectively. Further discussion is provided in Sec. VI.C.1.
5. Value input to control system was 0.033 MPa (4.8 psi) lower than measured.

TABLE III

EVENT TABLE FOR TEST 330302

Test Time (s)	Calculation Time (s)	Event Description
0.0	0.0	Start transient - loss of AFW to SG secondaries.
942.0	730.0	Primary system pressure increases to 16.41 MPa (2350 psia) and PORV lifted. PORV maintained open for remainder of test.
942.0	730.0	Core power decay ramp initiated.
1025.0	860.0	RVVVs first close.
1080.0	935.0	Pressurizer full.
1680.0	—	SG secondary isolated.
2142.0	1930.0	HPI started.
	4560.0	Calculation terminated (vessel refilled to near RVVV level).

TABLE IV

RESULTS OF SG NODING STUDY

	Time(s) to stated event		
	Divisions of bottom SG secondary cell		
Description	Standard Model	1 Cell into 5	1 Cell into 10
Time to SG-secondary dryout			
All standalone model inlet and exit conditions vary as measured in Test 330302	535	680	780
Full-model calculation	680	740	
Time to PORV set point			
Full-model calculation	742 (note)	728	739

NOTE:

This calculation was performed with same number of cells as standard SG model but with unequal cell heights for bottom two SG cells. Rather than equal cells of 1.5 m (4.92 ft), the bottom cell was 0.75 m (2.46 ft) and the next higher cell was 2.25 m (7.38 ft).

TABLE V

TAG EVALUATION OF ISSUES

Natural Circulation	
Single-phase natural circulation	D
Two-phase natural circulation	C
Boiler condenser natural circulation	A
Steam generator-driven instabilities	B
Cold-leg oscillations	B
Interruption/re-establishment	B
High point vents	A/D
Noncondensable gases	B
RVVVs	C
SBLOCA	
Break size	C
ECC system operation	C
Reactor-coolant pump operation	B
Location of break	D
Break isolation	B
RVVVs	B
Feed and Bleed	D
Steam-generator tube rupture	B

TABLE VI

PRIORITY OF SBLOCA EVENTS

Rank	Rating	SBLOCA Event
1	8	Hot-leg U-bend saturation and voiding
2	8	RVVV activation
3	8	Leak-HPI cooling
4	7	Reinitiation of natural circulation
5	7	SG condensation of primary steam
6	7	Downcomer and cold-leg voiding and condensation
7	7	Leak flow
8	7	Reactor-vessel upper-head voiding
9	7	Decoupling of SG
10	6	Spillover circulation (hot-leg U-bend refilled)
11	6	Primary repressurization
12	6	Venting of primary fluid
13	5	Feed and bleed primary cooldown
14	5	Controlled SG depressurization and primary cooldown
15	5	Compression of primary fluid
16	5	Asymmetric conditions among cold legs
17	4	Single-phase natural circulation
18	4	"Pump Bump"
19	4	Cooling of idle loop
20	4	Primary depressurization
21	4	Power and flow transient: reactor and coolant pump trip, feed transfer
22	3	Primary depressurization to core-flood tank/low-pressure injection pressures
23	3	Subcooling of primary components
24	3	SG repressurization
25	3	Pressurizer draining

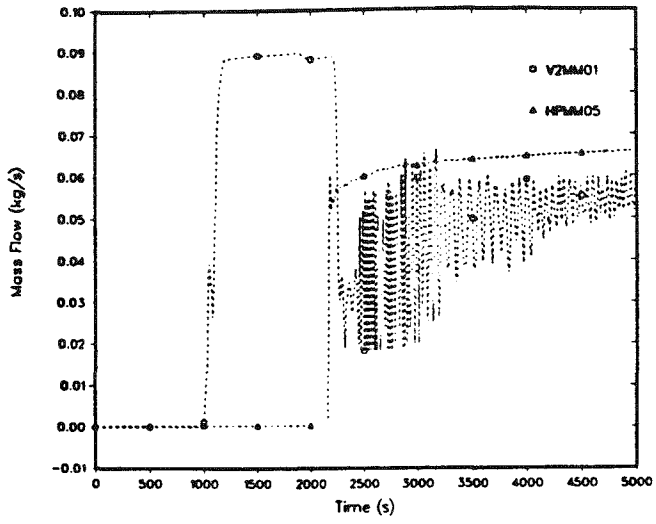

Fig. 1.c. PORV and HPI flows.

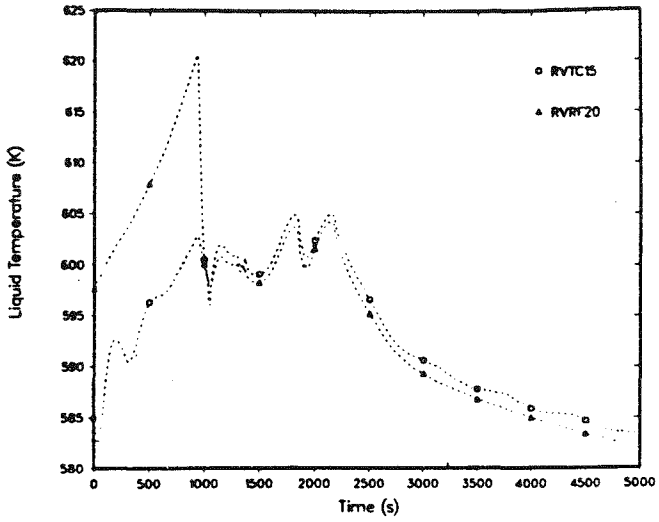

Fig. 1.d. Core exit liquid temperature compared to saturation.

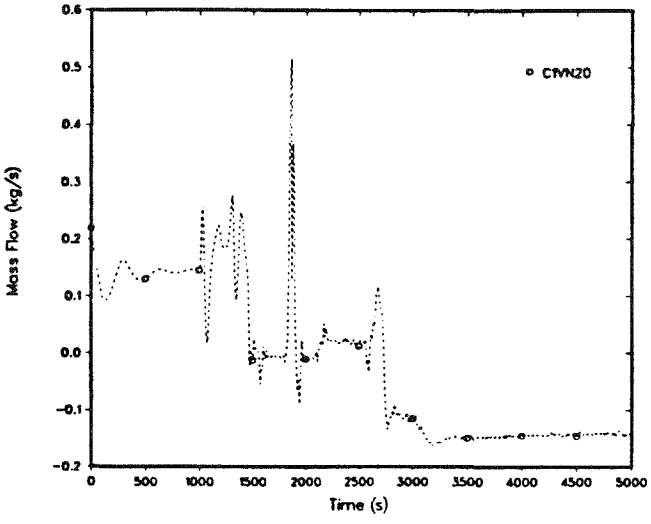

Fig. 1.g. Loop-A1 cold-leg mass flow.

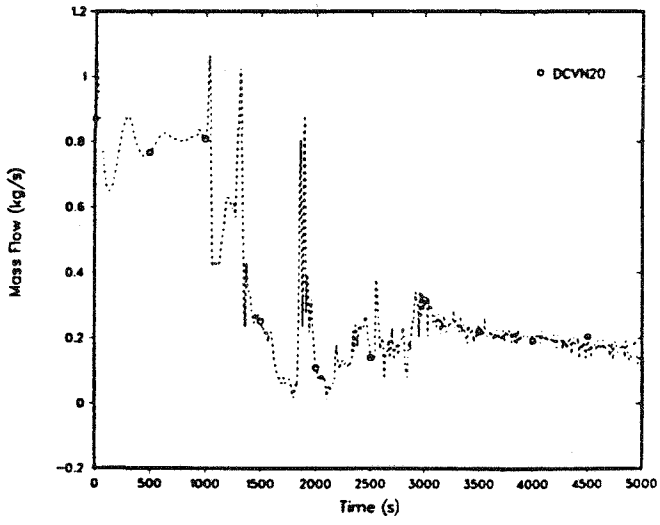

Fig. 1.h. Downcomer mass flow.

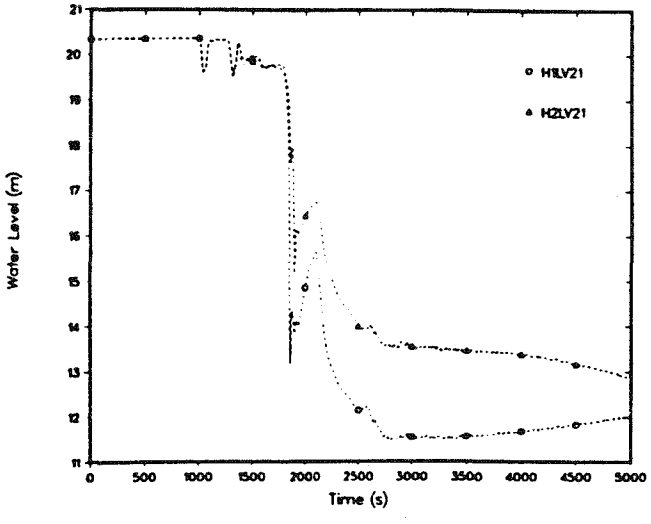

Fig. 1.k. Hot-leg collapsed liquid level.

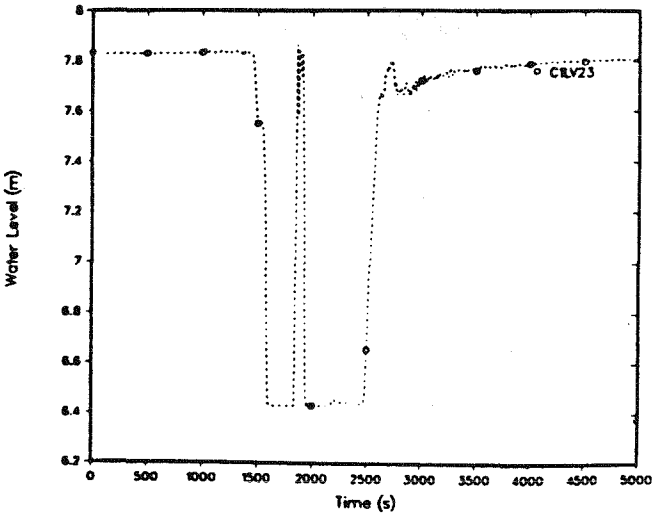

Fig. 1.l. Loop-A1 cold-leg collapsed liquid level.

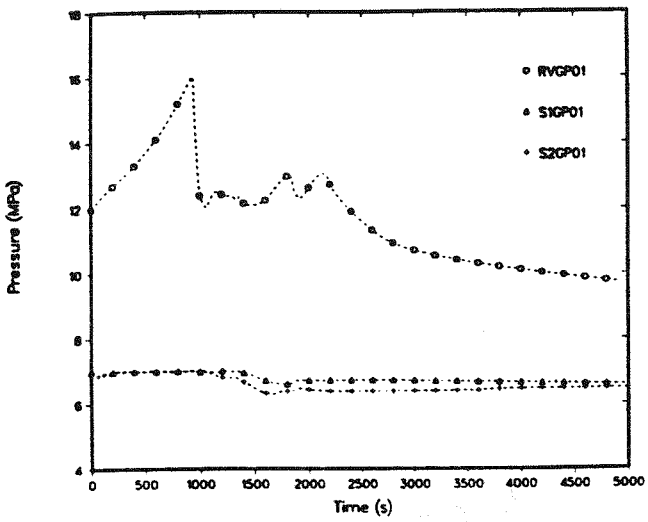

Fig. 1.a. Primary and secondary pressure.

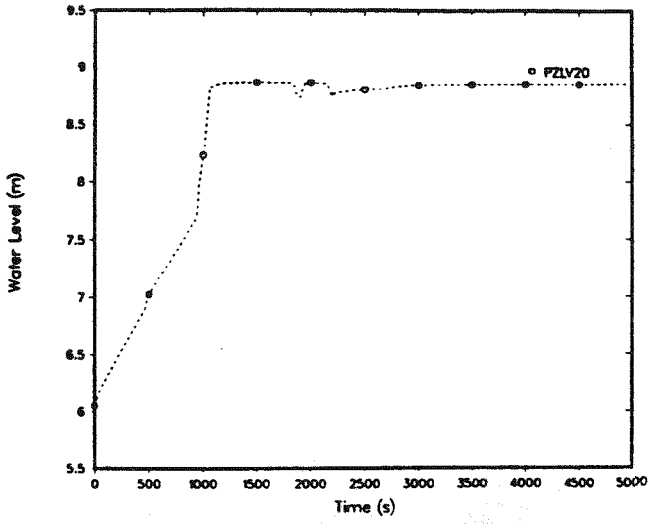

Fig. 1.b. Pressurizer water level.

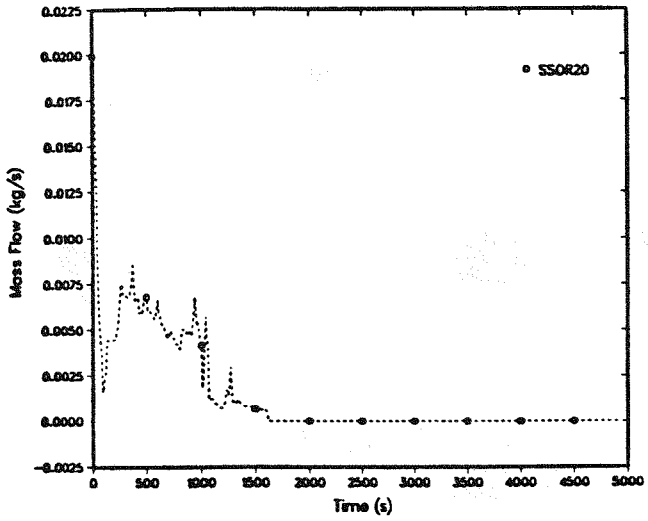

Fig. 1.e. Loop-A steam-generator secondary steam flow.

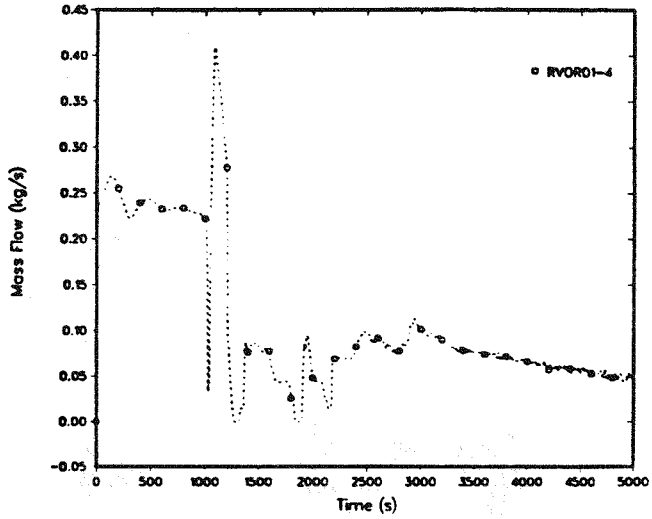

Fig. 1.f. Reactor-vessel vent-valve flow (total of four valves).

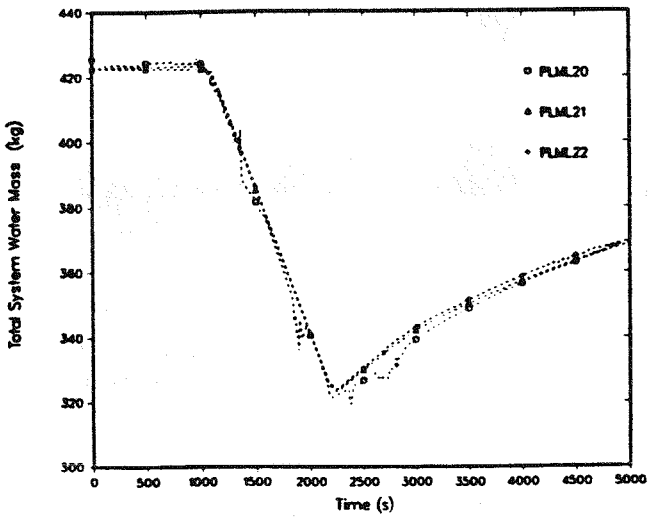

Fig. 1.i. Primary-side water mass.

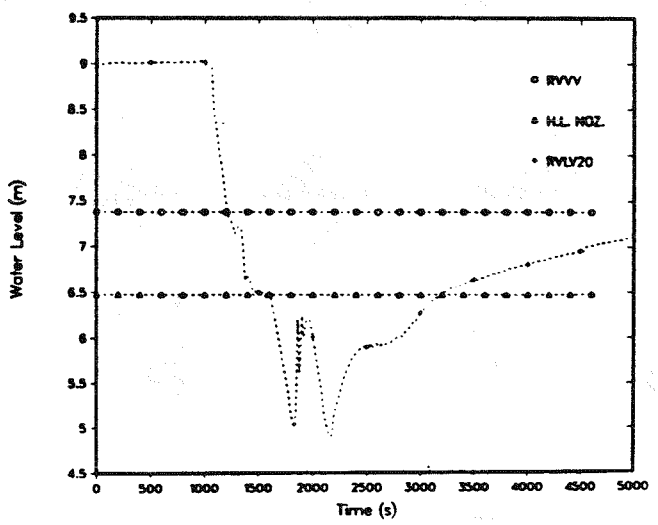

Fig. 1.j. Reactor-vessel collapsed liquid level.

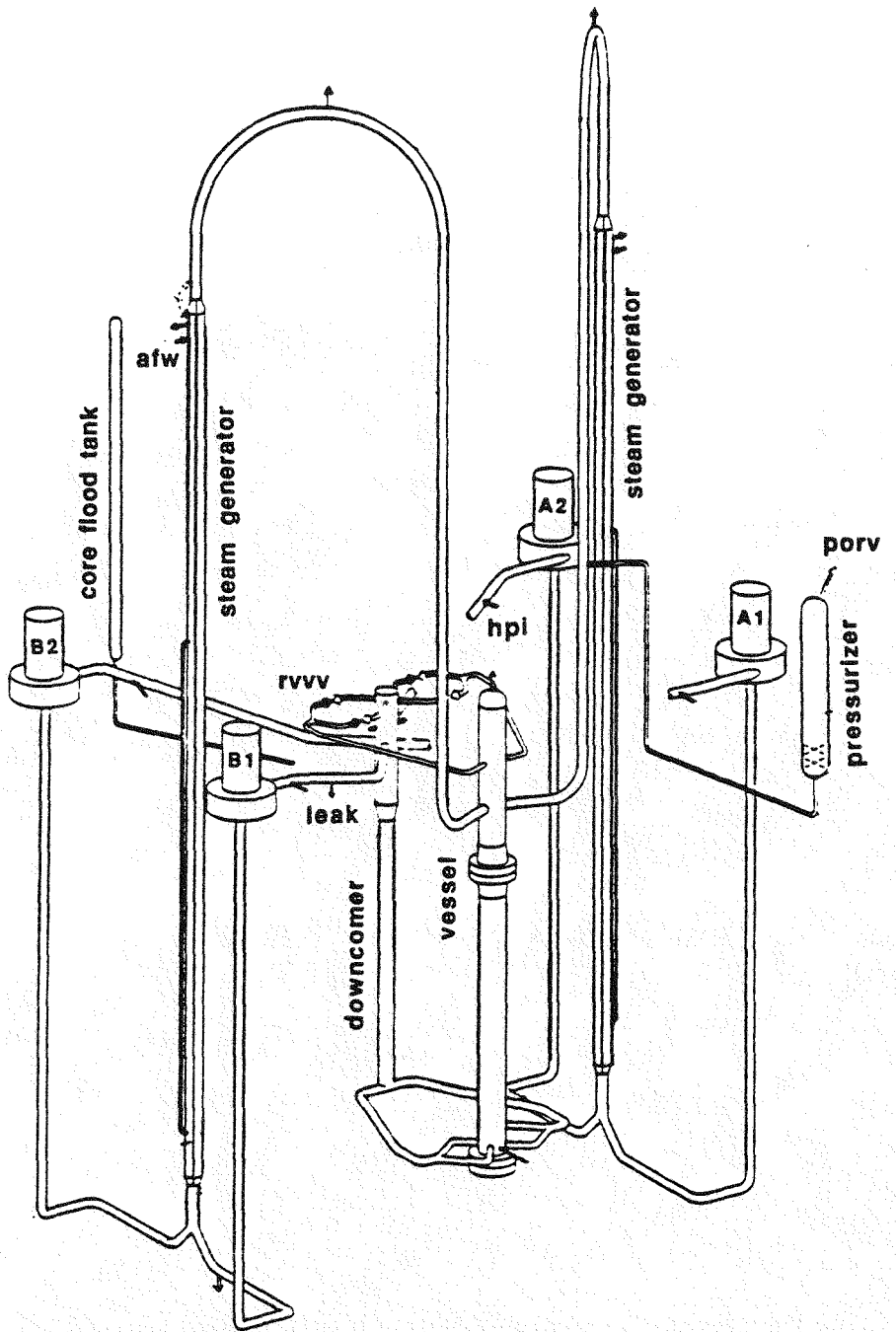

Fig. 1. Overview of measured results for MIST Test 330302.

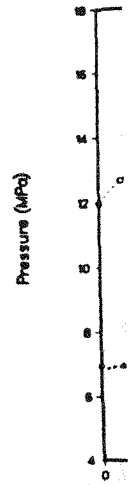

Fig.

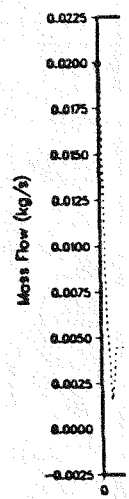

Fig. 1

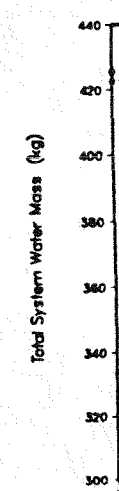

F

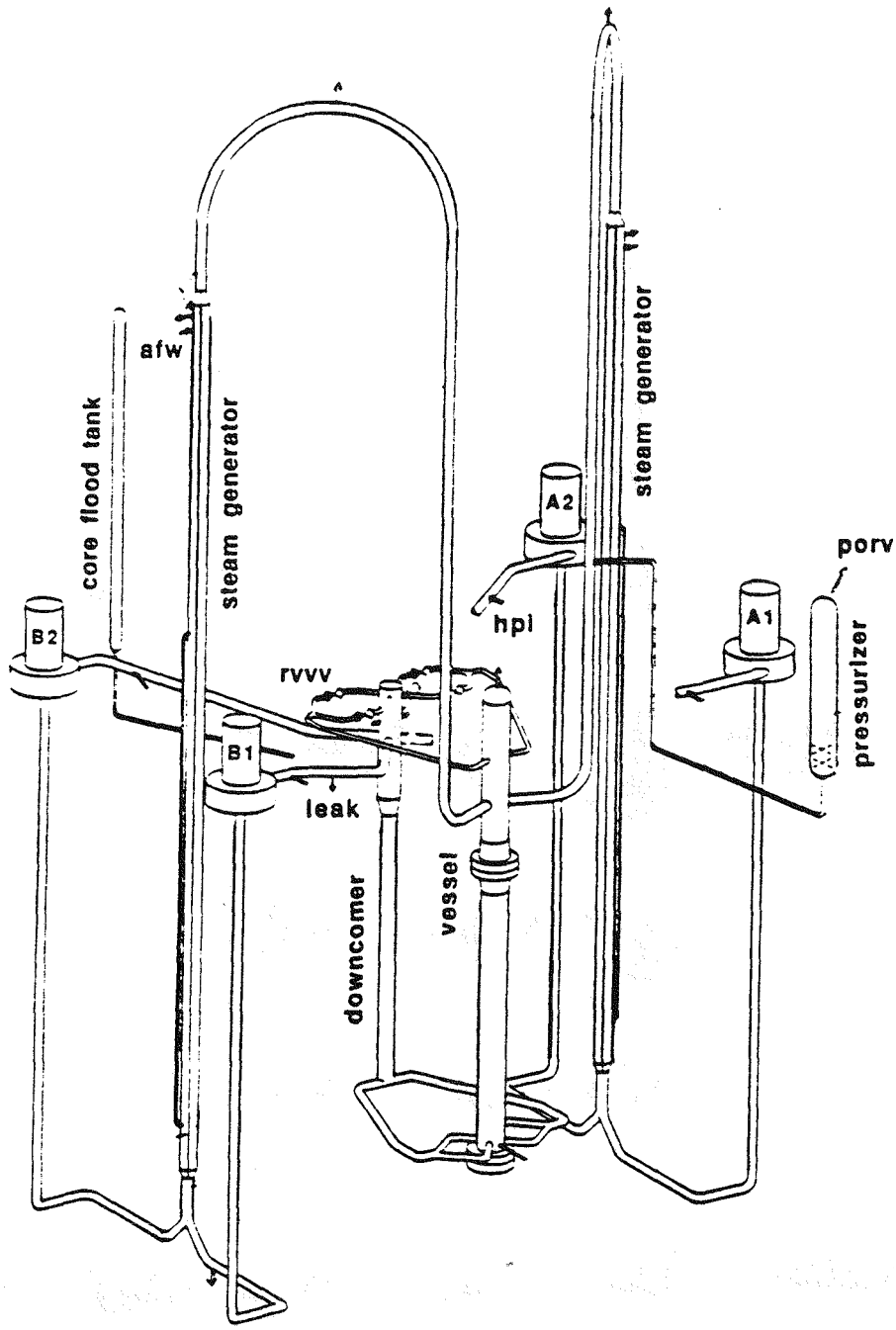

Fig. 2. Overview of code-experiment comparisons for MIST Test 330302.

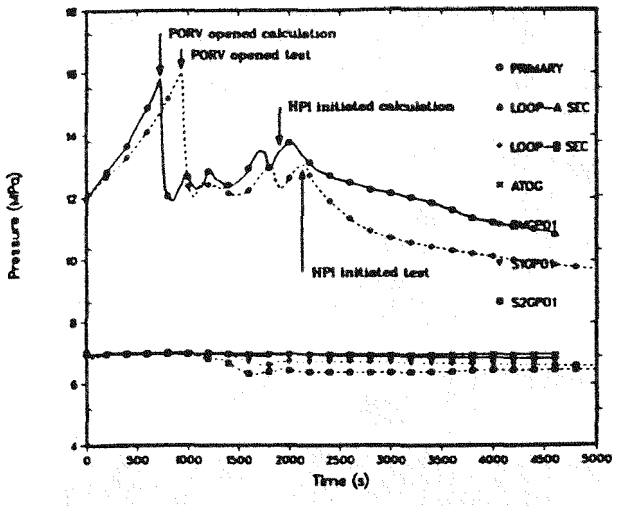

Fig. 2.a. Primary and secondary pressure.

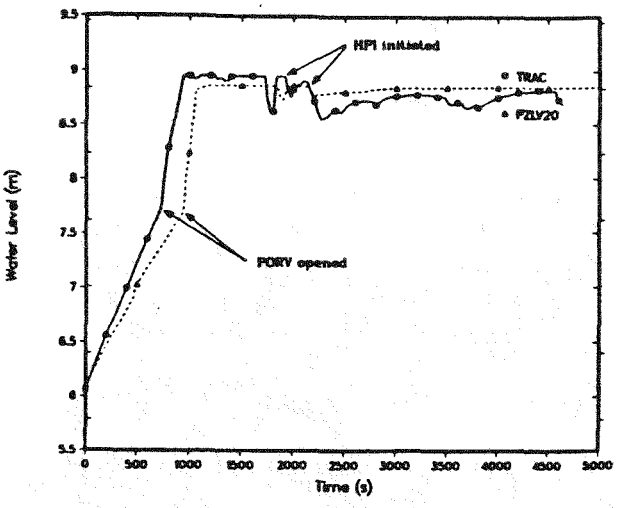

Fig. 2.b. Pressurizer water level.

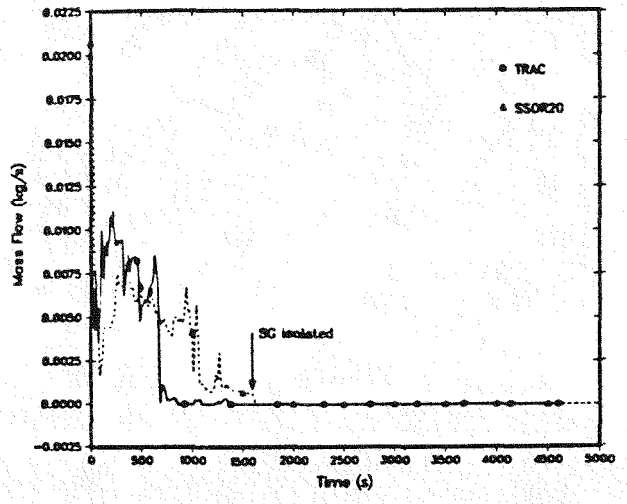

Fig. 2.e. Loop-A steam-generator secondary steam flow.

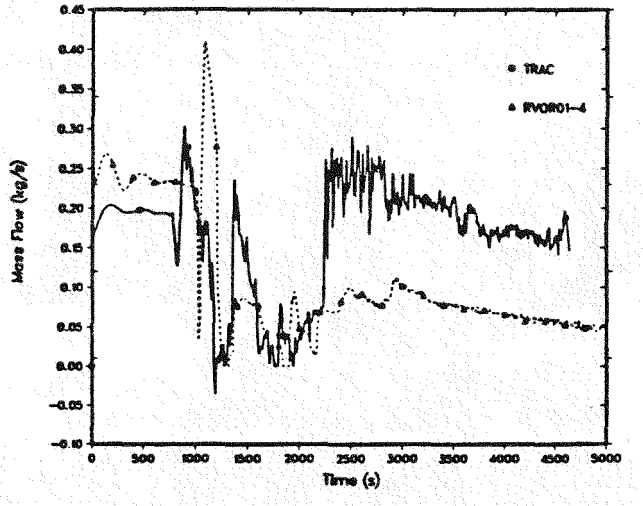

Fig. 2.f. Reactor-vessel vent-valve flow (total of four valves).

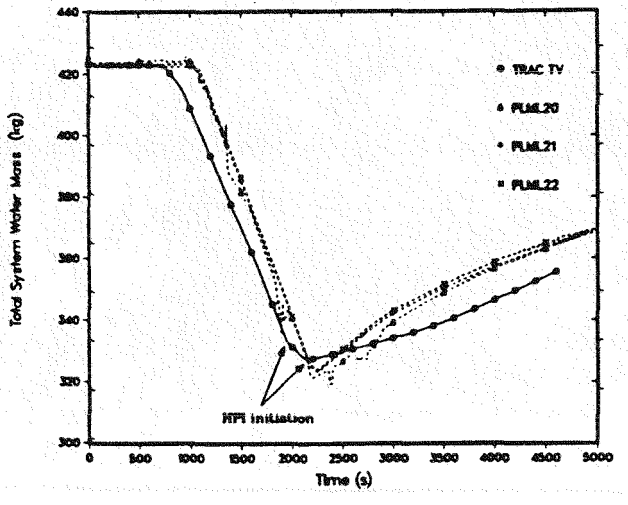

Fig. 2.i. Primary-side water mass.

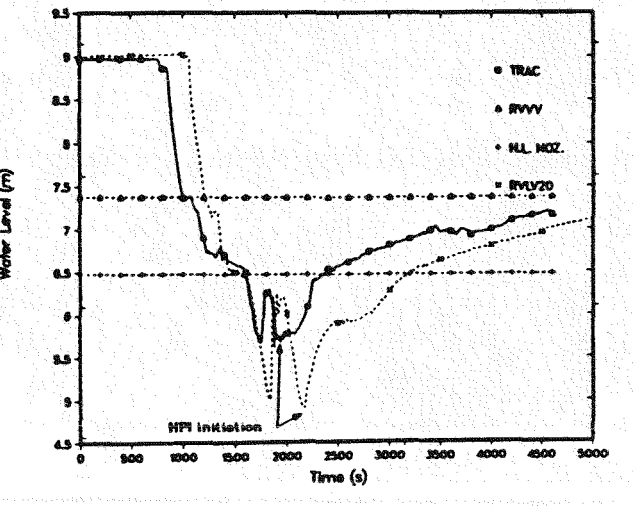

Fig. 2.j. Reactor-vessel collapsed liquid level.

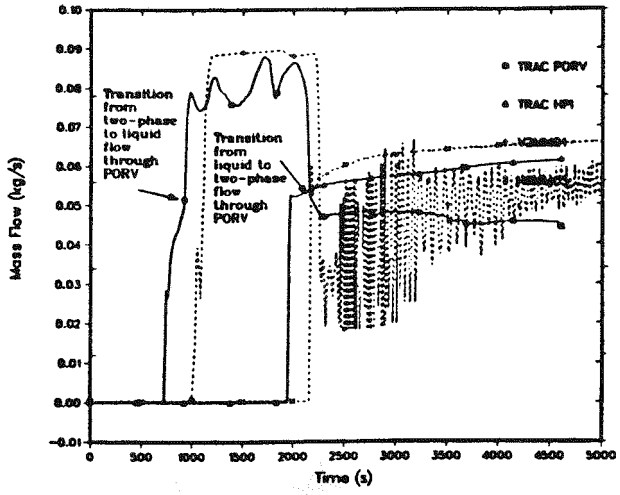

Fig. 2.c. PORV and HPI flows.

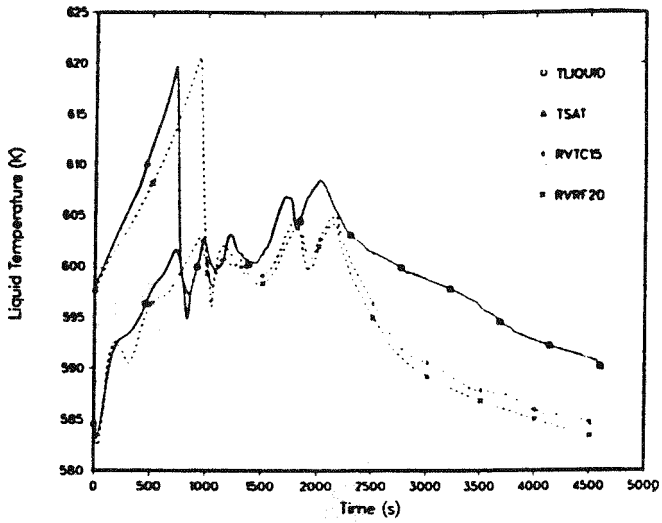

Fig. 2.d. Core exit liquid temperature compared to saturation.

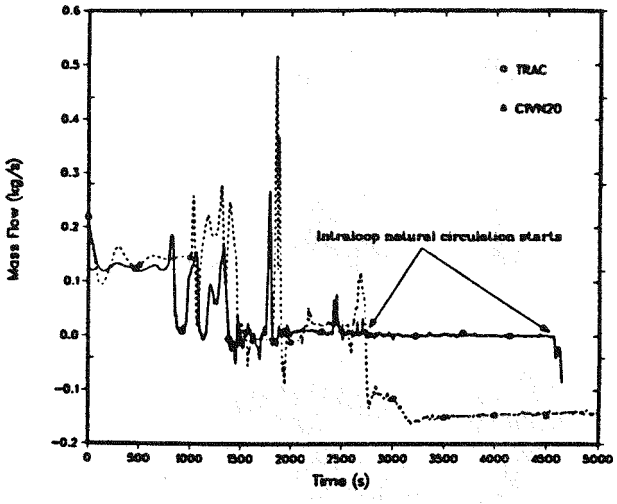

Fig. 2.g. Loop-A1 cold-leg mass flow.

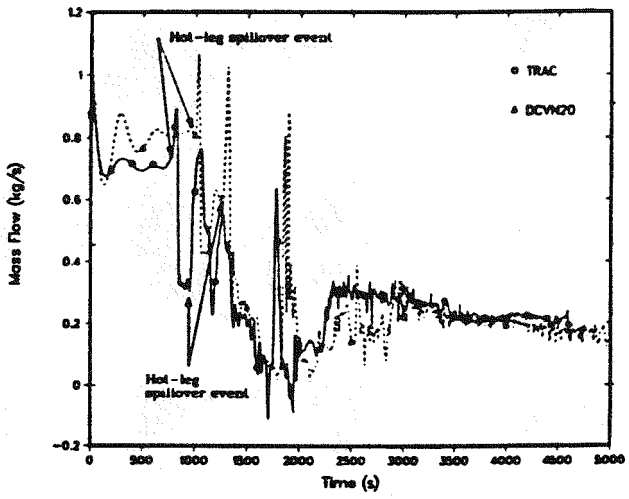

Fig. 2.h. Downcomer mass flow.

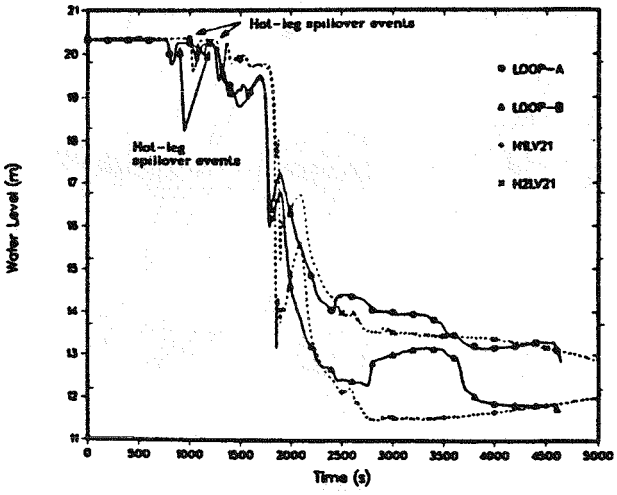

Fig. 2.k. Hot-leg collapsed liquid level.

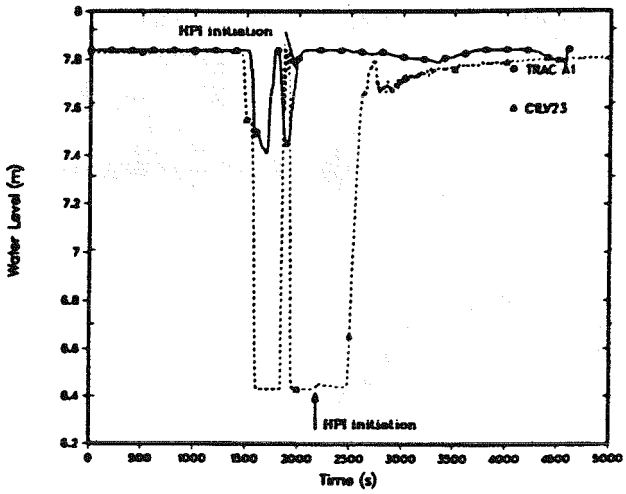

Fig. 2.l. Loop-A1 cold-leg collapsed liquid level.

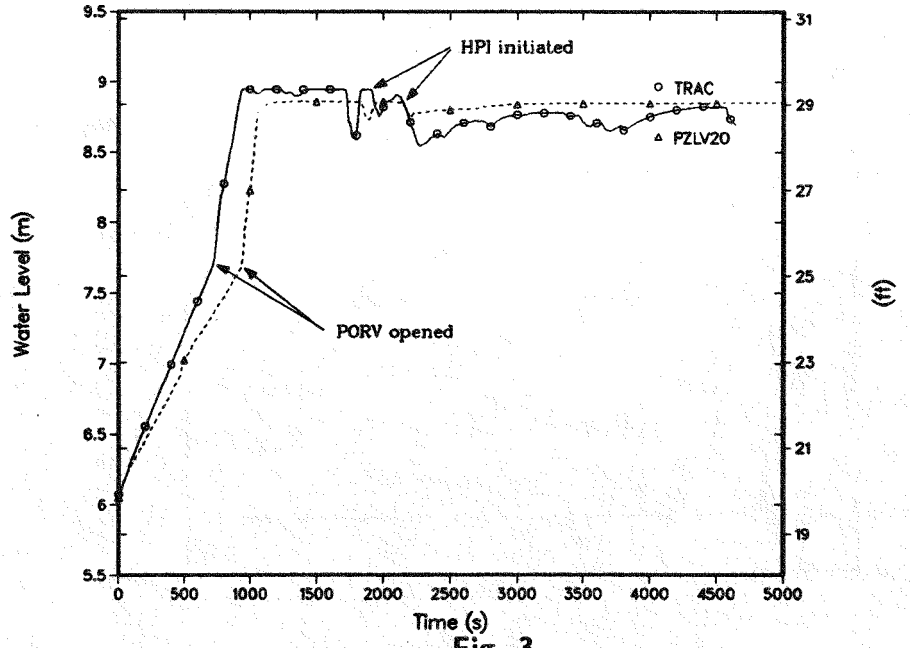

Fig. 3.
Primary and secondary pressures.

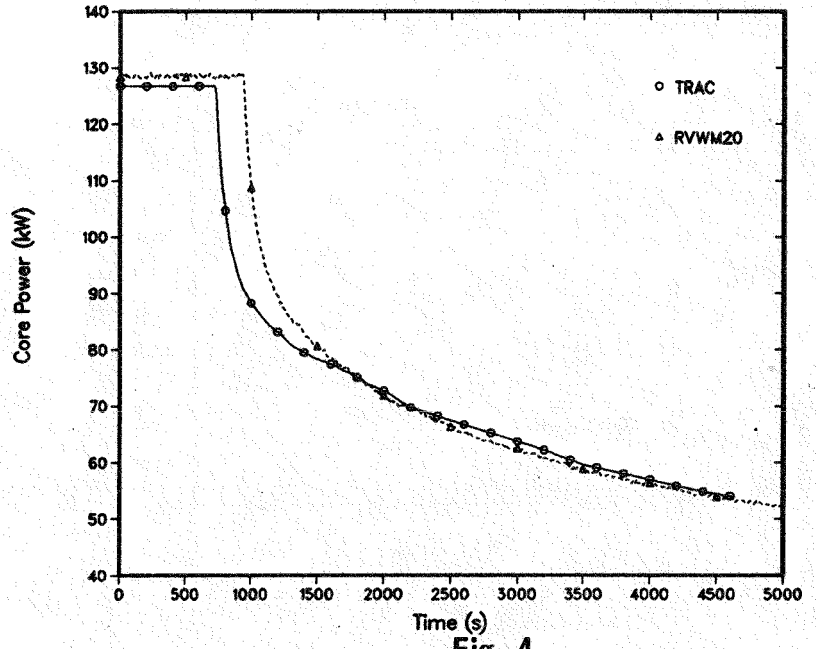

Fig. 4.
Pressurizer water level.

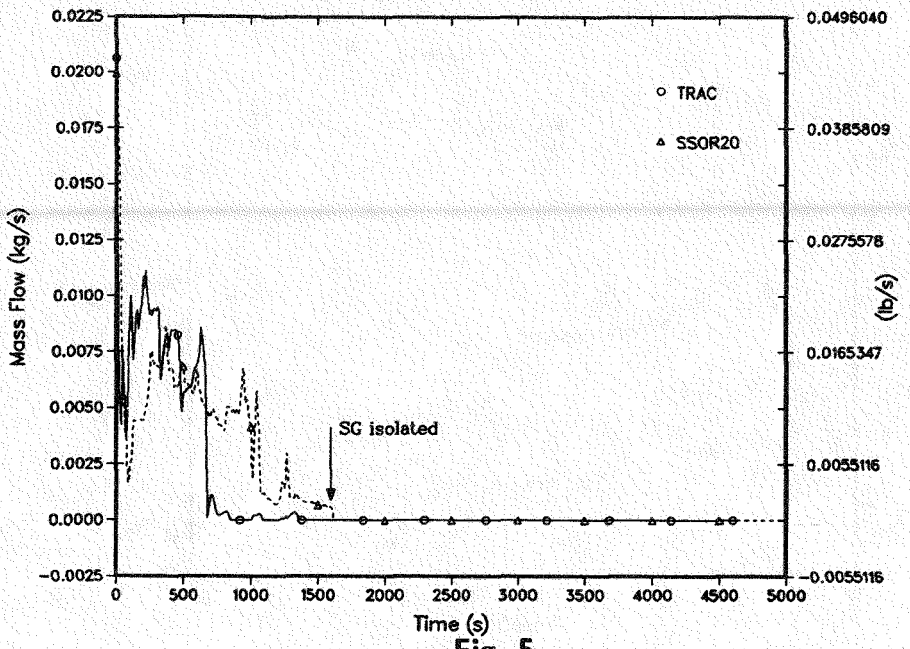

Fig. 5.
Measured and input core power.

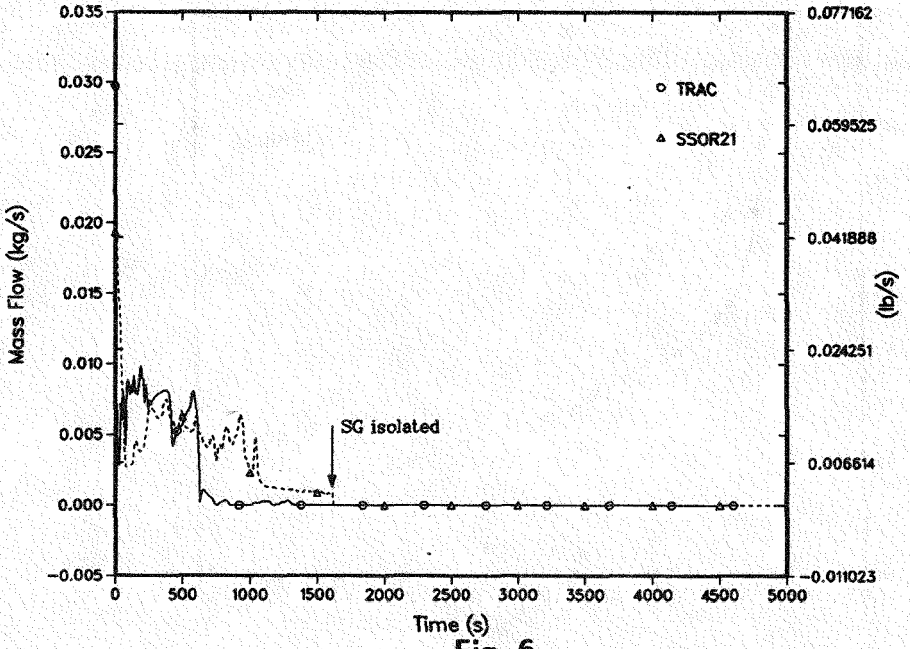

Fig. 6.
Loop-A SG-secondary steam flow.

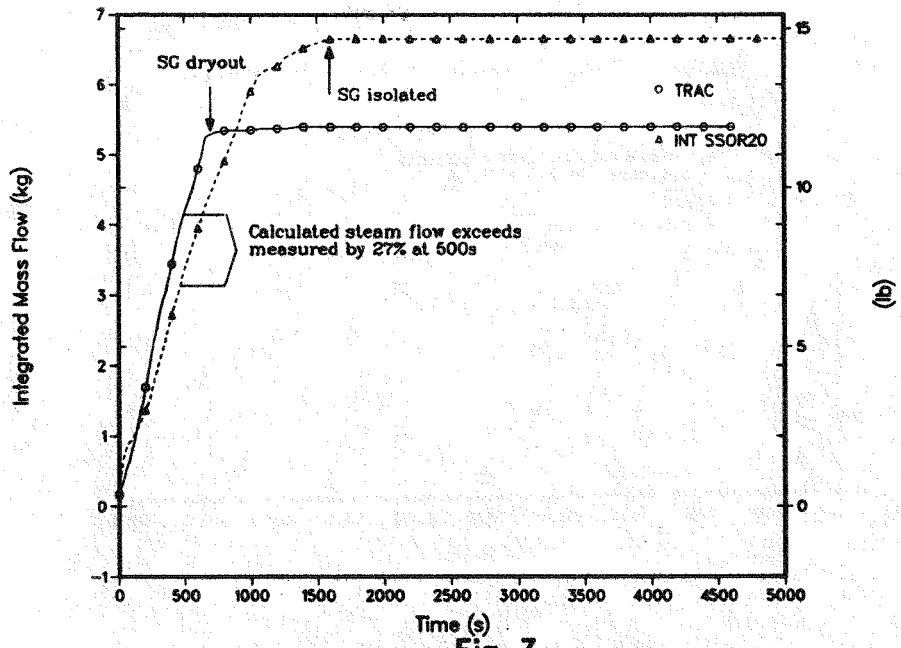

Fig. 7.
Loop-B SG-secondary steam flow.

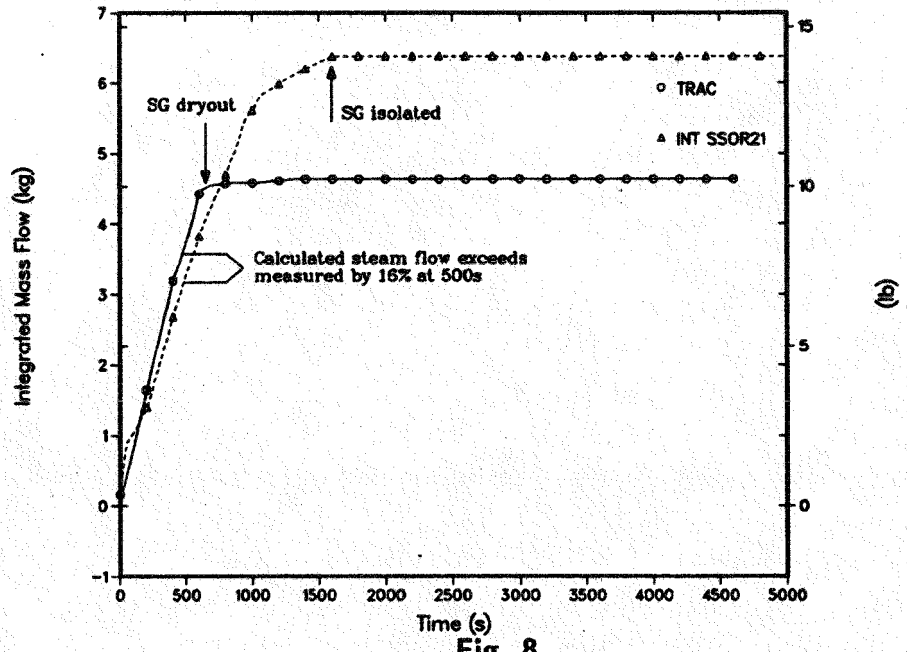

Fig. 8.
Integrated Loop-A SG-secondary steam flow.

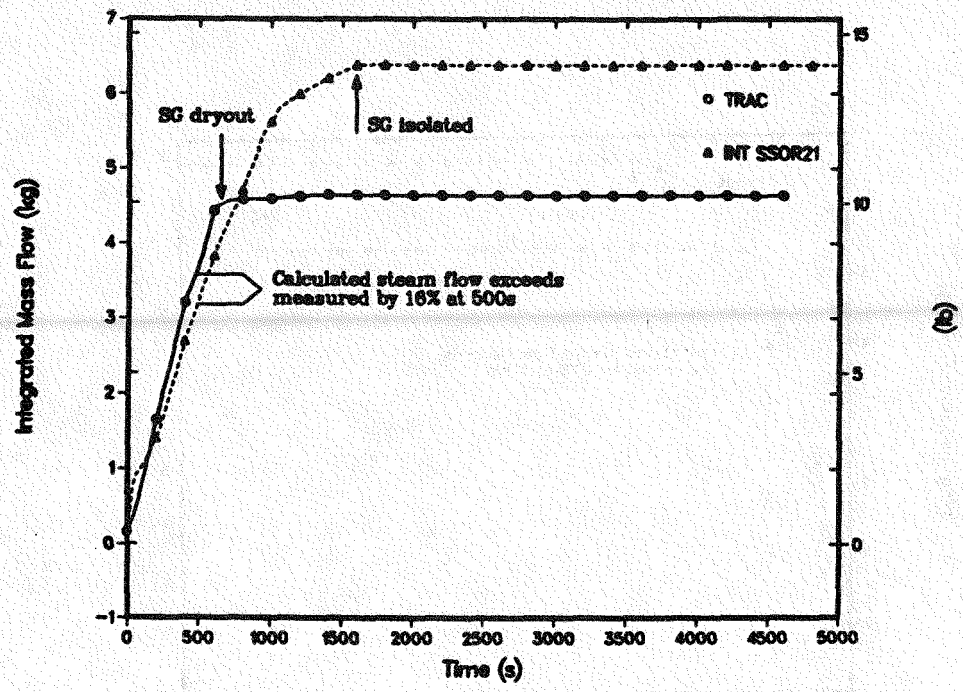

Fig. 9.
Integrated Loop-B SG-secondary steam flow.

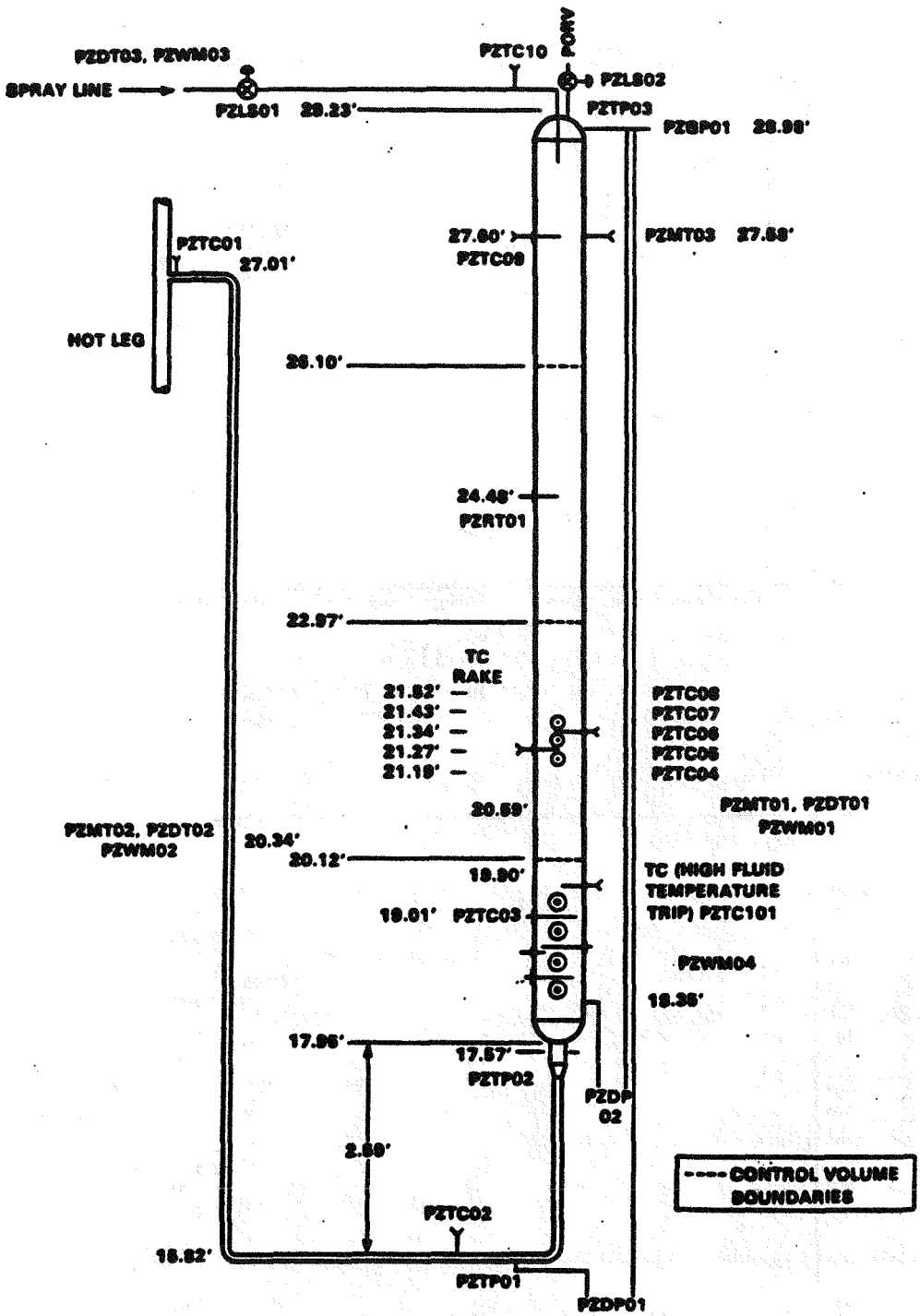

Fig. 10.
MIST pressurizer instrumentation.

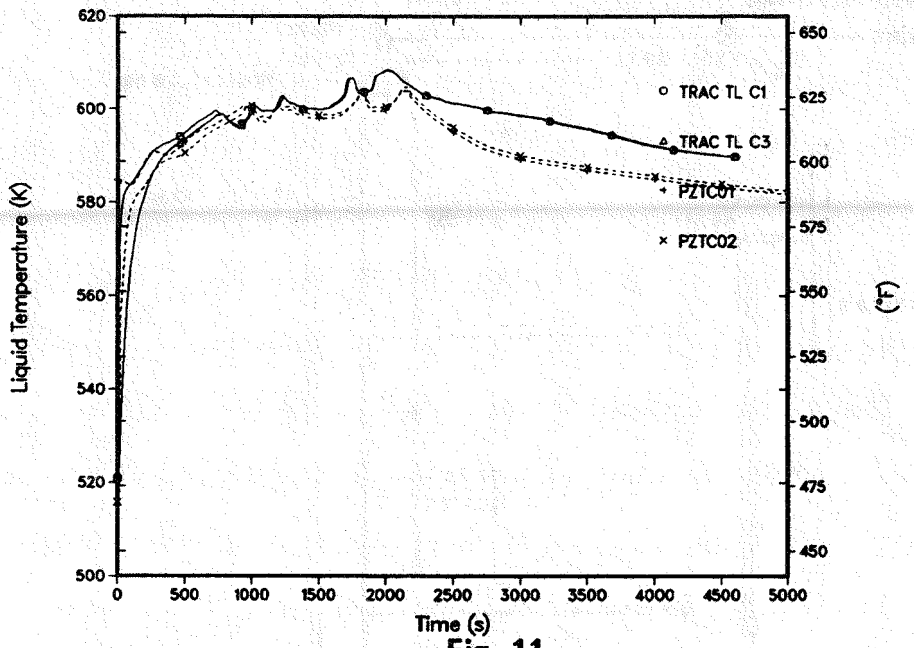

Fig. 11.
Pressurizer surge-line fluid temperatures

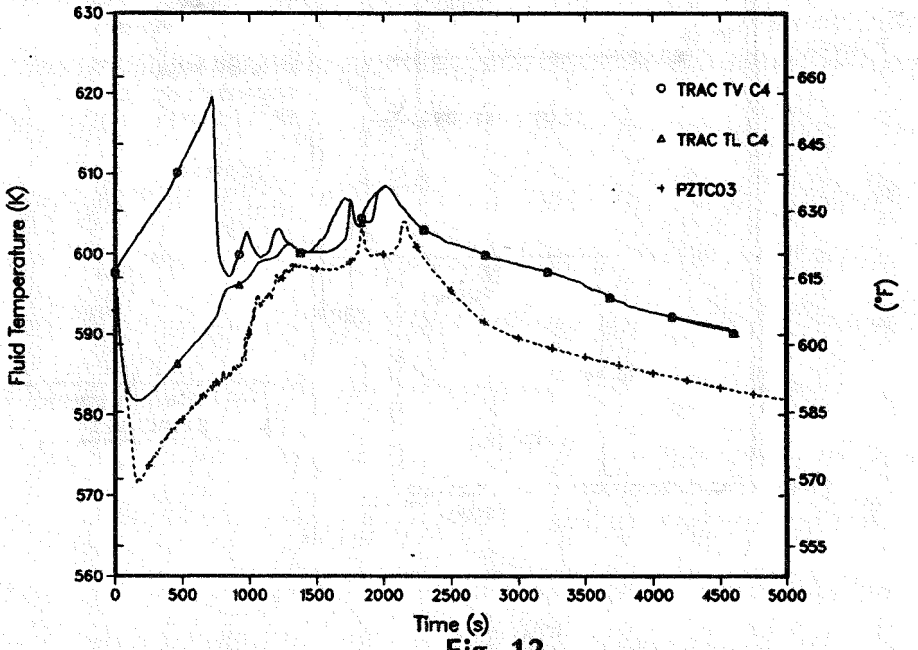

Fig. 12.
Pressurizer fluid temperatures, control volume 4.

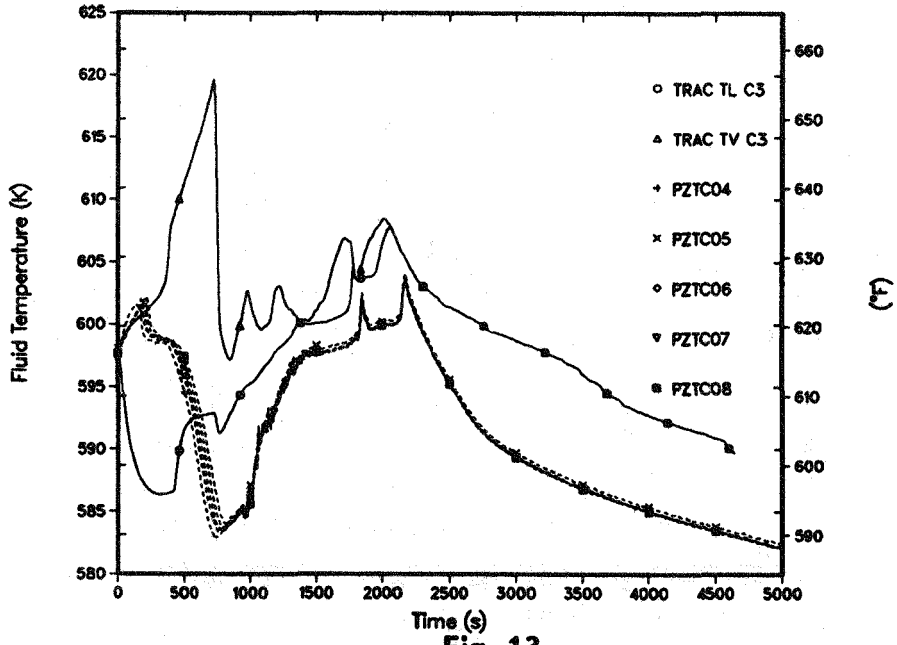

Fig. 13.

Pressurizer fluid temperatures, control volume 3.

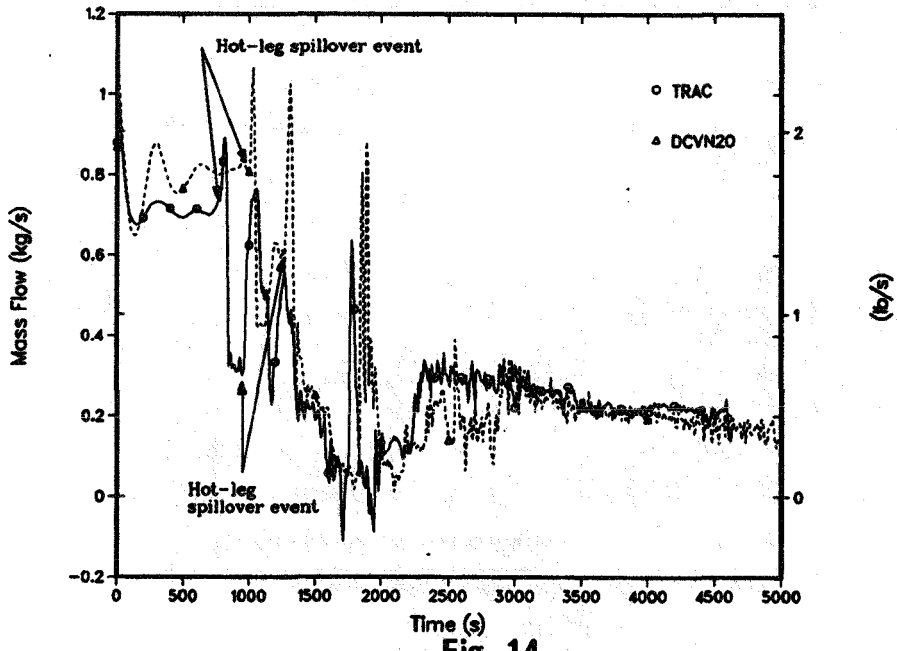

Fig. 14.

Downcomer mass flow.

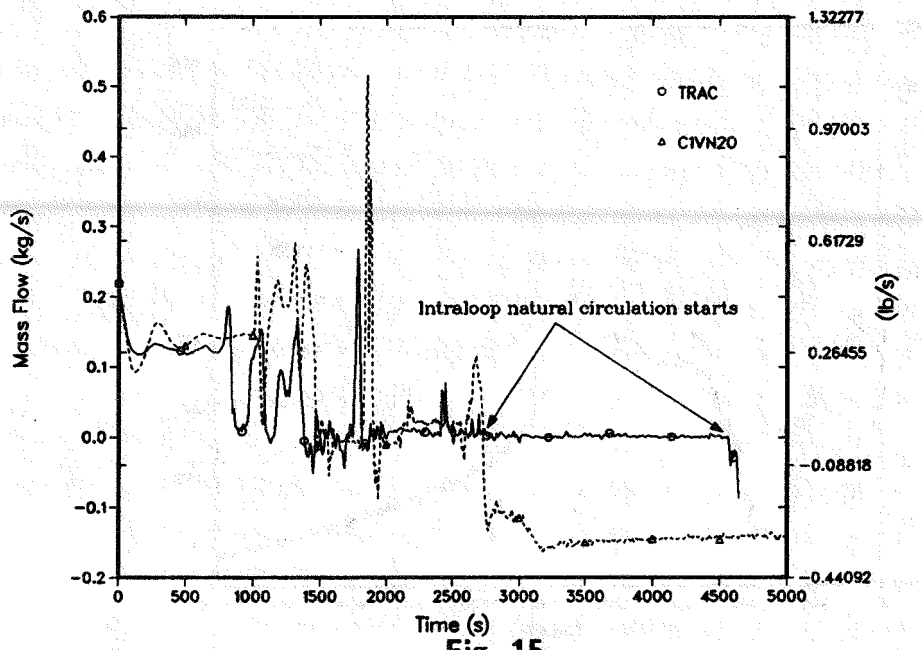

Fig. 15.
Cold-leg A1 mass flow.

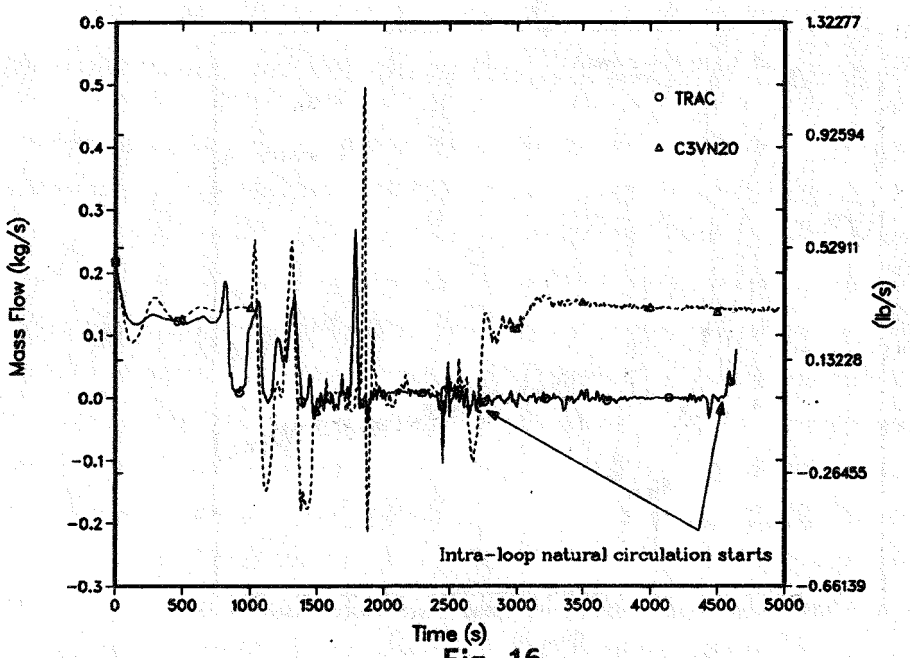

Fig. 16.
Cold-leg A2 mass flow.

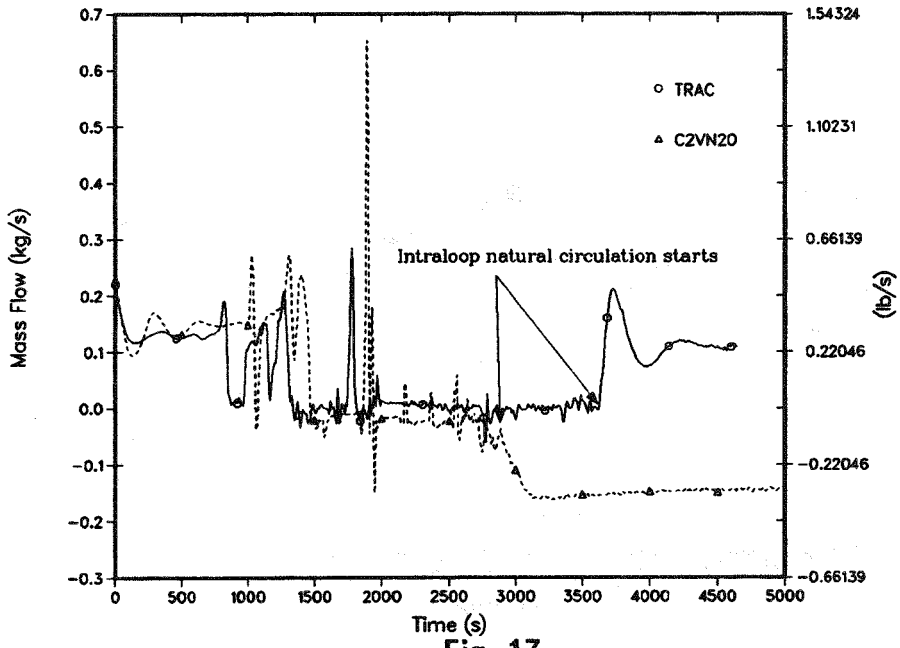

Fig. 17.
Cold-leg B1 mass flow.

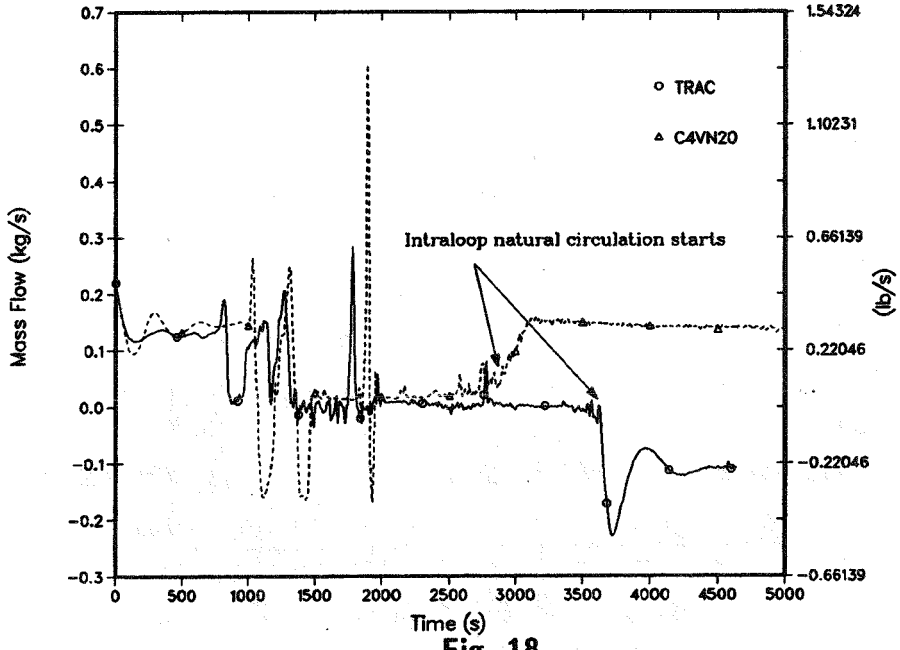

Fig. 18.
Cold-leg B2 mass flow.

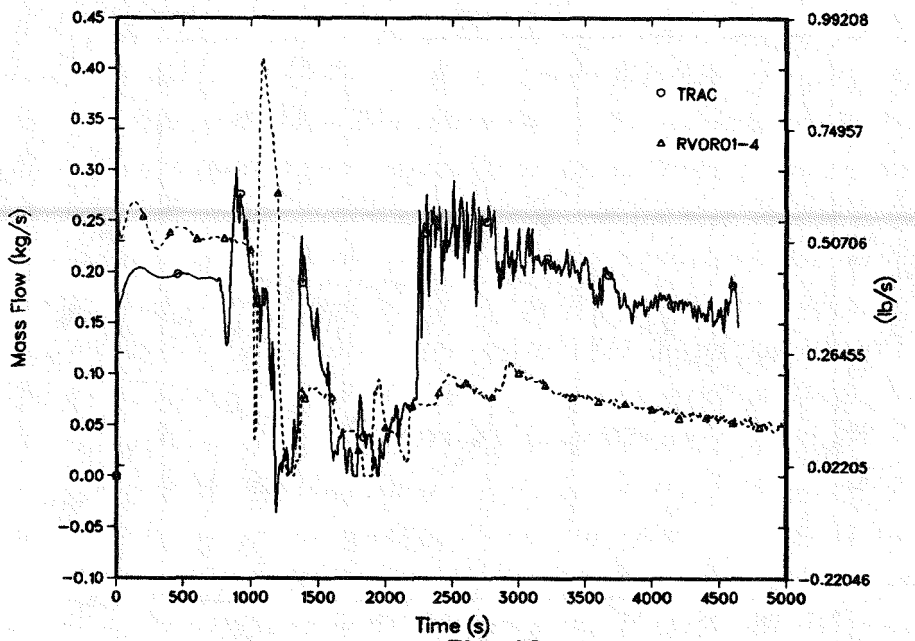

Fig. 19.
RVVV mass flow.

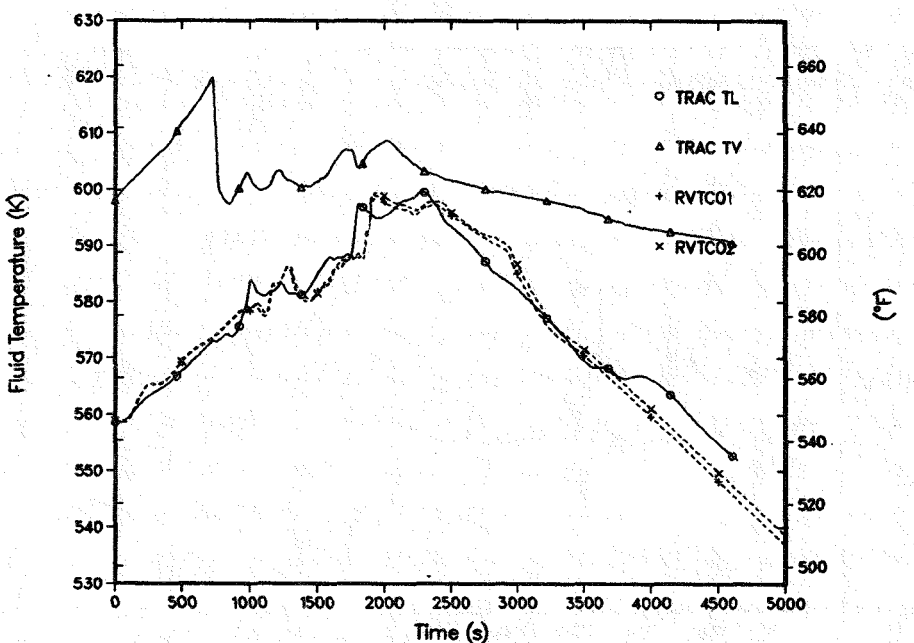

Fig. 20.
Core inlet fluid temperatures.

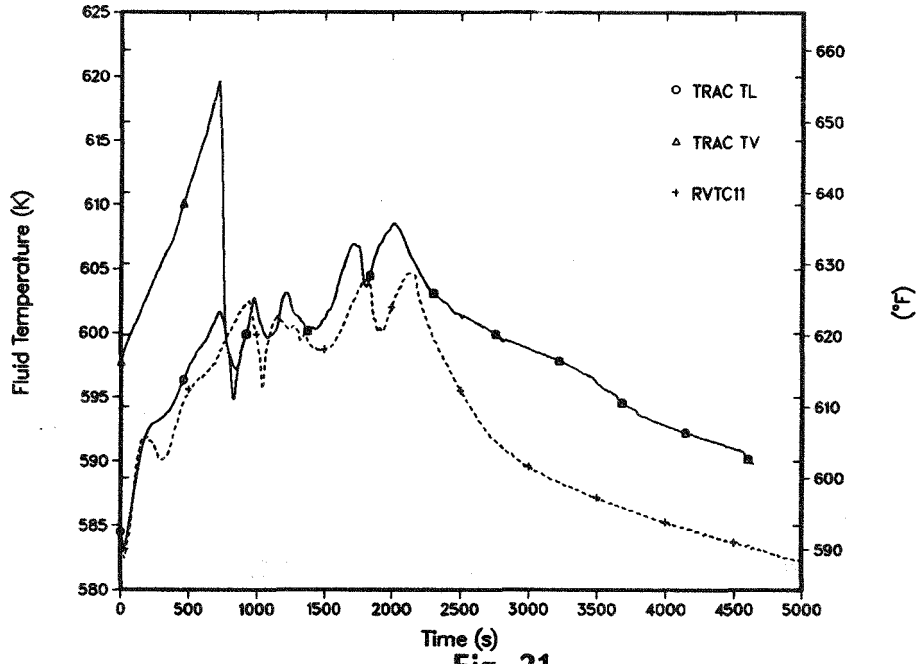

Fig. 21.
Core outlet fluid temperatures.

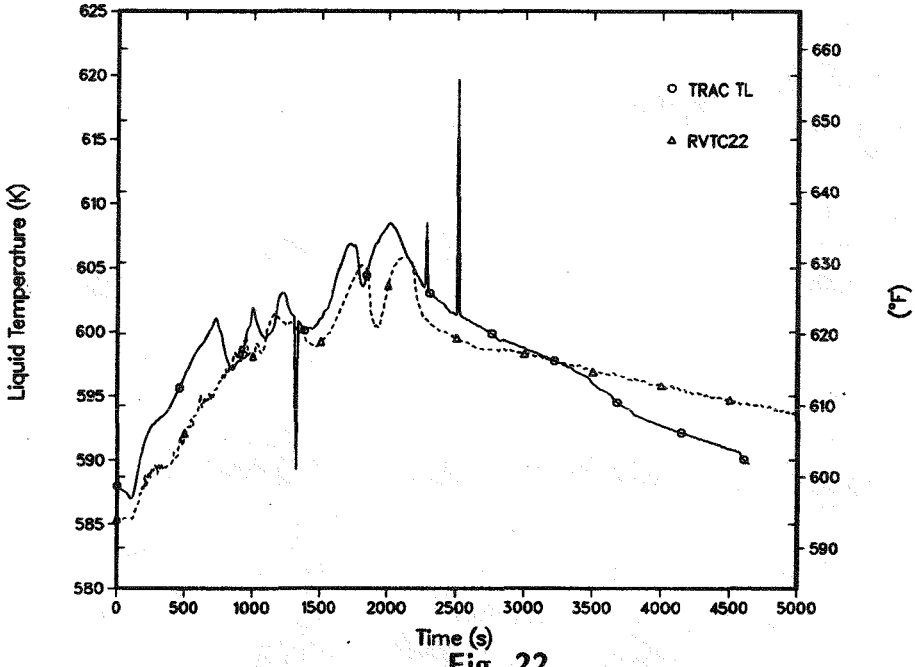

Fig. 22.
Upper-plenum fluid temperatures.

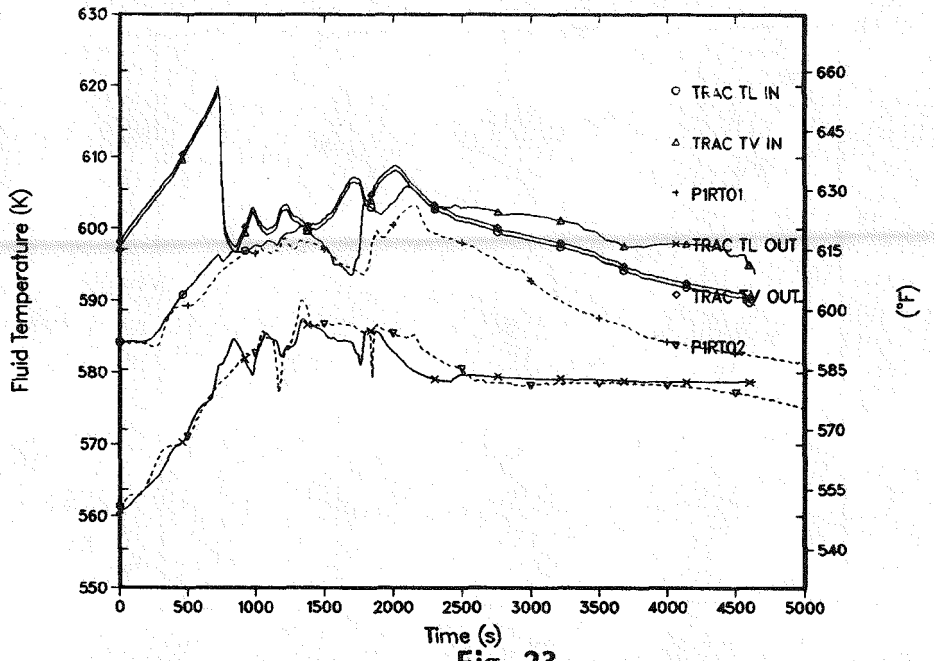

Fig. 23.

Loop-A inlet- and outlet-plenum fluid temperatures.

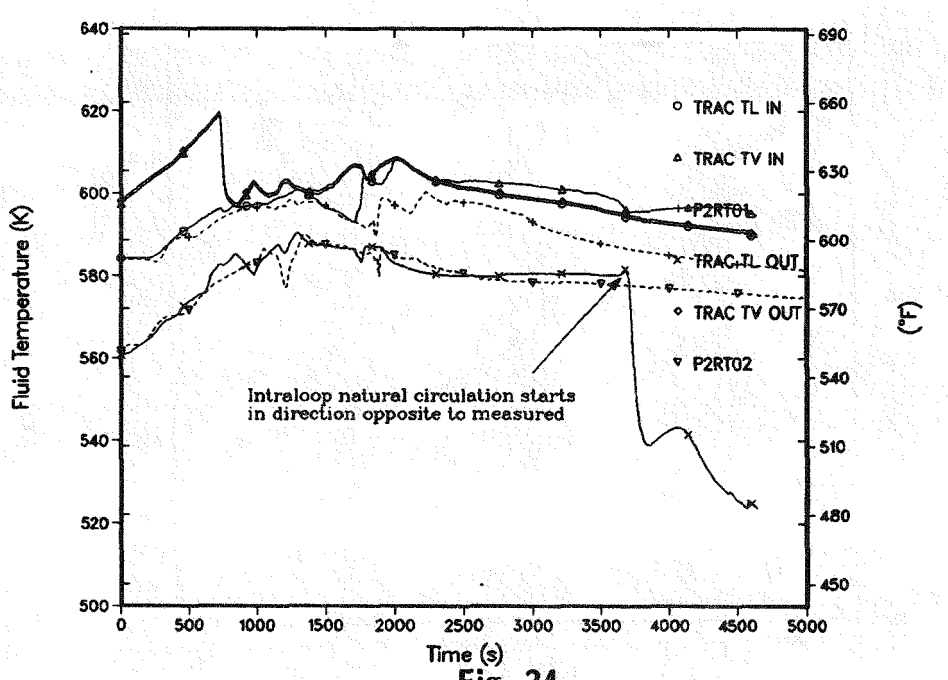

Fig. 24.

Loop-B inlet- and outlet-plenum fluid temperatures.

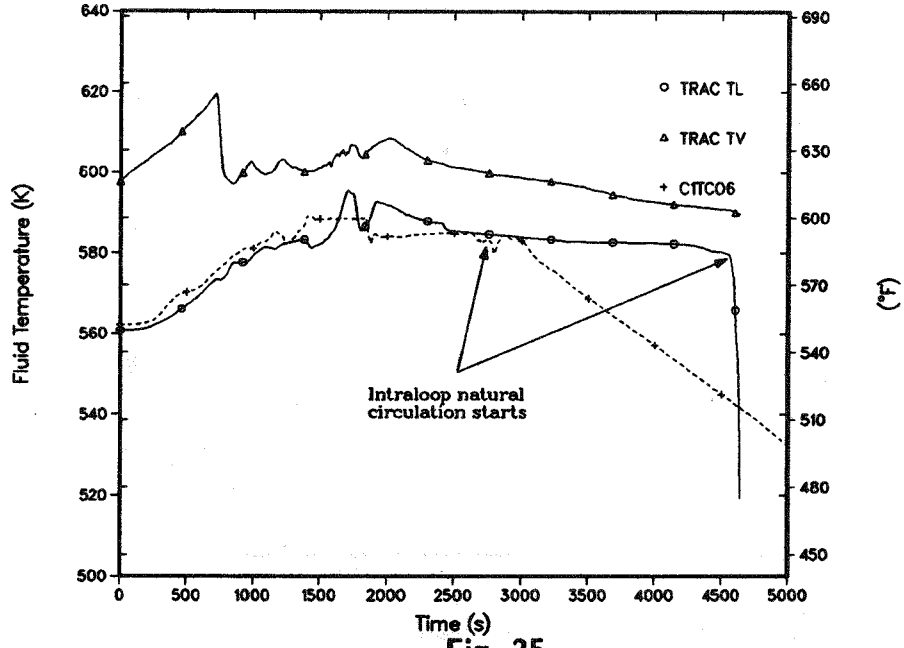

Fig. 25.
Loop-A1 pump-suction fluid temperatures.

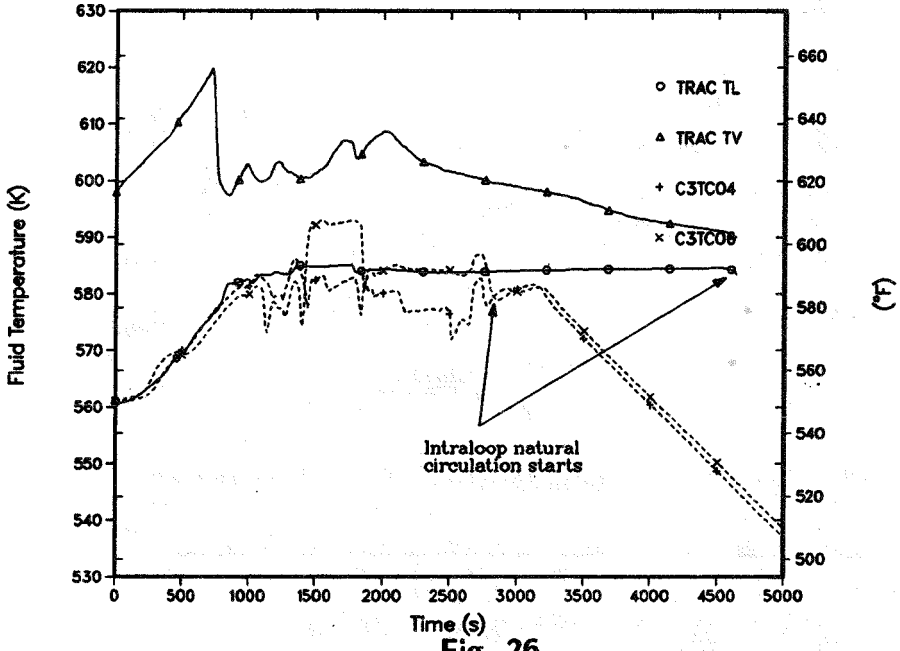

Fig. 26.
Loop-A2 pump-suction fluid temperatures.

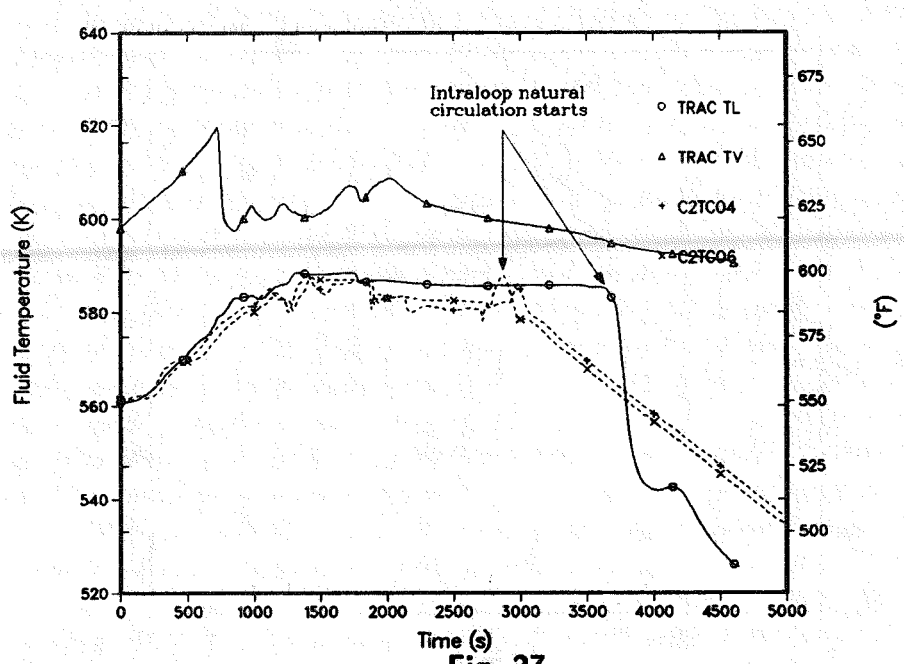

Fig. 27.

Loop-B1 pump-suction fluid temperatures.

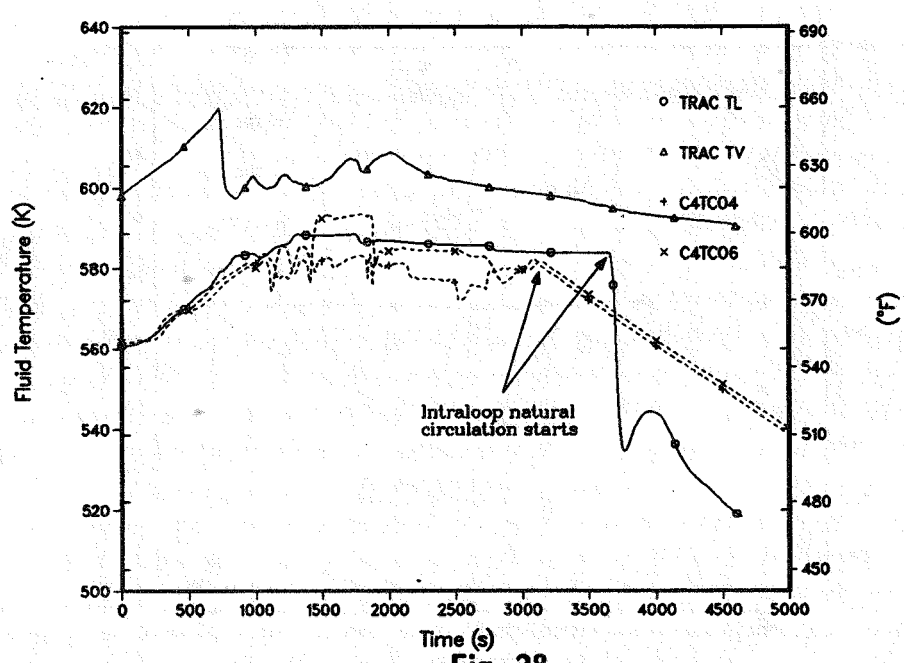

Fig. 28.

Loop-B2 pump-suction fluid temperatures.

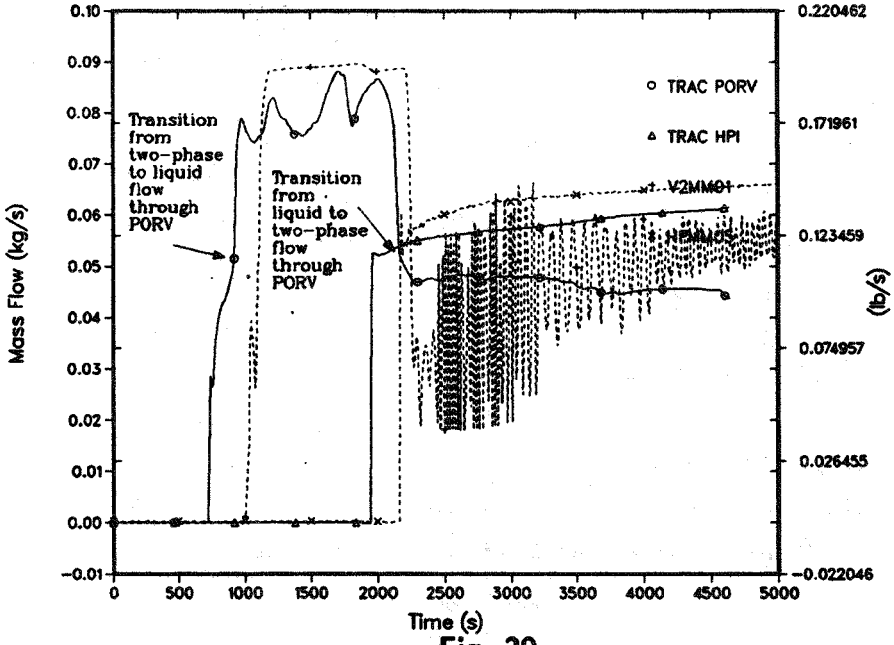

Fig. 29.
PORV and HPI mass flows.

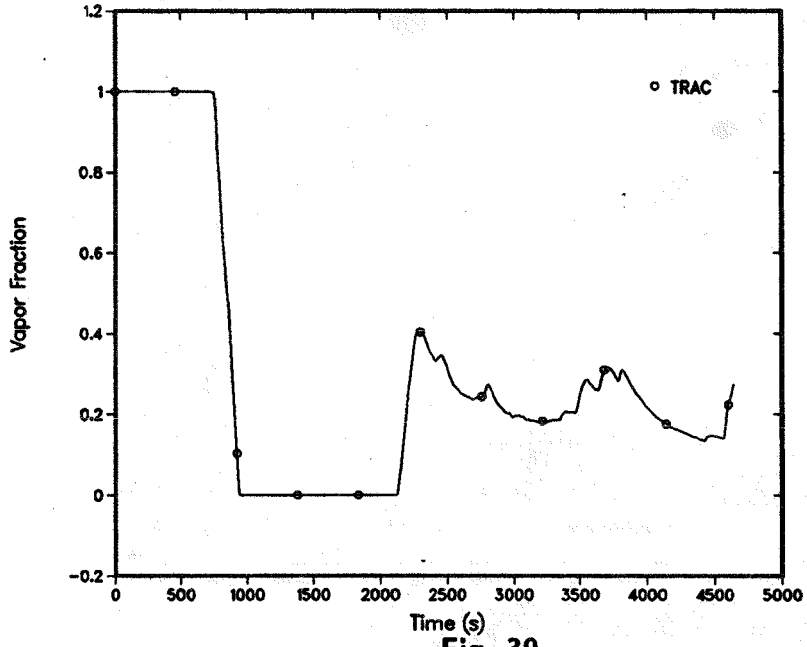

Fig. 30.
Vapor fraction upstream of PORV.

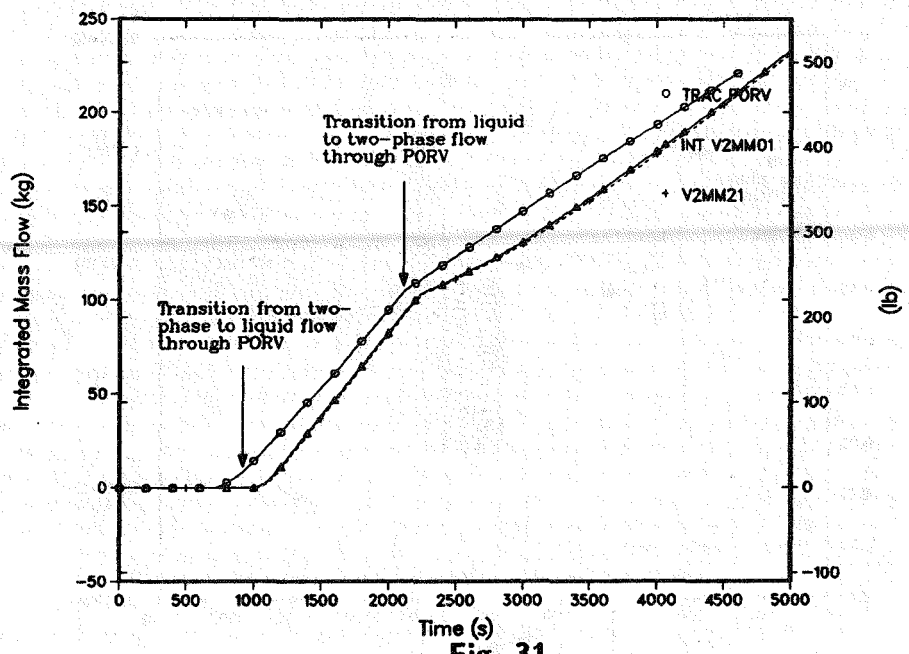

Fig. 31.
PORV integrated mass flow.

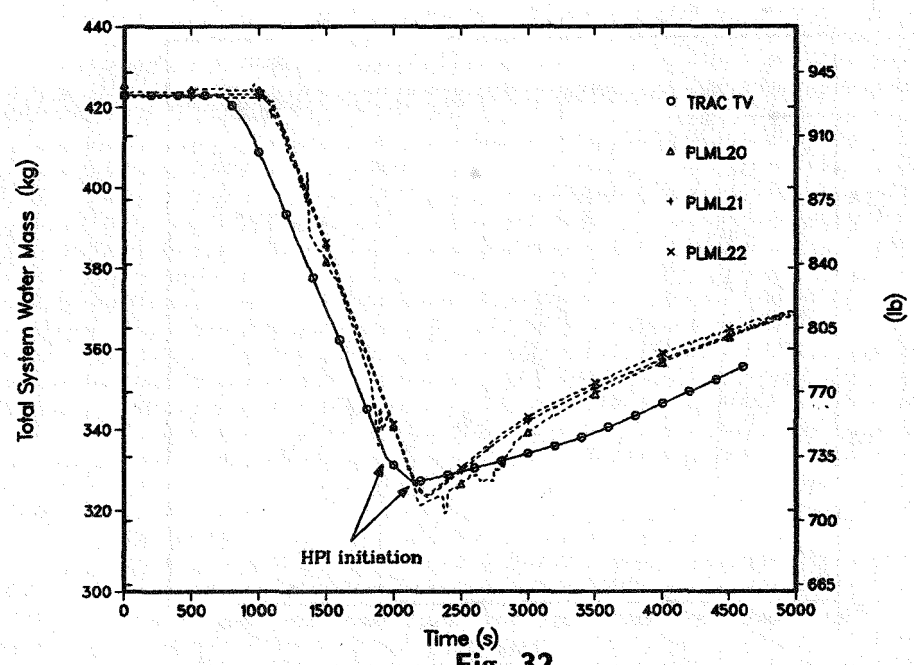

Fig. 32.
Primary-system water mass.

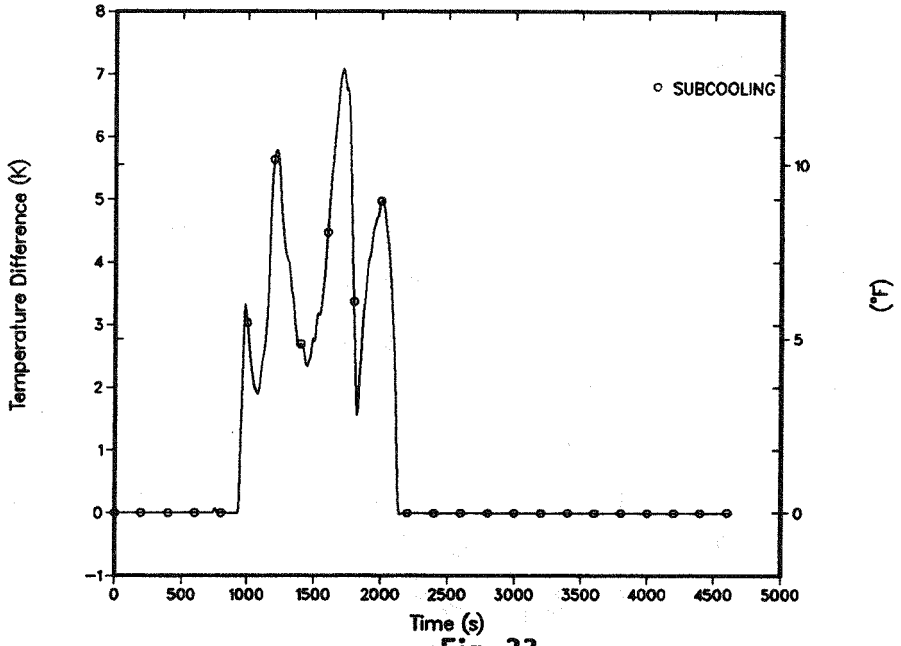

Fig. 33.
Liquid subcooling upstream of PORV.

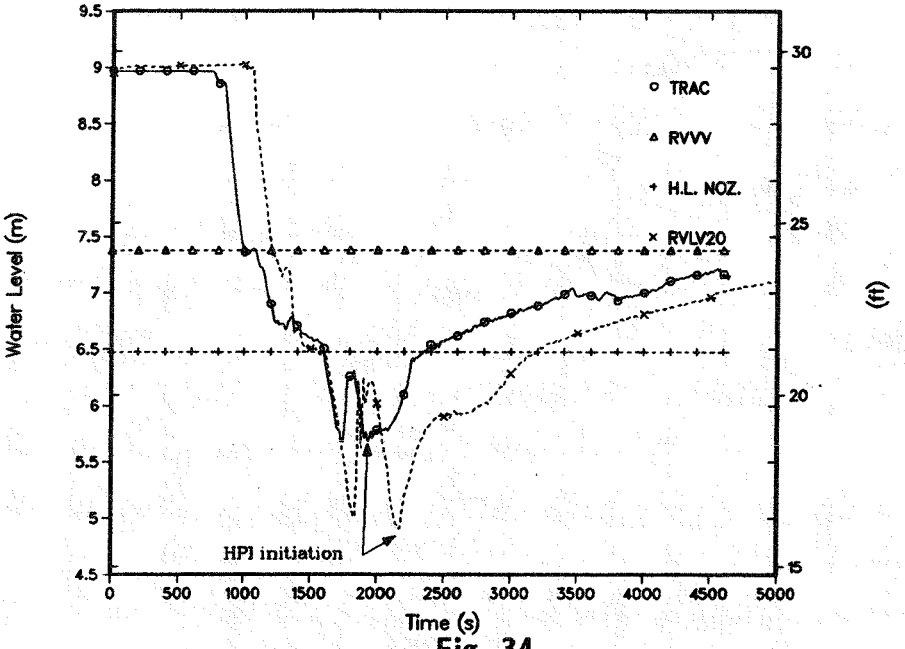

Fig. 34.
Reactor-vessel collapsed liquid level.

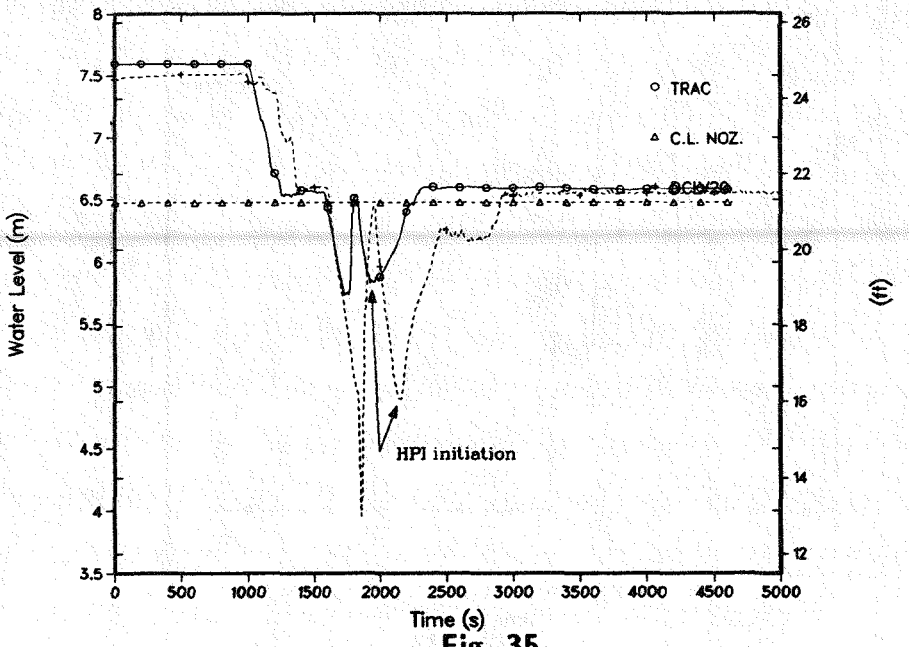

Fig. 35.

Downcomer collapsed liquid level.

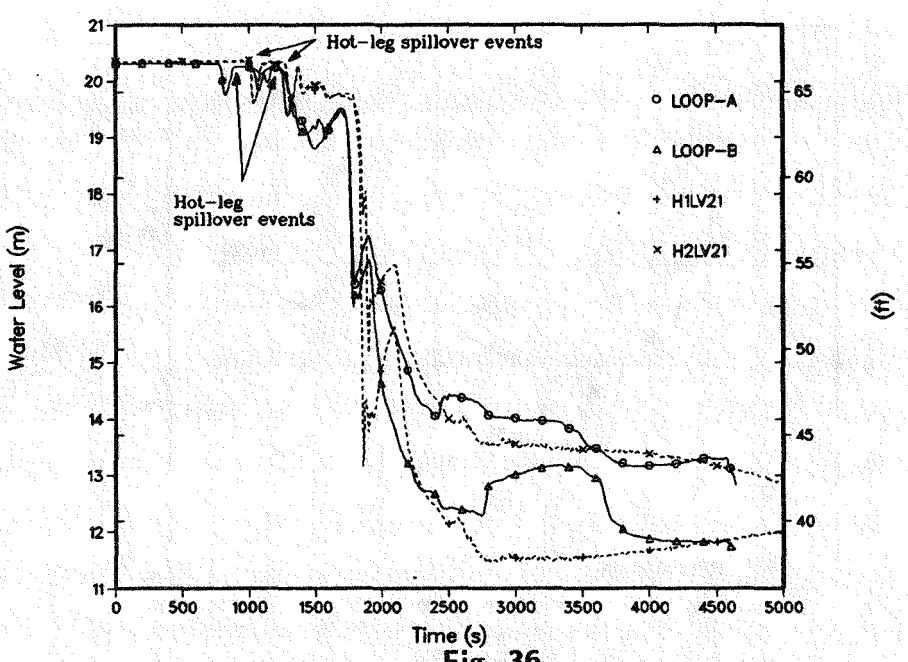

Fig. 36.

Hot-leg collapsed liquid levels.

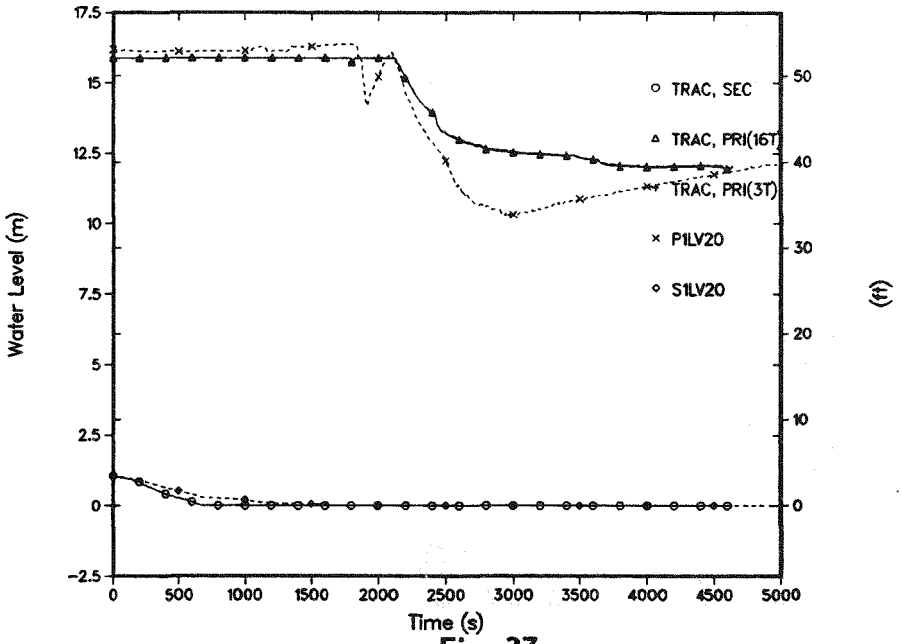

Fig. 37.

Loop-A SG primary and secondary collapsed liquid levels.

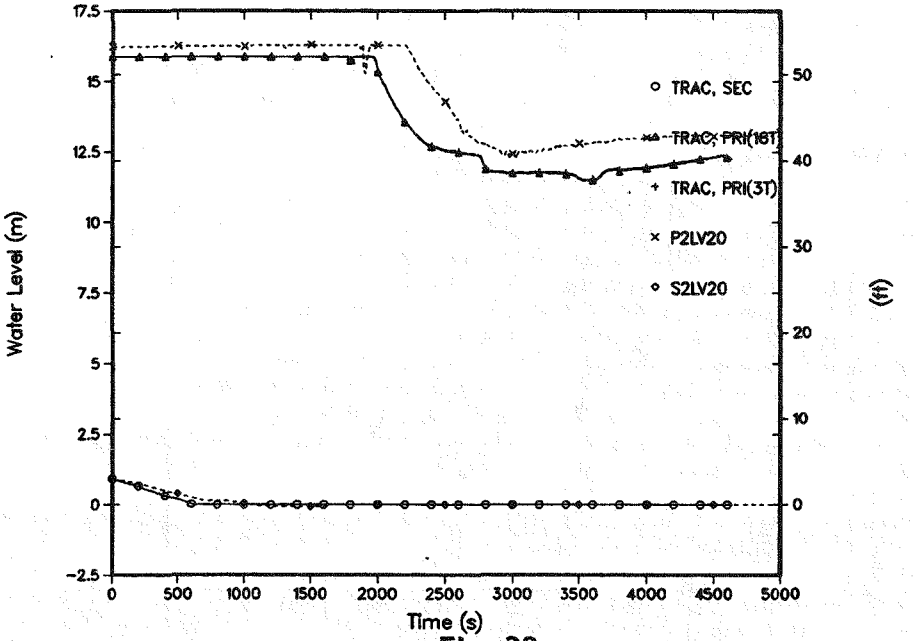

Fig. 38.

Loop-B SG primary and secondary collapsed liquid levels.

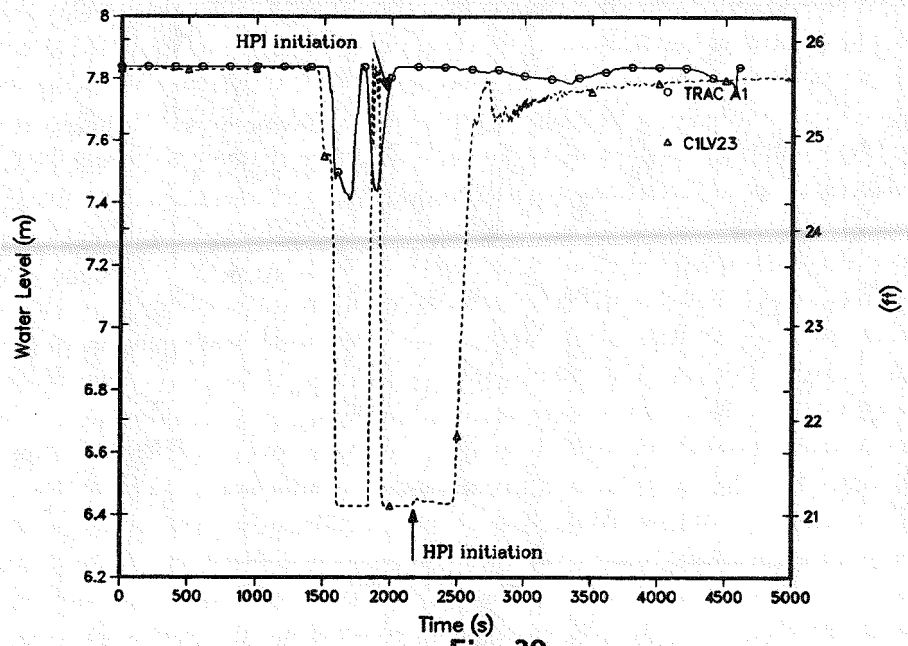

Fig. 39.

Loop-A1 cold-leg collapsed liquid levels.

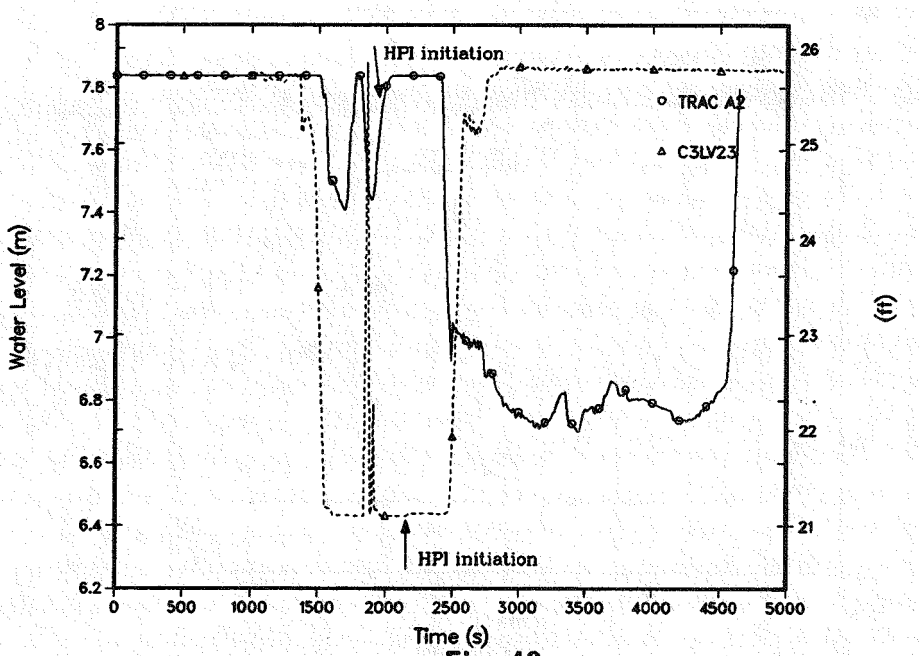

Fig. 40.

Loop-A2 cold-leg collapsed liquid levels.

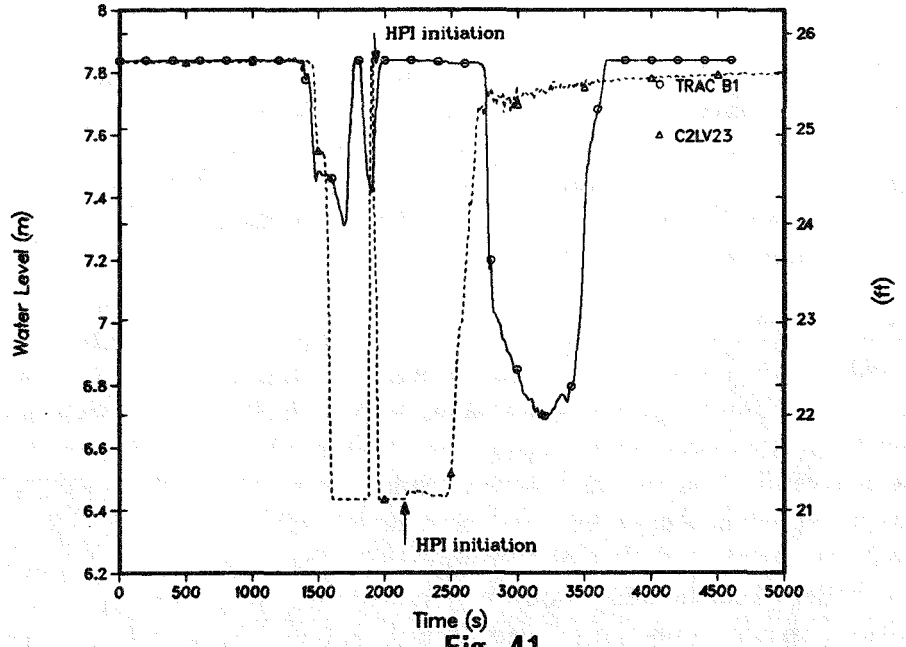

Fig. 41.
Loop-B1 cold-leg collapsed liquid levels.

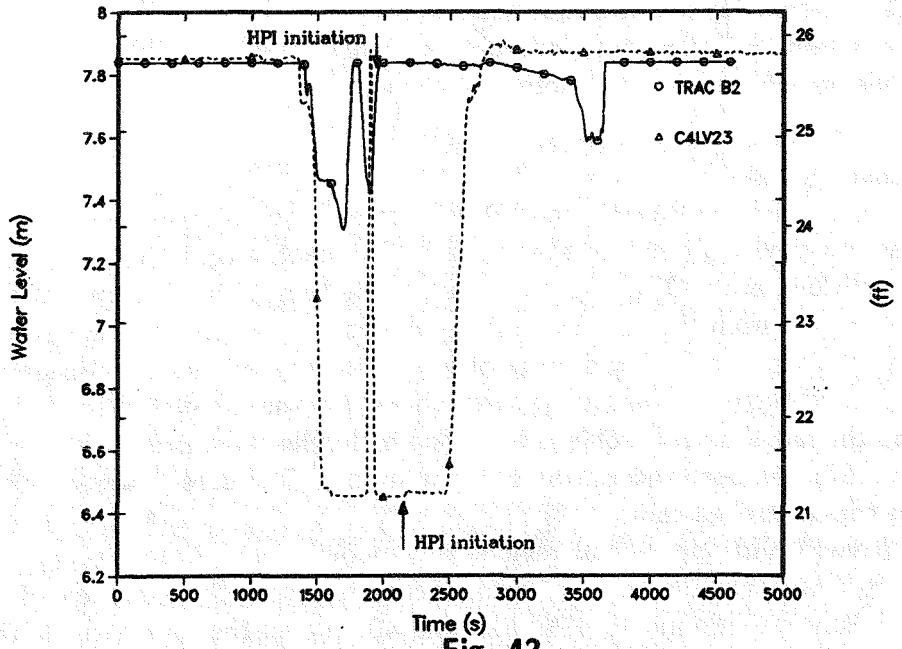

Fig. 42.
Loop-B2 cold-leg collapsed liquid levels.

APPENDIX A

TRAC Model of MIST Facility

The MIST facility, shown in Fig. A-1, is a scale model of a B&W nuclear power plant. The facility is designed to investigate the effectiveness of plant automatic safety systems and operational procedures during postulated small-break and operational transients. The facility is primarily intended to investigate events occurring after reactor trip and reactor coolant-pump coastdown. The MIST facility is scaled to a 2×4 lowered-loop prototype plant with 177 fuel assemblies. The scale factor is 1/817 for volume and power; component elevations are scaled one to one.

The TRAC model of the MIST facility has evolved over a period of time. The model was initially based on preliminary information provided in the MIST facility specification.[5] It has progressed to its present form as available, as-built facility information was received from B&W. The final model compares very closely to the B&W REDBL5 model described in the MIST design verification report.[6] Archival information about the TRAC model used in this study is presented in Appendix A. A component schematic of the MIST model is shown in Fig. A-2. The model consists of 77 components that have been subdivided into 251 fluid cells. This model is considered to be finely noded and should be capable of providing reasonable results as shown in previous Once-Through Integral System (OTIS) calculations. Table C-I lists the components used for the MIST model and the number of fluid cells in each component. The outer walls of the vessel and loop piping components are generally modeled as adiabatic boundaries since the MIST facility is guard heated to eliminate external heat losses. Localized uncompensated heat losses caused by cooled instruments are modeled using a constant heat-transfer coefficient at the component outer wall. The local heat-transfer coefficients were determined from heat-loss data provided by B&W. The following sections describe the modeling philosophy and actual modeling details of the various MIST facility components.

A. Reactor Vessel

A series of PIPE, TEE, PLENUM, and VALVE components has been connected to a 1-D CORE component to physically model the entire MIST reactor vessel (Fig. A-3). The 1-D CORE component (Component 3) is used to simulate the heated core region and a portion of the upper-plenum region from the core exit to an elevation slightly below the hot-leg nozzles. The heated core consists of a 7×7-rod array of which 45 rods are electrical heater rods and 4 rods simulate guide tubes. The axial power shape for the simulated rod is a chopped cosine profile and the radial power profile is flat. The hydraulic resistance from the rod-bundle grid spacers (k=0.57) has been incorporated in the model. The core-power decay history is modeled using a trip-controlled table.

The upper-plenum and upper-head regions are modeled with Components 401–412 as shown in Fig. A-3. These one-dimensional components represent the geometry of the upper-vessel region as follows: Components 401, 402, and 403 model the region inside the plenum cylinder; the annular region between the plenum cylinder and the vessel is modeled with Components 408–412; and the upper-head region above the plenum cylinder is represented by Components 404 and 405. The RVVVs and vent-valve nozzles are modeled with a VALVE component (Component 7) that is connected to PLENUM Component 411.

The MIST RVVV system consists of four vent valves and connecting lines from the upper plenum to the upper downcomer. The actual system has been modeled as a single valve and associated piping. The valve-stroke time of 2.0 s and hydraulic-loss coefficient of 95.0 have been modeled. A trip-control system controls the opening and closing of the valve based on opening the valve when the pressure drop across the valve is 861.8 Pa (0.125 psi) and closing at 275.8 Pa (0.040 psi). An outer heat-transfer coefficient was applied to the valve to model the uncompensated localized heat loss of the valves of 1480 W (5.05×10^3 Btu/h).

The primary tube of TEE Component 2 represents the lower-plenum region, whereas the secondary tube models all the piping configuration connecting the lower plenum and the vertical downcomer. Components 103 and 104 model the 0.076-m (3-in.) sch 80 piping and the lower portion of the downcomer annulus region slightly below the cold-leg nozzles. Component 103 represents the piping that contains the cooled thermocouple (TC) and includes an outer heat-loss coefficient to model the TC's uncompensated heat loss of 1100 W (3.855×10^3 Btu/h). Component 8 is a PLENUM component used to model the connections of the cold-leg nozzles to the downcomer annulus. The upper portion of the downcomer annulus, RVVV nozzle, and core-flood tank (CFT) nozzle are simulated with TEE Component 9.

The fluid in the downcomer annulus region was initially assumed to follow one-dimensional behavior, and this was later verified in a sensitivity study that incorporated a three-dimensional model of the downcomer annulus region. The results of this study showed that, although small multidimensional effects were present in the downcomer annulus, they did not affect vessel and loop behavior as compared to results obtained with the one-dimensional downcomer model.

An ACCUM and a VALVE component were used to model the CFT system (Components 10 and 11). The CFT is initially 75% full of 316.5 K (110.3°F) water at a pressure of 4.137 MPa (600 psi). The surge line and valve are connected to the upper-downcomer region at the 7.087-m (23.25-ft) elevation. The VALVE component models the CFT isolation valve, which is dependent on calculated system conditions.

B. Intact Loop

In the MIST facility, the intact loop was designated as the loop containing the pressurizer. All components of the intact loop are shown in Fig. A-4 and described in Table A-1. The hot-leg nozzle and piping to the pressurizer surge line are simulated by the primary tube of Component 21. Also, an outer heat loss of 640 W (2.18×10^3 Btu/h) was modeled to simulate the heat loss of the viewports and densitometer located near the hot-leg nozzle region. The secondary tube represents the pressurizer surge line. Components 22 and 23 model the pressurizer and power-operated relief valve (PORV), respectively. The balance of the hot leg is represented by Components 108, 25, and 109. Component 25 included a connection to the high-point vent (HPV) valve and an outer heat-transfer coefficient to model an uncompensated heat loss of 170 W (0.58×10^3 Btu/h) through a viewport in the U-bend.

The MIST intact loop SG was modeled with a STGEN component (Component 29) and two PLENUM components (Components 28 and 30) as shown in Fig. A-5. Considerable effort was expended on the SG model during the OTIS posttest calculations and in preliminary MIST posttest calculations. The STGEN Component 29 includes two parallel fluid channels to represent the primary side of the intact loop MIST SG. The first channel represents the sixteen tubes not wetted on the outside by the AFW, and the second channel represents the three tubes adjacent to the AFW injection nozzle on the secondary. Both of the primary

channels are divided into twelve axial cells. The secondary side of the MIST intact loop SG was modeled with a single fluid channel, also consisting of twelve axial cells. Three tees and a pipe were used for the secondary side. Two tee side legs were used for the SG downcomer. The falling film heat transfer from the AFW is calculated using a code update that redistributes the liquid in each of the secondary cells to the heat slabs connected to the 3-tube primary channel. In addition to the liquid redistribution, a multiplier is applied to the Chen correlation heat transfer coefficient for the wetted channel heat slabs. The head-vs-flow curve for the SG AFW is modeled with FILL Component 31.

Components 28 and 30 model the inlet and exit plena, respectively, and provide the connection between the loop piping and SG primary tubes. The lower tube sheet and outer shell wall have been included in the heat-transfer data. No special code models have been used to vary the tube wetted areas or the heat-transfer coefficients based on AFW flow.

The split cold legs from the SG exit plenum to the downcomer consist of Components 34, 117, 118, 36, 38, 115, 116, and 40. The pump-suction piping, pump-discharge piping, and HPI ports are modeled by these components. Each pump suction and discharge line is constructed of 0.051-m (2-in.) sch 80 piping, 10.82 m (35.5 ft) and 1.75 m (5.74 ft) in length, respectively. The two primary-coolant pumps located in the intact-loop cold legs are modeled with PUMP Components 35 and 39. Each of the identical PUMP components represents a fluid volume of 0.007334 m^3 (0.26 ft^3) and a flow length of 1.608 m (5.28 ft) and models the locked-rotor resistance of the MIST pumps. Uncompensated local heat losses of 1350 W (4.61×10^3 Btu/h) per pump are modeled by outer heat-transfer coefficients in the PUMP components.

C. Broken Loop

The broken-loop piping and SG components are shown in Figs. A-6 and A-7. These components are described in Table A-1, and they are identical to the corresponding intact-loop components, except that there is no pressurizer connection to the broken loop. Thus, PIPE Component 105 in the broken-loop hot leg is identical to the primary side of TEE Component 21 in the intact-loop hot leg. The broken loop SG in modeled in exactly the same manner as the intact loop SG with STGEN Component 54 and PLENUM Components 53 and 55.

D. HPI System

The HPI system is modeled with Components 41, 59, and 37. FILL Component 41 is used to model the HPI fluid conditions and flow rate. The HPI flow rate used in Component 41 is determined in a series of control blocks, which monitor the calculated cold-leg pressure, pressurizer level, and core-exit subcooling. Using these parameters, the control blocks model the head-flow characteristics of the HPI pump and the logic for the HPI actuation and throttling of the HPI flow. The HPI flow rate determined in the control blocks is then used in FILL Component 41. The HPI piping and manifold are modeled with PIPE Component 59 and PLENUM Component 37, the latter of which is connected to each cold-leg pump discharge.

E. Controls

The steady-state and transient-control functions are modeled using signal variables, control blocks, and trips. These control parameters are used to control the core power, SG AFW and discharge flows, HPI flow, RVVVs, the PORV, and the CFT isolation valve. The transient

control logic is implemented in the input for the steady-state calculation, thus simplifying the transient restart input. Most of the control logic is modeled using control blocks; the control parameters are evaluated once each time step.

TABLE A-I
COMPONENT DESCRIPTION OF MIST MODEL

Component Numbers	Component Description	Number of Cells
1	Bottom of reactor vessel	1
2	Lower plenum and lower downcomer	3
3	Core and upper plenum	7
401	Upper plenum, hot-leg elevation	3
402	Upper plenum, middle section	2
403	Upper plenum, upper section	2
404	Upper head, lower section	1
405	Upper head, upper section	1
406	Top of reactor vessel	1
407	Upper-plenum cylinder, bottom cap	1
408	Upper-plenum cylinder, lower section	1
409	Upper-plenum cylinder, hot leg connections	1
410	Upper-plenum cylinder, middle section	1
411	Upper-plenum cylinder, vent valve connections	1
412	Upper-plenum cylinder, upper section	1
7	Reactor vessel vent valve	4
8	Downcomer (cold leg nozzle connections)	1
9	Upper downcomer	5
103	Lower downcomer	1
104	Lower downcomer	4
10	Core flood tank valve	2
11	Core flood tank	3
21	Loop A hot leg (lower section)	8
22	Pressurizer	4
23	PORV	2
24	Pressurizer atmospheric boundary	1
108	Loop A hot leg	4
25	Loop A hot leg (upper section)	2
26	Loop A high point vent valve	2
27	Loop A high-point vent (HPV) atmospheric boundary	1
109	Loop A hot leg	3
28	Loop A STGEN inlet plenum	1
29	Loop A STGEN	42
30	Loop A STGEN exit plenum	1
31	Loop A STGEN high AFW fill	1

TABLE A-I (cont.)
COMPONENT DESCRIPTION OF MIST MODEL

Component Numbers	Component Description	Number of Cells
91	Steam Line	2
32	Loop A STGEN secondary atm. boundary	1
34	Cold-leg A1 pump suction	2
117	Cold-leg pump suction	1
118	Cold-leg pump suction	3
35	Cold-leg A1 pump	2
36	Cold-leg A1 pump discharge	5
38	Cold-leg A2 pump suction	2
115	Cold-leg pump suction	1
116	Cold-leg pump suction	3
39	Cold-leg A2 pump	2
40	Cold-leg A2 pump discharge	5
105	Loop B hot leg (lower section)	4
106	Loop B hot leg (upper section)	4
50	Loop B hot leg	2
51	Loop B high point vent valve	2
52	Loop B HPV atmospheric boundary	1
107	Loop B hot leg	3
53	Loop B STGEN inlet plenum	1
54	Loop B STGEN	42
95	Steam line	2
69	Loop B STGEN secondary atmospheric boundary	1
68	Loop B STGEN upper auxiliary feed	1
55	Loop B STGEN exit plenum	1
56	Cold-leg B2 pump suction	2
119	Cold-leg B2 pump suction	1
120	Cold-leg B2 pump suction	3
57	Cold-leg B2 pump	2
58	Cold-leg B2 pump discharge	5
60	Cold-leg B1 pump suction	3
61	Cold-leg B1 pump-suction leak valve	2
62	Leak atmospheric boundary	1
121	Cold-leg B1 pump suction	1
63	Cold-leg B1 pump	2
122	Cold-leg B1 pump suction	3
64	Cold-leg B1 pump discharge (upper)	4
66	Cold-leg B1 pump discharge (lower)	2

TABLE A-I (cont.)
COMPONENT DESCRIPTION OF MIST MODEL

Component Numbers	Component Description	Number of Cells
67	Cold-leg B1 pump-discharge leak valve	2
80	Leak atmospheric boundary	1
37	HPI manifold	1
41	HPI fill	1
59	Connection between HPI fill and manifold	1
	components	77
	fluid cells	276

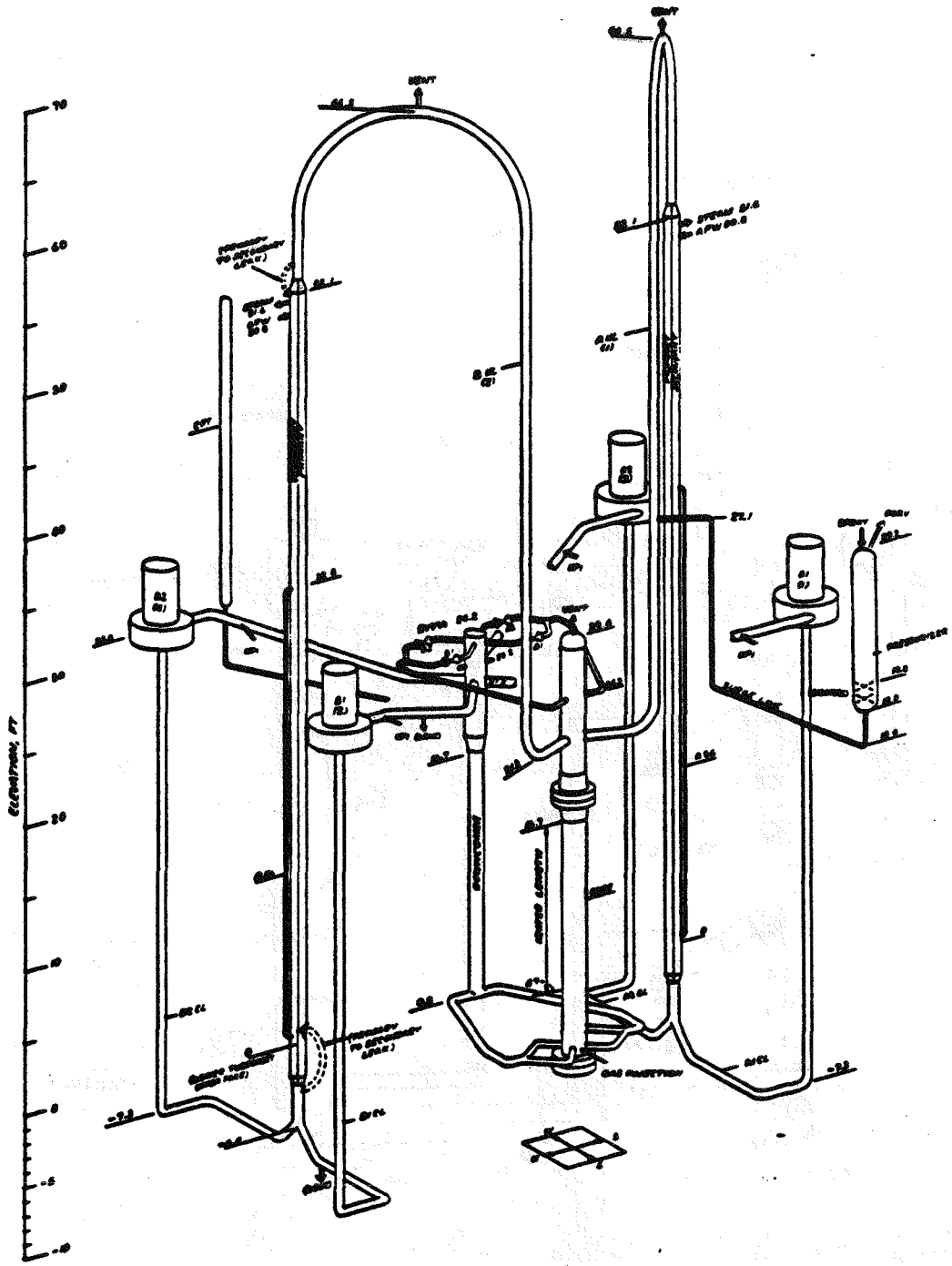

Fig. A-1.
MIST facility isometric.

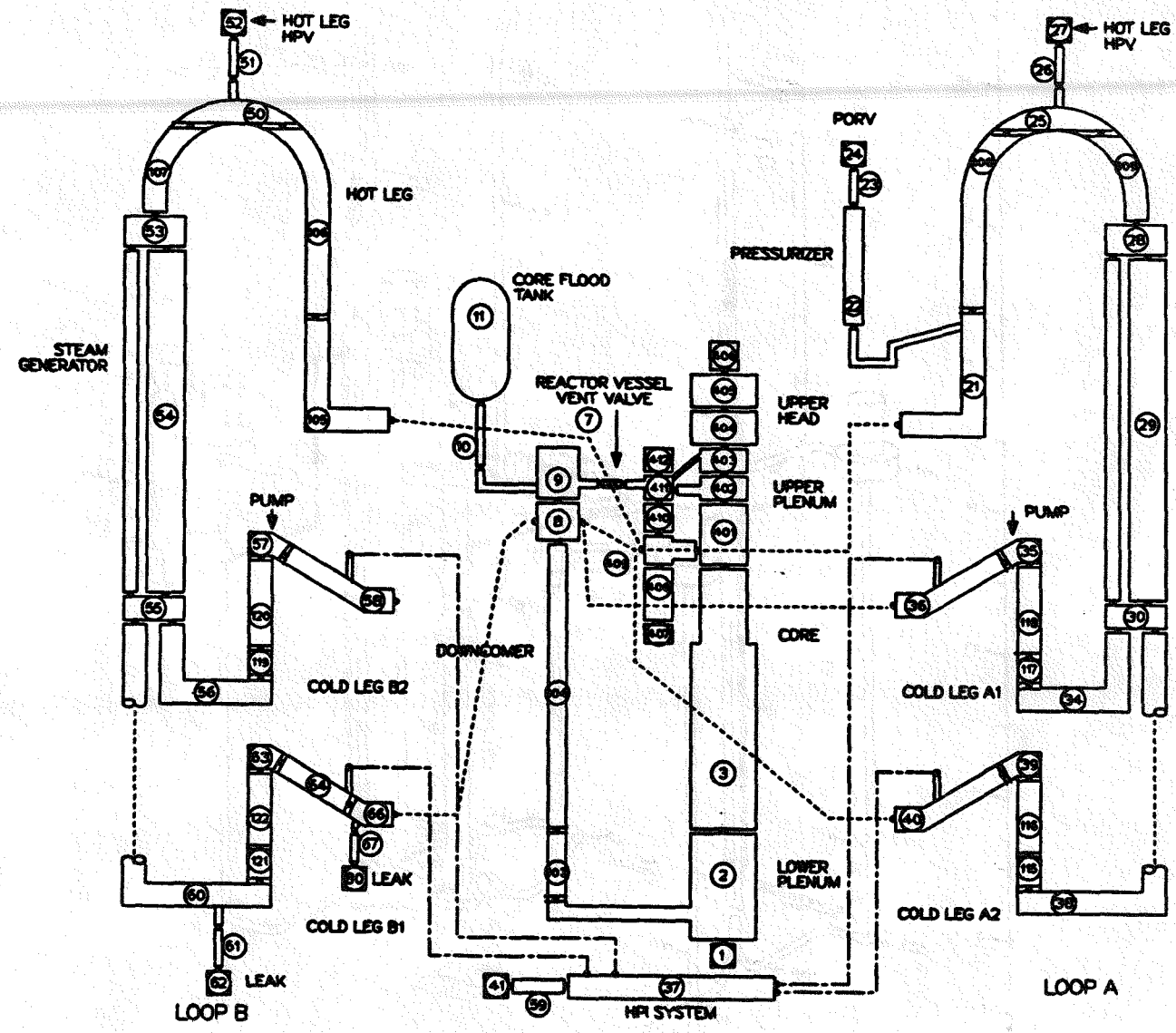

Fig. A-2.
TRAC component noding schematic of MIST facility.

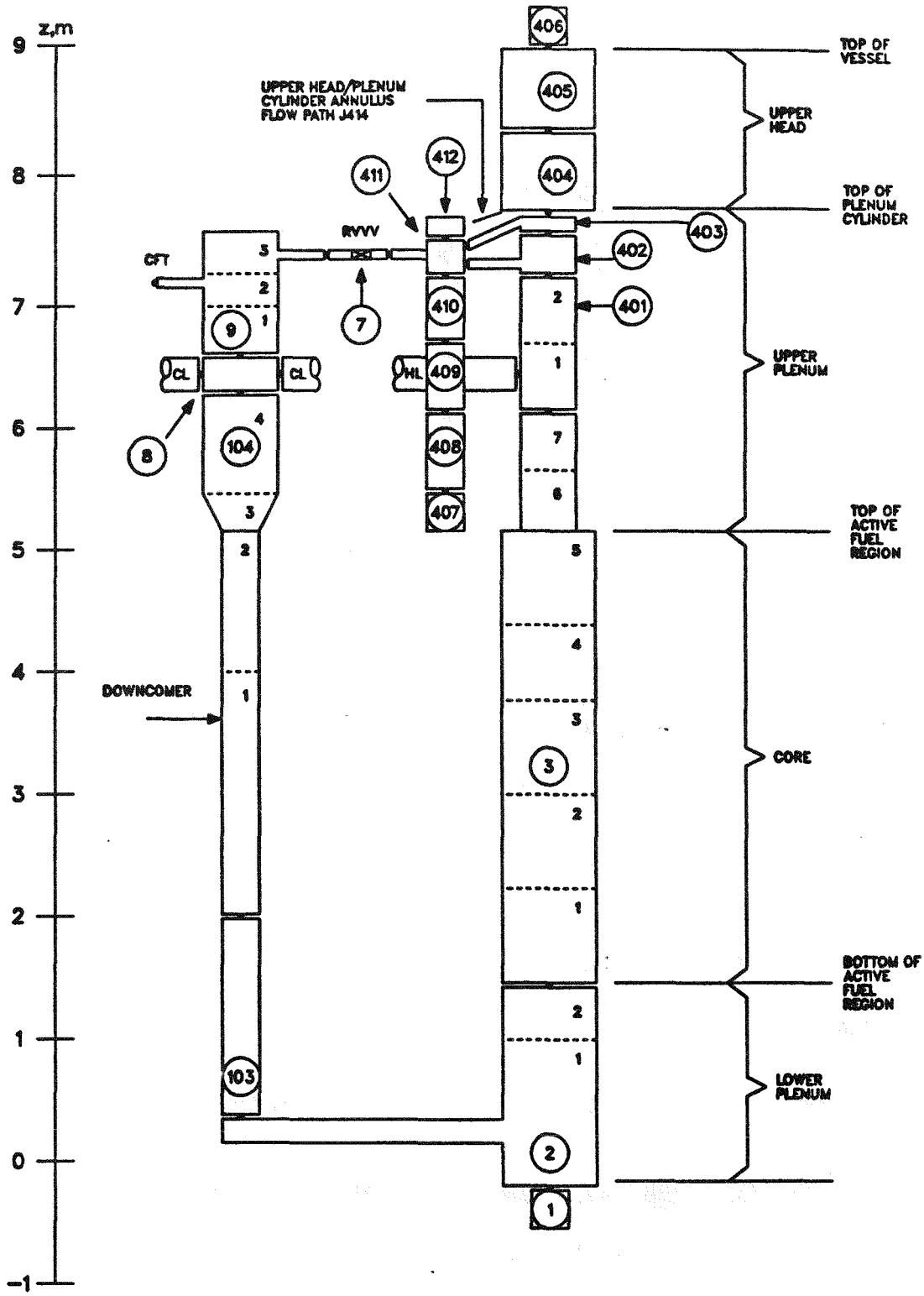

Fig. A-3.
TRAC reactor-vessel noding schematic of MIST facility.

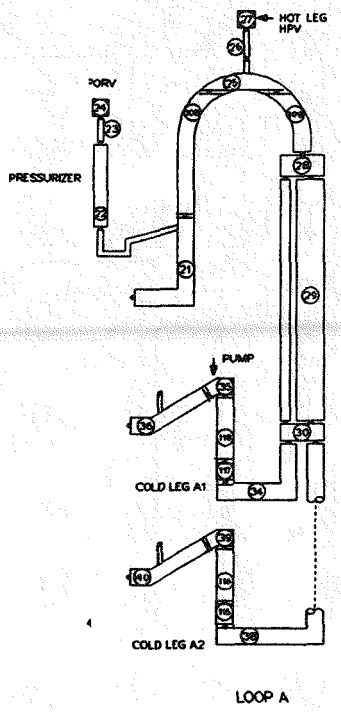

Fig. A-4.
TRAC Loop-A noding schematic of MIST facility.

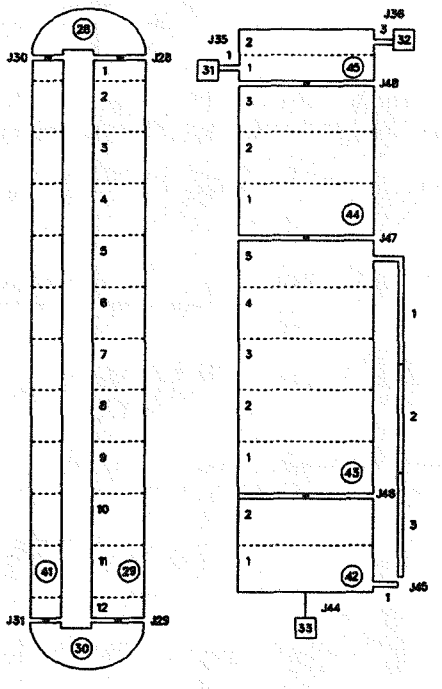

Fig. A-5.
TRAC Loop-A steam-generator noding schematic of MIST facility.

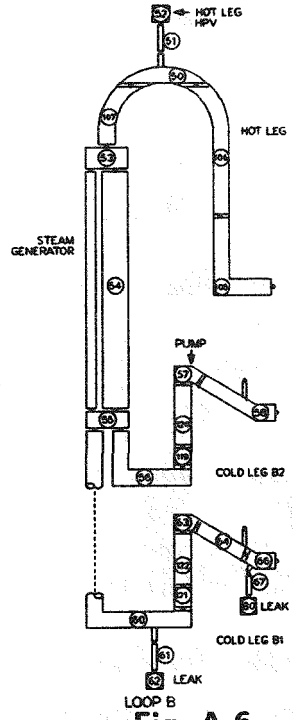

Fig. A-6.
TRAC Loop-B noding schematic of MIST facility.

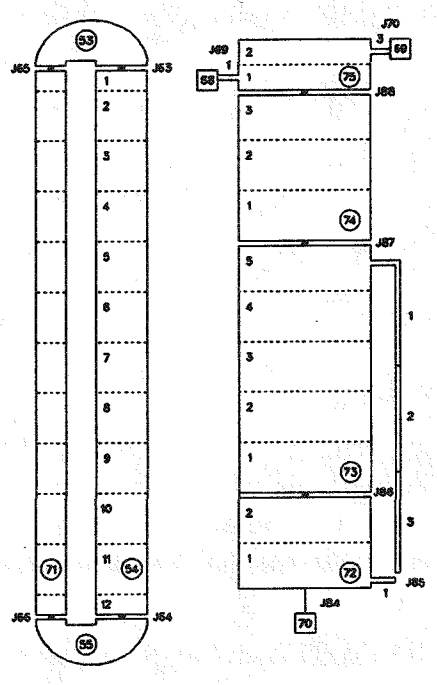

Fig. A-7.
TRAC Loop-B steam-generator noding schematic of MIST facility.

APPENDIX B
ARCHIVAL INFORMATION

I. CODE IDENTIFICATION AND STORAGE

TRAC-PF1/MOD1 with error correction sets through 14.3 was used for the posttest calculation of MIST 330302. The program library and updates required to recreate this code are stored on the Los Alamos Central File System (CFS) and may be accessed through the following path:

/Q9TRAC/ARCHIVES/14.3

In addition, a MIST specific code update named STGN1X was used. Initialization of the MIST facility in natural circulation rather than pumped flow caused modeling difficulties unique to this facility. An accurate prediction of SG heat-transfer distribution is necessary to correctly predict steady-state loop flows and hence initial system pressure and temperatures. Code modifications were required to achieve this. A listing of this update is provided at the end of this appendix.

II. INPUT DECK STORAGE

The TRAC input deck which contains the model of the MIST facility is permanently stored in the TRAC Input Deck Archive (TIDA) on the Los Alamos CFS and may be accessed through the following path:

/TIDA/EXPERIMENT/MIST/number of this report, *e.g.*, LA-CP-XX-XXXX

III. CALCULATION FILE STORAGE

The output (TRCMSG, TRCOUT, TRCGRF, TRCDMP) files generated by TRAC during the calculation of MIST 330302 are stored on the Los Alamos CFS and may be accessed through the following path:

/ISTP/MIST/POSTTEST/330302

These files will be maintained for a minimum of one year from the publication date of this report.

IV. UPDATE STGN1X LISTING

This update is a hardwired change to the code logic for distributing high-elevation AFW between wetted and unwetted tube regions on the SG secondary. This update is specific to the MIST facility and will not be incorporated into a released version of TRAC-PF1/MOD1. This update is permanently stored in the TIDA on the Los Alamos CFS and may be accessed through the following path:

/TIDA/EXPERIMENT/MIST/number of this report, *e.g.*, LA-CP-XX-XXXX

```
*id mistcu
*i stgn1x.15                    stgn1x
c
c  iflgw is flag to detect steam generator tube heat
c          structure which is wetted by the afw
c
c  iflgwc is flag to detect a wetted steam generator tube heat
c          structure to which the chen multiplier is applied
c
c  iflgd is flag to detect steam generator tube heat
c          structure which is not wetted by the afw
c
c  hlc1 and hlc0 are the multiplier and additive constant for
c  the liquid heat transfer coefficient
c
c  hvc1 and hvc0 are the multiplier and additive constant for
c          the vapor heat transfer coefficient
c
c  alphamw is the maximum void fraction used to determine
c          the heat transfer coefficients for the wetted
c          steam generator tubes above the pool
c
c  alphad is the void fraction used to determine the heat
c          transfer coefficients for the unwetted steam
c          generator tubes above the pool
c
c  alpha0 is the minimum void fraction for identifying steam
c          generator secondary cells which are above the liquid pool
c
c  alpha1 is the minimum void fraction for reducing the void
c          fraction used to determine the heat transfer coefficients
c          for the wetted steam generator tubes above the pool
c
c          alpha2 is the maximum void fraction for reducing the void
c  fraction used to determine the heat transfer coefficients
c  for the wetted steam generator tubes above the pool
c
      data iflgw     , iflgwc   , iflgd   / 0.0 , 0.0    , 0.0    /
      data alpha0    , alpha1   , alpha2  / 0.9 , 0.95   , 0.9999 /
      data alphamw   , alphad             / 1.0 , 0.9965 /
      data hlc0      , hlc1               / 0.0 , 1.8    /
      data hvc0      , hvc1               / 0.0 , 1.0    /
c
*i uphgam.144
c
c  check for slab which is wetted by the afw
c
   if(i .ge. (ncell1 + 1) .and. i .le. (2*ncell1-1)) iflgw = 1
c
c  check wetted slab to determine whether to apply chen multiplier
c
   if(iflgw .eq. 1 .and. a(lalp+io) .ge. alpha0
   +          .and. a(lalp+io) .lt. alpha2) iflgwc = 1
c
c  check for slab which is not wetted by the afw
c
   if(i .ge. 1 .and. i .le. (ncell1-1)) iflgd = 1
c
c
   alpha = a(lalp+io)
c
c
c  reset alpha for dry slabs above pool
c
```

```
      if(iflgd .eq. 1 .and. a(lalp+io) .ge. alpha0) then
        if(a(lalp+io) .le. alpha2) alpha = alphad
        if(a(lalp+io) .gt. alpha2) alpha = amax1(a(lalp+io),alphad)
      endif
c
c
c     reset alpha for wetted slabs above pool
c
      if(iflgw .eq. 1 .and. a(lalp+io) .ge. alpha0) then
        if(a(lalp+io) .gt. alpha2) alphamw = 1.
        if(a(lalp+io) .le. alpha2) alphamw = alpha1
        alpha = amin1(a(lalp+io),alphamw)
      endif
c
c
*d stgn1x.86
      * alpha,a(lsig+io),grvg,vlz,vlz,zero,vvz,zero,zero,
*i uphgam.146
c
c     apply chen multiplier for slab with iflgwc = 1
c     and heat transfer mode = 2
c
      if (iflgwc .eq. 1 .and. a(lidgho+im1) .eq. 2.) then
        a(lholgn+im1) = a(lholgn+im1) * hlc1 + hlc0
        a(lhovgn+im1) = a(lhovgn+im1) * hvc1 + hvc0
      endif
c
      iflgw = 0
      iflgwc = 0
      iflgd = 0
c
```

APPENDIX C

CODE ASSESSMENT DESCRIPTOR DEFINITIONS

The descriptors will be used to provide an overall characterization of how TRAC predicted (1) the thermal-hydraulic behavior in the MIST facility. Four descriptors are used to characterize the degree of agreement and the application consequences of either the agreement or lack of agreement. The four descriptors are **excellent agreement**, **reasonable agreement**, **minimal agreement**, and **insufficient agreement**. Each of these descriptions will be defined below along with the consequences for future application of the code in the given area being characterized and the perceived need for additional code development.

Excellent agreement is an appropriate descriptor when the code exhibits no deficiencies in modeling a given behavior. Major and minor phenomena and trends are correctly predicted. The calculated results are judged by the analyst to be close to the data with which a comparison is being made. If the uncertainty of the data has been identified and made available to the analyst, the calculation will, with few exceptions, lie within the uncertainty band of the data. The code may be used with confidence in similar applications. Neither code models nor the facility noding model require examination or change.

Reasonable agreement is an appropriate descriptor when the code exhibits deficiencies, but the deficiencies are minor; that is, the deficiencies are acceptable because the code provides an acceptable prediction of the test. All major trends and phenomena are correctly predicted. Differences between the test and calculated traces of parameters identified as important by the analyst are greater than those deemed necessary for excellent agreement. If uncertainty data are available, the calculation will frequently lie outside the uncertainty band. However, the analyst believes that the discrepancies are not sufficiently large to require a warning to potential users of the code in similar applications. The assessment analyst believes that the correct conclusions about trends and phenomena would be reached if the code were used in similar applications. The code models and/or facility noding model should be reviewed to see if improvements can be made.

Minimal agreement is an appropriate descriptor when the code exhibits deficiencies and the deficiencies are significant; that is, the deficiencies are such that the code provides a prediction of the test that is only conditionally acceptable. Some major trends or phenomena are not predicted correctly while others are predicted correctly. Some TRAC-calculated values lie far outside the uncertainty band of the data with which a comparison is being made. The assessment analyst believes that incorrect conclusions about trends and phenomena may be reached if the code were used in similar applications. The analyst believes that certain code models and/or the facility noding model must be reviewed, corrections made, and a limited assessment of the revised code or input models made before the code can be used with confidence for similar applications. A warning should be issued to the TRAC user community that the user applying the code in similar applications risks drawing incorrect conclusions. This warning should stay in force until the identified review, modification, and limited assessment activities are completed and the resultant characterization descriptor is "reasonable" or better.

Insufficient agreement is an appropriate descriptor when the code exhibits major deficiencies; that is, the deficiencies are such that the code provides a prediction of the test that is unacceptable. Major trends are not predicted correctly. Most TRAC-calculated values lie far

outside the uncertainty band of the data with which a comparison is being made. The assessment analyst believes that incorrect conclusions about trends and phenomena are probable if the code is used in similar applications. The analyst believes that certain code models and/or the facility noding model must be reviewed, corrections made, and a limited assessment of the revised code or facility noding model made before the code can be used with confidence for similar applications. A warning should be issued to the TRAC user community that the code must not be used for similar applications until the identified review, modification, and limited assessment activities are completed and the resultant characterization descriptor is "reasonable" or better.

APPENDIX D

CODE PERFORMANCE INDICATORS

A comparison of CPU time versus real time for the calculation of MIST 330302 on the Cray-1S computer at Los Alamos National Laboratory is presented in Fig. D-1. Plots of time-step size versus real time and number of time steps versus real time are presented in Figs. D-2 and D-3, respectively. The time-step data presented in Fig. D-2 illustrate that larger time steps up to the input limit of 0.15 s were possible when the primary system was in single-phase natural circulation. After the PORV was opened at 728 s and the primary system began to void, the code selected a reduced time-step size. The mean time step after PORV opening was about 0.050 s.

The "grind" time for this calculation is calculated from the equation:

$$\text{Time} = (\text{CPU} \times 10^3) \quad / \quad (\text{C} \times \text{DT})$$

where CPU = total execution time in seconds,
C = total number of volumes in the model, and
DT = total number of time steps.

The resultant time is expressed in milliseconds per computational volume per time step.

For the MIST Test 330302, the CPU time was 50000 s, the total number of volumes in the MIST facility model was 251, and the total number of time steps was 104000. Thus,

$$\text{Time} = (5 \times 10^4 \times 10^3) \quad / \quad (251 \times 1.04 \times 10^5)$$

$$\text{Time} = 1.9 \text{ milliseconds per volume per time step.}$$

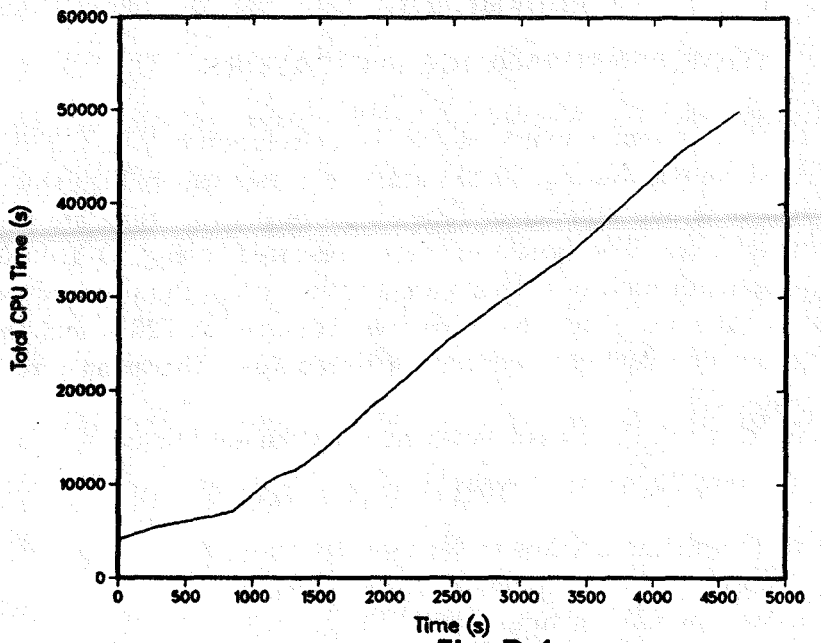

Fig. D-1.
CPU time versus real time for Test 330302.

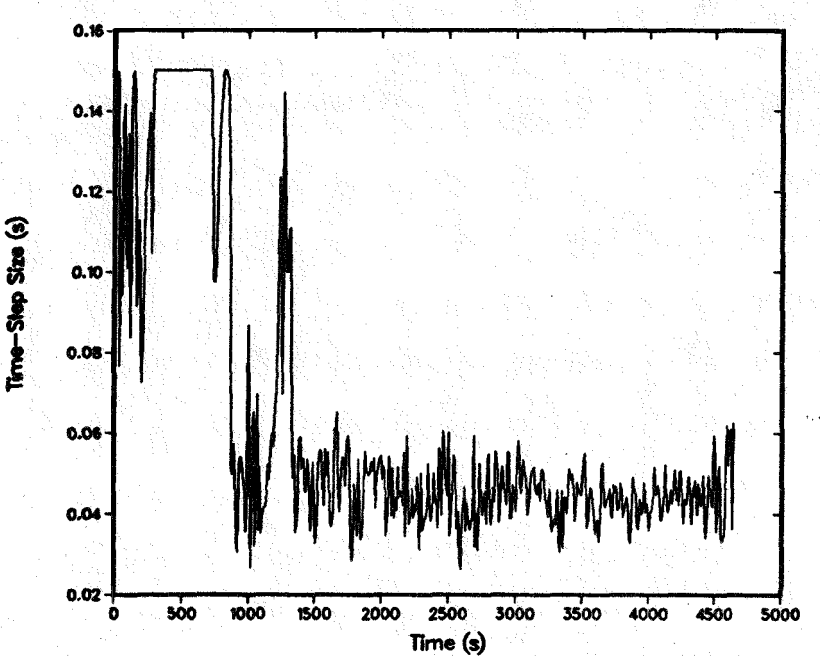

Fig. D-2.
Time-step size versus real time for Test 330302.

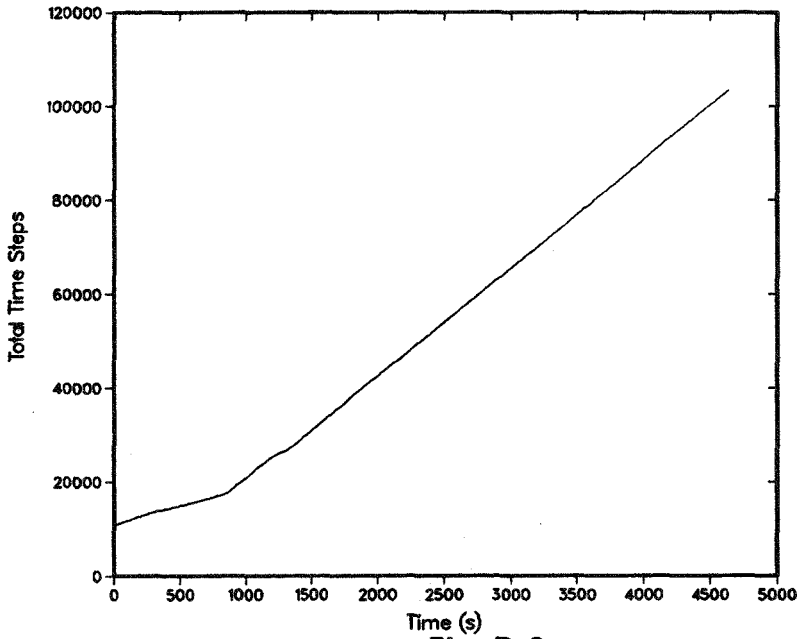

Fig. D-3.

Number of time steps versus real time for Test 330302.

NRC FORM 335 (2-89) NRCM 1102, 3201, 3202

U.S. NUCLEAR REGULATORY COMMISSION

BIBLIOGRAPHIC DATA SHEET

1. REPORT NUMBER (Assigned by NRC,Add Vol., Supp., Rev., and Addendum Numbers, if any.)

NUREG/CR-5889
LA-UR-88-1937

2. TITLE AND SUBTITLE

Posttest Analysis of MIST Test 330302 Using TRAC-PF1/MOD1

3. DATE REPORT PUBLISHED

MONTH: September | YEAR: 1992

4. FIN OR GRANT NUMBER

A7311

5. AUTHOR(S)

Brent E. Boyack

6. TYPE OF REPORT

Technical

7. PERIOD COVERED *(Inclusive Dates)*

8. PERFORMING ORGANIZATION – NAME AND ADDRESS *(If NRC, provide Division, Office or Region, U.S. Nuclear Regulatory Commission, and mailing address; if contractor, provide name and mailing address.)*

Los Alamos National Laboratory
Los Alamos, New Mexico 87545

9. SPONSORING ORGANIZATION – NAME AND ADDRESS *(If NRC, type "Same as above"; if contractor, provide NRC Division, Office or Region, U. S. Nuclear Regulatory Commission, and mailing address.)*

Division of Systems Research
Office of Nuclear Regulatory Research
U. S. Nuclear Regulatory Commission
Washington, DC 20555

10. SUPPLEMENTARY NOTES

None

11. ABSTRACT *(200 words or less)*

A posttest analysis of Multi-loop Integral System Test (MIST) 330302 has been performed using TRAC-PF1/MOD1. This test was one of a group performed in the MIST facility to investigate high-pressure injection (HPI)-power-operated relief valve (PORV) cooling, also known as feed-and-bleed cooling. In Test 330302, HPI cooling was delayed 20 min after opening and locking the PORV open to induce extensive system voiding. MIST 330302 displayed many phenomena of interest. These included a steam-generator-secondary boiloff, slow primary-system inventory, single- and two-phase fluid flows through the PORV, hot-leg spillover events, cold-leg and downcomer flow interruption and recovery, effects of late HPI injection into a voided primary system, and primary-system refill. We have concluded that the TRAC-calculated results are in reasonable overall agreement with the data for Test 330302. All major trends and phenomena were correctly predicted. Differences observed between the measured and calculated results have been traced and related, in part, to deficiencies in our knowledge of the facility configuration and operation. We have identified two models for which additional review is appropriate. However, in general, the TRAC closure models and correlations appear to be adequate for the prediction of the phenomena expected to occur during feed-and-bleed transients in the MIST facility. We believe that the correct conclusions about trends and phenomena will be reached if the code is used in similar applications. Conclusions reached regarding use of the code to calculate similar phenomena in full-size plants (scaling implications) and regulatory implications of this work are also presented.

12. KEY WORDS/DESCRIPTORS *(List words or phrases that will assist researchers in locating the report.)*

Thermal Hydraulic Analysis
Multi-Loop Integral System Test (MIST)
Small-break loss-of-coolant accident (SBLOCA)
TRAC-PF1/MOD1
MIST Test 330302
Power-operated relief valve (PORV)

13. AVAILABILITY STATEMENT

Unlimited

14. SECURITY CLASSIFICATION

(This Page) Unclassified

(This Report) Unclassified

15. NUMBER OF PAGES

16. PRICE

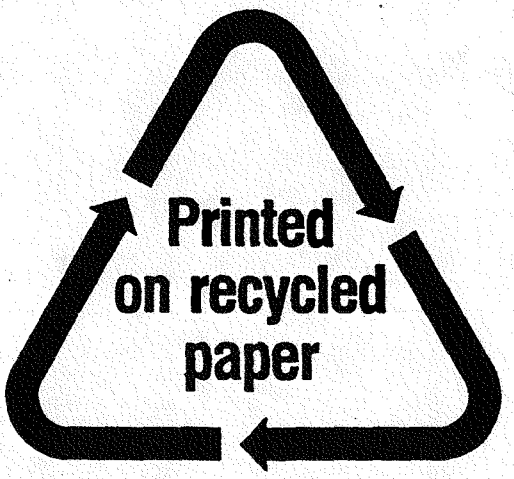

Federal Recycling Program

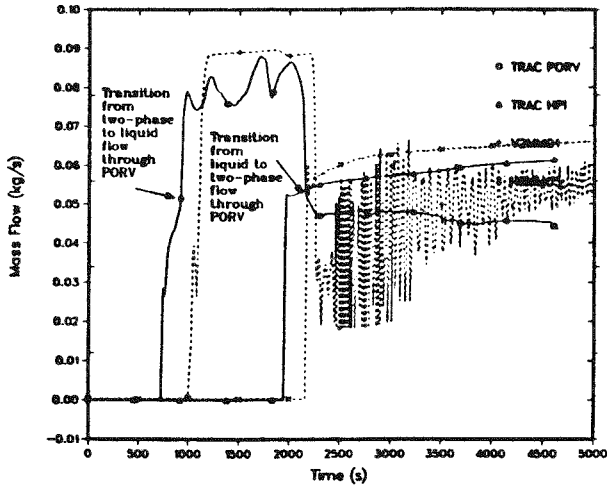

Fig. 2.c. PORV and HPI flows.

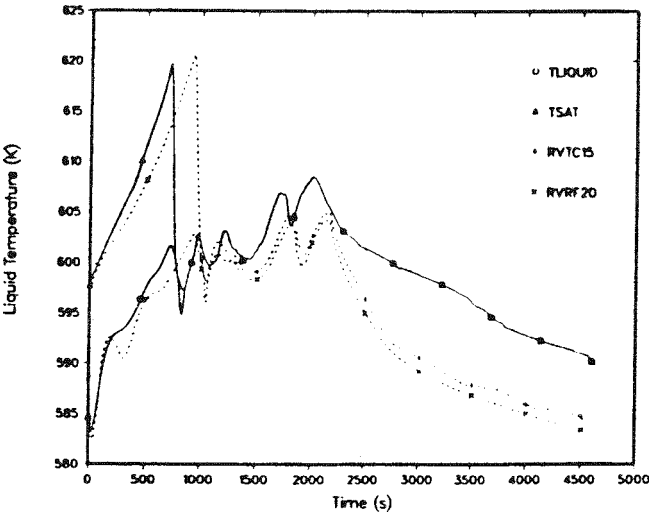

Fig. 2.d. Core exit liquid temperature compared to saturation.

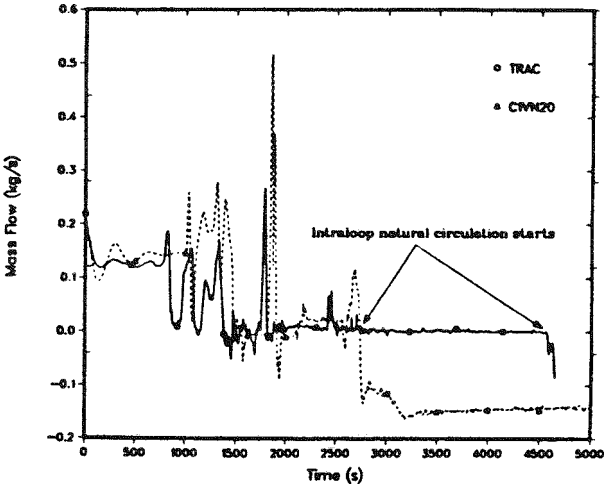

Fig. 2.g. Loop-A1 cold-leg mass flow.

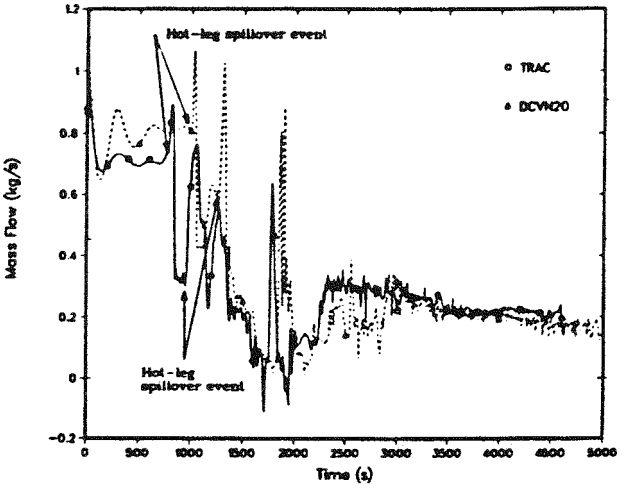

Fig. 2.h. Downcomer mass flow.

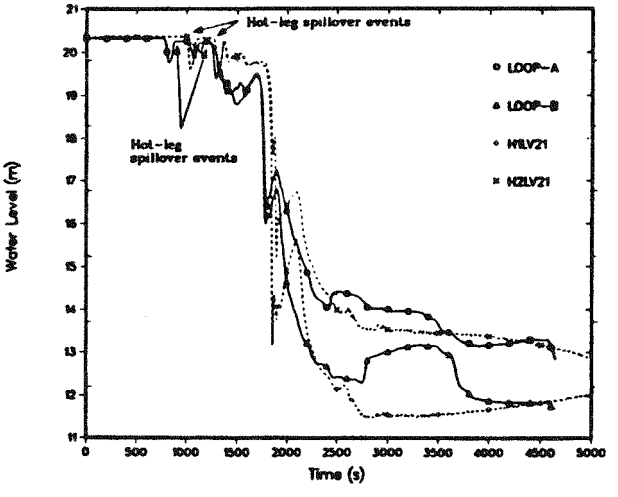

Fig. 2.k. Hot-leg collapsed liquid level.

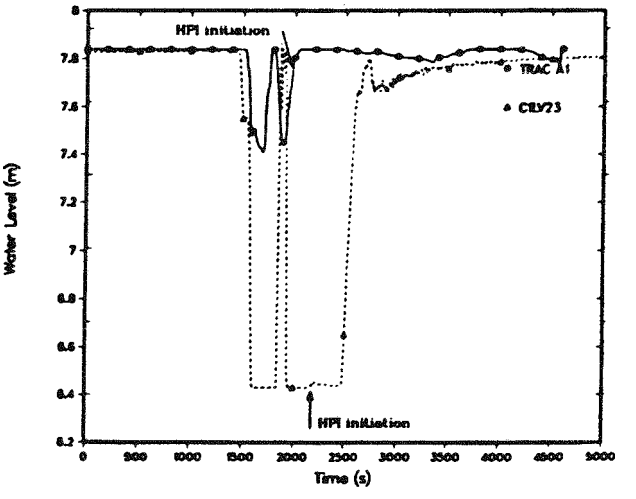

Fig. 2.l. Loop-A1 cold-leg collapsed liquid level.

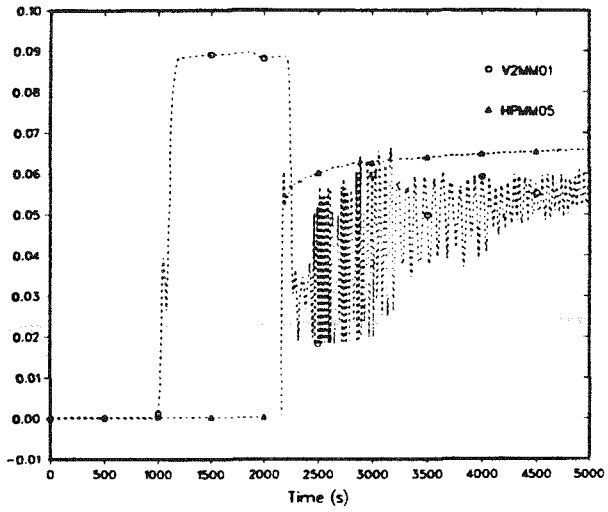

Fig. 1.c. PORV and HPI flows.

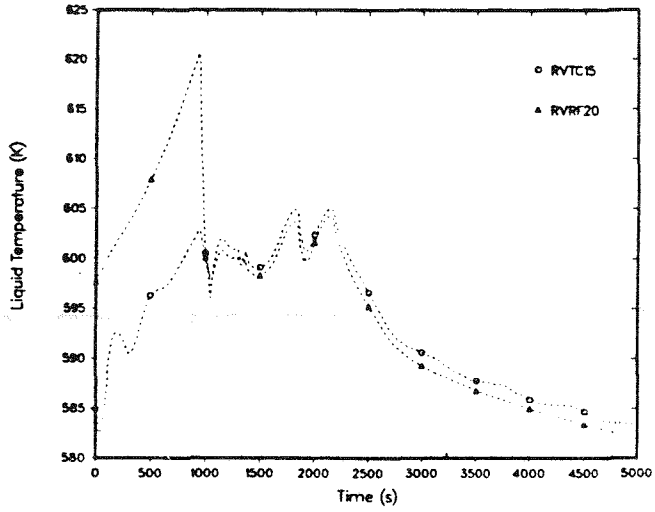

Fig. 1.d. Core exit liquid temperature compared to saturation.

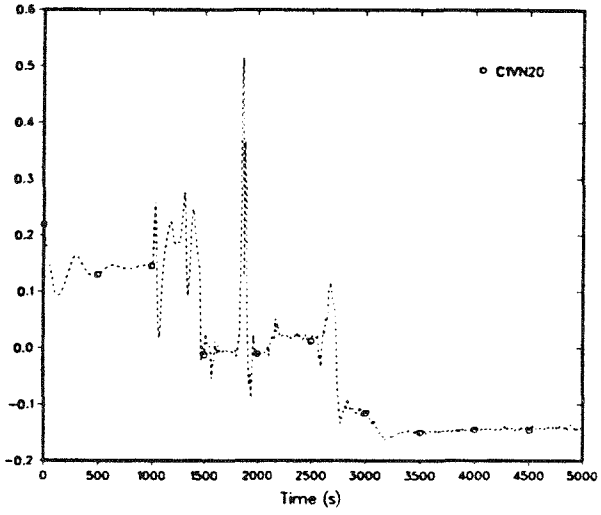

Fig. 1.g. Loop-A1 cold-leg mass flow.

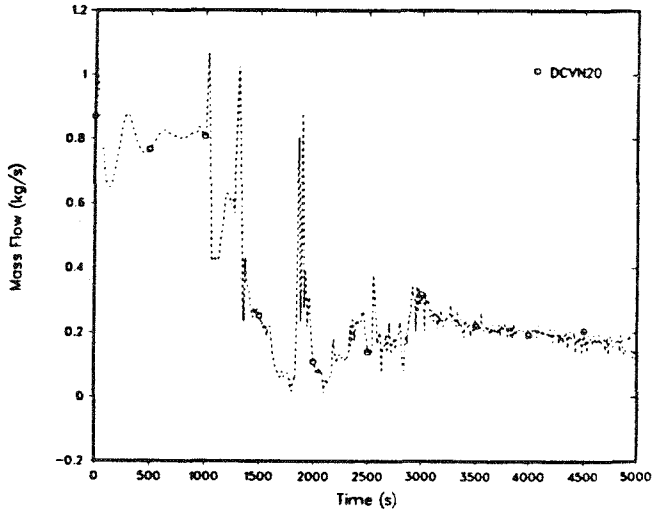

Fig. 1.h. Downcomer mass flow.

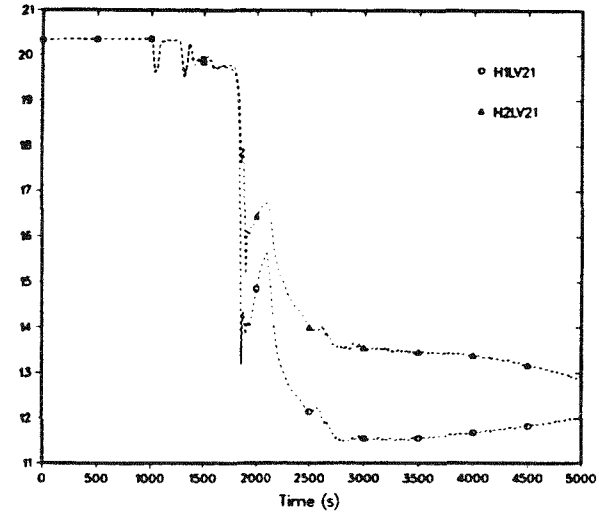

Fig. 1.k. Hot-leg collapsed liquid level.

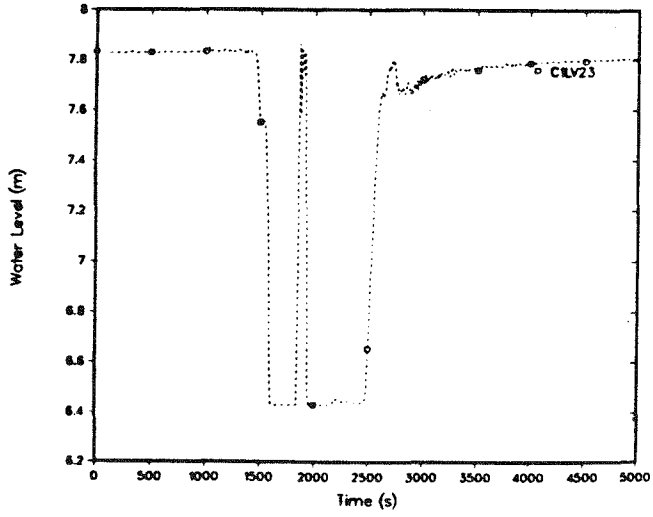

Fig. 1.l. Loop-A1 cold-leg collapsed liquid level.